

Master's thesis

Emphasis: Theoretical particle physics

**Resummation predictions for slepton particle production
at the LHC
and implications for dark matter**

*Resummations-Vorhersagen für Slepton-Produktion am LHC
und Konsequenzen für Dunkle Materie*

by Marcel Rothering

Münster, November 12, 2012

Submitted in partial fulfilment of the requirements for the
degree of Master of Science in physics
by research at the Westfälische Wilhelms-Universität Münster

Supervisor & first examiner: Prof. Dr. Michael Klasen
Second examiner: Jun. Prof. Dr. Anna Kulesza
Time allowed for completion: From April 23 to December 27, 2012

Contents

1	Introduction	1
2	Theoretical background	3
2.1	Supersymmetry and the MSSM	3
2.1.1	Motivation	3
2.1.2	Concepts of Supersymmetry	5
2.1.3	The Minimal Supersymmetric Standard Model	9
2.2	QCD at the LHC	16
2.2.1	The Drell-Yan process	17
2.2.2	Parton distribution functions	19
2.2.3	Collider kinematics and important distributions	25
3	Resummation	29
3.1	The basic ideas behind resummation	30
3.2	Soft photon resummation	31
3.3	Threshold resummation	33
3.4	Transverse momentum resummation	39
4	Slepton pair production	44
4.1	Analytical results	44
4.2	Numerical results	49
4.2.1	Experimental constraints	50
4.2.2	Benchmark scenarios	51
4.2.3	Total cross sections	52
4.2.4	Invariant mass distributions	58
4.2.5	Transverse momentum distributions	62
4.3	Implications for dark matter	65
4.3.1	Sneutrino as a dark matter candidate	65

4.3.2	The monojet analysis	68
5	Conclusion and outlook	74
A	Feynman rules	76
B	Feynman amplitudes	77
B.1	Leading-order process	78
B.2	Virtual corrections	79
B.2.1	The quark self energy	79
B.2.2	SUSY self energy for quarks	80
B.2.3	The gluon vertex correction	81
B.2.4	The SUSY vertex correction	82
B.3	The real corrections	83
B.3.1	Real gluon emission	83
B.3.2	Real quark emission	85
B.3.3	Real antiquark emission	86
C	Gaugino pair production	87

1 Introduction

Understanding the laws of nature is probably one of the most exciting challenges Mankind can accept. The concept of symmetries provides an extremely successful approach to derive the rules the universe obeys. With the combination of space-time and internal gauge symmetries, a Quantum Field Theory (QFT) has been created with a tremendous predictive power, the Standard Model of particle physics (SM). Since the construction of the Large Hadron Collider (LHC) at CERN we have a source for highly accurate experimental results to check the validity of the SM. All comparisons seem to be in perfect agreement and with the discovery of a particle, consistent with the properties of the Higgs, even the last element of the SM may have been found. Certainly this will not be the end of the challenge. There are open questions the SM can never answer, some of them by its construction alone: What is the source of gravitation? What is dark matter (DM)? Why are the neutrinos massive? Why is there a matter-antimatter asymmetry? ... What could be more beautiful than finding the answers in a larger symmetry nature exhibits? This is what Supersymmetry (SUSY) does.

With the LHC we are confident to explore things beyond the SM (BSM). We know it will discover something new, but we do not know what. It might be SUSY. In order to verify a new discovery the necessity of highly precise predictions for proton-proton collisions is indispensable. Therefore the techniques of perturbative Quantum Chromodynamics (QCD) have been established as an effective tool. Nevertheless, in a certain region of the particle phase space the fixed order computations show a large discrepancy compared to the experimental results. Furthermore these regions somehow spoil the convergence of the perturbative series and our computations become unreliable. This is where resummation makes its important contribution for the improvement of the fixed order computations and to assure the predictive power even in the critical kinematic regions. The Minimal Supersymmetric Standard Model (MSSM) is one of the most promising candidates BSM we are looking for. It contains superpartners for each SM particle. Among them the sleptons are the supersymmetric counterparts of the leptons and our particles of interest during this thesis. Due to their only electroweak gauge couplings,

sleptons are among the lightest superpartners containing the sneutrino as a possible DM candidate if it is the lightest stable supersymmetric particle (LSP). Even if this is not the case, slepton phenomenology is of high interest. They would decay into the LSP, probably the neutralino in minimal Supergravity (mSUGRA) or the gravitino in gauge mediated SUSY-breaking models (GMSB), and their corresponding lepton. For slepton pair production this would lead to a highly energetic lepton pair, which can be easily detected, and some missing energy.

Our main goal of the thesis is making precise predictions for slepton pair production at the LHC. We therefore will firstly study the necessary theoretical background of SUSY and QCD at the LHC in Ch. 2.1 and 2.2, respectively. Afterward, we present in Ch. 3 all the important formulas to apply threshold and transverse momentum resummation. This is followed by its applications to slepton pair production in Ch. 4, which is divided in an analytical and numerical part and the implications for DM. Finally, we will come to the conclusion of the work and give a brief outlook in Ch. 5.

Apart from the main chapters, we will present all the necessary computations for the used Feynman amplitudes in App. A and B. In addition, updated results for gaugino pair production are stated in App. C, since the program code developed in this thesis is an extension of Jonathan Debove's, originally created for resummation techniques applied to gaugino pair production [1].

2 Theoretical background

2.1 Supersymmetry and the MSSM

The probably most important approach to understand nature is to study its symmetries. Most of the progress made in understanding the laws and mechanisms of particle physics has been achieved through studying the symmetries of the particles they exhibit. It is known, thanks to the *Noether theorem* that every global symmetry corresponds to a conserved quantity. So the origin for the possibility to label our particles with different quantum numbers lies in the symmetries, a given theory, i.e. a Lagrangian, obeys. The fundamental Lorentz invariance, the Abelian and non-Abelian gauge symmetries and the study of flavor symmetries play an important role for the research and development of QFT. But a symmetry unlike all the others has been proposed and brought to attention by Wess and Zumino in 1974. Its name is *Supersymmetry*. [2]

In this section we want to mention and briefly explain all the necessary basics to pursue the study of slepton pair production in this thesis. Firstly, we will show reasonable motivations to look for physics BSM and deal with SUSY. After the introduction of the general concepts we will directly go to the model of interest, the MSSM.

The whole section will be based on the Refs. [3] and [4].

2.1.1 Motivation

With the discovery of a new boson at the LHC, which is consistent with the properties of the SM Higgs particle, the final missing ingredient of the SM could have been found. Yet even then the chapter of particle physics would not be closed. There are still open questions, even apart from the trivially missing gravitational force. Until now the SM provides a remarkable description of the world we live in and it fits incredibly well the experimental measurements. But not all of them!

From the experimental data of, e.g. WMAP, we know that only a little piece the universe consists of can be described by the SM. There is roughly 95% of energy which

is unknown. We have no clue about the origin yet, but we know that the SM cannot explain that part of *dark energy* and *dark matter*. In addition, we have other unsolvable problems like the matter and anti matter asymmetry in the universe or the neutrino oscillations. There are also unsatisfactory aspects in the SM like the grand unification of the three SM forces at high energies, which is not fulfilled in the SM, or the hierarchy problem, which describes the large M_P/M_W ratio of the Planck mass and W boson mass. It is rather obvious that there must be physics between those 16 orders of magnitude. This comes along with the *fine-tuning* problem, which is due to the scalar nature of the Higgs particle. Therefore the corrections to its mass depend quadratically, and so tremendously on Λ_{UV} , which is the upper scale limit up to which we think the SM is valid. Since all the masses of the SM particles are generated with the *Higgs mechanism* the whole theory is directly or indirectly sensitive to Λ_{UV} . So we have to either accept this, avoid it with theories without a *Higgs mechanism* or to extend the SM somehow with respect to the mentioned problems.

All this opens the field for physics BSM, e.g. *extra dimensions*, *technicolor*, *seesaw mechanisms*, *LR-models*, . . . and of course SUSY.

Let us have a closer look at the *fine-tuning* problem. We know that the *bare* mass of every particle in the Lagrangian receives corrections from loop diagrams. It is relatively easy to compute those diagrams while introducing a cut-off scale Λ_{UV} , a scale up to which our theory is supposed to be valid, e.g. the Planck scale M_P . For fermions and vector bosons this will lead to a logarithmically dependence on Λ_{UV} , which is not large even if the scale is. For the Higgs it is different. In the SM the Higgs mass will get its corrections from fermion loops depicted in Fig. 2.1 (a).

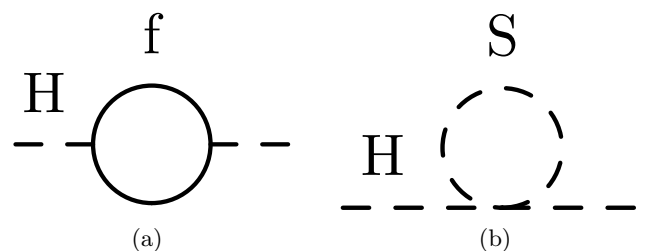


Figure 2.1: Virtual corrections contributing to the Higgs mass. (a) shows a virtual fermion and (b) a virtual scalar particle.

This will give us the contribution

$$\Delta m_H^2 = \frac{|\lambda_f|^2}{16\pi^2} \left[-2\Lambda_{\text{UV}}^2 + 6m_f^2 \ln \frac{\Lambda_{\text{UV}}}{m_f} \right], \quad (2.1)$$

where λ_f is a Yukawa coupling. It shows the quadratic dependence. If the scale for new physics would be the Planck scale, this would lead to a correction 30 orders of magnitude larger than the expected value of $(100 \text{ GeV})^2$. But maybe Λ_{UV} is smaller and of the order of 1 TeV and there SUSY comes into the scene. Therewith we will get scalar superpartners of the fermions, the sfermions. They will also couple to the Higgs (Fig.2.1 (b)) and lead to a contribution

$$\Delta m_H^2 = \frac{\lambda_s}{16\pi^2} \left[\Lambda_{\text{UV}}^2 - 2m_s^2 \ln \frac{\Lambda_{\text{UV}}}{m_s} \right]. \quad (2.2)$$

In SUSY each chiral fermion state has its own superpartner. Therefore the quadratic dependence exactly cancels if $\lambda_s = |\lambda_f|^2$. Now only a logarithmic dependence remains that we can handle.

Unfortunately SUSY is not an exact symmetry of nature, otherwise we would have seen e.g. a massless particle with spin 1/2. So why bother about such a theory? Firstly it has an undoubted mathematical fascination and some physicists incline that ‘‘God’’ must have made use of such a nice symmetry to create Mother Nature. Secondly, it can partially solve our open questions and can be combined with other theories to get a very large symmetry nature could have obeyed until it was broken.

2.1.2 Concepts of Supersymmetry

SUSY is a theory in which fermions can be transformed into bosons and vice versa. Therefore the Poincaré group has to be enlarged and is then called the Super-Poincaré-Group. The Poincaré transformations (PT) include Lorentz transformations and translations. The infinitesimal generators are P^μ for the translations and $K^{\mu\nu}$ for rotations and boosts. They fulfill the Poincaré algebra

$$[P^\mu, P^\nu] = 0, \quad (2.3)$$

$$[P^\mu, K^{\nu\sigma}] = i(g^{\mu\nu} P^\sigma - g^{\mu\sigma} P^\nu), \quad (2.4)$$

$$[K^{\mu\nu}, K^{\sigma\rho}] = -i(g^{\mu\sigma} K^{\nu\rho} + g^{\nu\rho} K^{\mu\sigma} - g^{\mu\rho} K^{\nu\sigma} - g^{\nu\sigma} K^{\mu\rho}) \quad (2.5)$$

and therewith we can do a finite transformation on a field:

$$\phi(x) \rightarrow \phi'(x) = e^{ia^\mu P_\mu + \frac{i}{2}\omega^{\mu\nu} K_{\mu\nu}} \phi(x). \quad (2.6)$$

The explicit form of the generators depends on the field's nature. E.g. for a spin 1/2 field it is

$$P^\mu = i\partial^\mu, \quad (2.7)$$

$$K^{\mu\nu} = i(x^\mu \partial^\nu - x^\nu \partial^\mu) + \frac{i}{4}[\gamma^\mu, \gamma^\nu]. \quad (2.8)$$

All these are *bosonic operators* which act only in the 4-momentum vector space and cannot change the spin of a particle. So why are there no *fermionic operators* which can lead to a symmetry in nature? This is what SUSY does and it is the only way to enlarge the Poincaré group ¹. Therefore we have to enlarge our 4-dimensional space time and add two Grassmann valued spinors as components $X(x^\mu, \theta^a, \bar{\theta}^{\dot{a}})$. The quantum fields which depend on X are called superfields.

During this thesis we will not make use of the superfield formalism, even if it is more elegant and opens a nice access to the enlarged PT. It is enough to consider an easy supersymmetric example. Therefore we show one of the first-mentioned supersymmetric Lagrangians. It is convenient to use Weyl spinor formalism, because this is the irreducible representation of the Lorentz group for spin 1/2 fields. For fixing the notations we will write the Dirac spinor as

$$\Psi_D = \begin{pmatrix} \psi_\alpha \\ \chi^{\dagger\dot{\alpha}} \end{pmatrix}, \quad \gamma^\mu = \begin{pmatrix} 0 & \sigma^\mu \\ \bar{\sigma}^\mu & 0 \end{pmatrix}, \quad \sigma^\mu = (1, \vec{\sigma}), \quad (2.9)$$

where α and $\dot{\alpha}$ are spinor indices and σ_i are the Pauli matrices.

For any kind of symmetry the action of the theory must be invariant under the corresponding transformation. First we want to find a theory with two free massless fields, where one is a Weyl spinor field ψ and the other one a complex scalar field ϕ . The action reads then

$$S = \int d^4x (\mathcal{L}_{scalar} + \mathcal{L}_{fermion}) \quad (2.10)$$

$$= \int d^4x (-\partial^\mu \phi^* \partial_\mu \phi + i\psi^\dagger \bar{\sigma}^\mu \partial_\mu \psi). \quad (2.11)$$

¹This is based on the *Haag-Lopuszanski-Sohnius theorem*.

The field content corresponds to a single chiral multiplet. A simple supersymmetric transformation is

$$\delta\phi = \epsilon\psi \qquad \delta\phi^* = \epsilon^\dagger\psi^\dagger, \qquad (2.12)$$

$$\delta\psi_\alpha = -i(\sigma^\mu\epsilon^\dagger)_\alpha\partial_\mu\phi + \epsilon_\alpha F, \qquad \delta\psi_{\dot{\alpha}} = i(\sigma^\mu\epsilon^\dagger)_{\dot{\alpha}}\partial_\mu\phi^* + \epsilon_{\dot{\alpha}}^\dagger F^*, \qquad (2.13)$$

where we have introduced an auxiliary complex scalar field F with two degrees of freedom to satisfy the invariance also off-shell and to get a closed group. Due to the *Noether theorem* this symmetry gives rise to a conserved current, called the *supercurrent* J^μ . Its integrated time component J^0 over the spatial space leads to the conserved charges Q and Q^\dagger , which are the generators of the supersymmetric transformations.

$$Q_\alpha|\text{bos}\rangle = |\text{ferm}\rangle_\alpha \qquad Q_\alpha|\text{ferm}\rangle^\alpha = |\text{bos}\rangle \qquad (2.14)$$

This gives us the enlarged Poincaré group which includes now also fermionic generators and fulfills the algebra

$$[Q_\alpha, P^\mu] = 0, \qquad (2.15)$$

$$\{Q_\alpha, \bar{Q}_{\dot{\beta}}\} = 2(\sigma^\mu)_{\alpha\dot{\beta}}P_\mu, \qquad (2.16)$$

$$[K^{\mu\nu}, Q_\alpha] = -i(\sigma^{\mu\nu})_\alpha{}^\beta Q_\beta, \qquad (2.17)$$

$$\{Q_\alpha, Q_\beta\} = \{\bar{Q}_{\dot{\alpha}}, \bar{Q}_{\dot{\beta}}\} = 0. \qquad (2.18)$$

Until now we have seen a free supersymmetric chiral field theory. Before we will consider the gauge part we want to look at the most general supersymmetric non gauge interactions. It can be shown that the most general renormalizable and supersymmetric interaction is

$$\mathcal{L}_W = \left(-\frac{1}{2}W^{ij}\psi_i\psi_j + W^i F_i\right) + \text{c.c.}, \qquad (2.19)$$

where

$$W^{ij} = \frac{\delta^2 W}{\delta\phi_i\delta\phi_j}, \qquad W^i = \frac{\delta W}{\delta\phi_i} \qquad (2.20)$$

and W is a holomorphic function of the scalar fields, the *superpotential*

$$W = \frac{1}{2}M^{ij}\phi_i\phi_j + \frac{1}{6}y^{ijk}\phi_i\phi_j\phi_k. \qquad (2.21)$$

Here M^{ij} is a symmetric mass matrix for the fermion fields and y^{ijk} is a Yukawa coupling of a scalar and two fermionic fields. We can express the auxiliary field F in terms of the *superpotential* W . The whole Lagrangian now reads

$$\begin{aligned} \mathcal{L} = & -\partial^\mu \phi^{*i} \partial_\mu \phi_i - V(\phi, \phi^*) + i\psi^{\dagger i} \bar{\sigma}^\mu \partial_\mu \psi_i \\ & - \frac{1}{2} M^{ij} \psi_i \psi_j - \frac{1}{2} M_{ij}^* \psi^{\dagger i} \psi^{\dagger j} - \frac{1}{2} y^{ijk} \phi_i \psi_j \psi_k - \frac{1}{2} y_{ijk}^* \phi^{*i} \psi^{\dagger j} \psi^{\dagger k}, \end{aligned} \quad (2.22)$$

where we have defined the scalar potential for the theory as

$$\begin{aligned} V(\phi, \phi^*) = & W^k W_k^* = F^k F_k^* \\ = & M_{ik}^* M^{kj} \phi^{*i} \phi_j + \frac{1}{2} M^{in} y_{jkn}^* \phi_i \phi^{*j} \phi^{*k} \\ & + \frac{1}{2} M_{in}^* y^{jkn} \phi^{*i} \phi_j \phi_k + \frac{1}{4} y^{ijn} y_{kln}^* \phi_i \phi_j \phi^{*k} \phi^{*l}. \end{aligned} \quad (2.23)$$

Using the *Euler Lagrange equations* and looking at the linearized equations of motion (EOM) we will get e.g.

$$\partial^\mu \partial_\mu \phi_i = M_{ik}^* M^{kj} \phi_j + \dots, \quad (2.24)$$

$$\partial^\mu \partial_\mu \psi_i = M_{ik}^* M^{kj} \psi_j + \dots. \quad (2.25)$$

So we have the same EOM for the fields in the chiral supermultiplet. If we now diagonalize the mass matrices and redefine the fields with unitary matrices we see that the superpartners have exactly the same mass. Therefore we must break SUSY.

The steps to construct the supersymmetric gauge part of the theory is more or less the same. The field content are vectorfields A_μ^a , where $a = 1, \dots, n^2 - 1$ for a SU(N), $a = 1$ for U(1), and their supersymmetric partners λ^a , called gauginos. Again we need an auxiliary field D^a which makes sure that the group closes off-shell. It has, like F , no mass term and no kinetic term. The Lagrangian density of the gauge supermultiplet is

$$\mathcal{L} = -\frac{1}{4} F_{\mu\nu}^a F^{\mu\nu a} + i\lambda^{\dagger a} \bar{\sigma}^\mu D_\mu \lambda^a + \frac{1}{2} D^a D^a, \quad (2.26)$$

$$F_{\mu\nu}^a = \partial_\mu A_\nu^a - \partial_\nu A_\mu^a + g f^{abs} A_\mu^b A_\nu^c, \quad (2.27)$$

$$D_\mu \lambda^a = \partial_\mu \lambda^a + g f^{abc} A_\mu^b \lambda^c, \quad (2.28)$$

while using the expression for the usual Yang Mills field strength tensor, the covariant derivative of the gaugino field D_μ , and the structure constants of the gauge group. If we couple the chiral multiplet with the gauge multiplet the EOM for the D^a field will

change to gain still a supersymmetric action of the theory.

Since SUSY and gauge transformations commute the supersymmetric chiral fields must be in the same representation of the gauge group. In addition to the common gauge interactions, which we get after the introduction of the covariant derivative, it is also allowed to have gauge interactions including the gaugino and D^a fields. Our supersymmetric Lagrangian is

$$\mathcal{L} = \mathcal{L}_{chiral} + \mathcal{L}_{gauge} - \sqrt{2}g(\phi^*T^a\psi)\lambda^a - \sqrt{2}g\lambda^{\dagger a}(\psi^\dagger T^a\phi) + g(\phi^*T^a\phi)D^a. \quad (2.29)$$

The first additional two terms are *supersymmetrizations* of the original SM gauge terms. Again we can replace the part of the auxiliary field by changing the scalar potential:

$$V(\phi, \phi^*) = F^{*i}F_i + \frac{1}{2}D^aD^a = W_i^*W^i + \frac{1}{2}\sum_a g_a^2(\phi^*T^a\phi)^2. \quad (2.30)$$

We call the two parts the *F-term* and the *D-term* and they will be essential for SUSY-breaking. The sum over a indicates the different gauge group couplings. Now we have found a complete SUSY theory.

2.1.3 The Minimal Supersymmetric Standard Model

Lagrangian and particle content

With the knowledge of the previous section we already know the particle content of the MSSM, shown in Tab. 2.1 and 2.2 with their corresponding representations of the gauge groups. The only novelty is an additional Higgs doublet to assure that all particles will get their mass.

Table 2.1: The chiral supermultiplets in the MSSM and their gauge group representations.

Names	Field	Spin 0	Spin 1/2	SU(3) _c , SU(2) _L , U(1) _Y
Squarks & quarks	Q	$(\tilde{u}_L, \tilde{d}_L)$	(u_L, d_L)	$(\mathbf{3}, \mathbf{2}, 1/3)$
	\bar{u}	$\tilde{\bar{u}}_L$	\bar{u}_L	$(\bar{\mathbf{3}}, \mathbf{1}, -4/3)$
	\bar{d}	$\tilde{\bar{d}}_L^*$	\bar{d}_L	$(\bar{\mathbf{3}}, \mathbf{1}, 2/3)$
Sleptons & leptons	L	$(\tilde{\nu}_{e_L}, \tilde{e}_L)$	(ν_{e_L}, e_L)	$(\mathbf{1}, \mathbf{2}, -1)$
	\bar{e}	$\tilde{\bar{e}}_L$	\bar{e}_L	$(\mathbf{1}, \mathbf{1}, 1)$
Higgs & Higgsino	H_u	(H_u^+, H_u^0)	$(\tilde{H}_u^+, \tilde{H}_u^0)$	$(\mathbf{1}, \mathbf{2}, 1)$
	H_d	(H_d^0, H_d^-)	$(\tilde{H}_d^0, \tilde{H}_d^-)$	$(\mathbf{1}, \mathbf{2}, -1)$

Table 2.2: The gauge supermultiplets in the MSSM and their gauge group representations.

Names	Spin 1/2	Spin 1	SU(3) _c , SU(2) _L , U(1) _Y
Gluino & gluon	\tilde{g}	g	(8 , 1 , 0)
Wino & W	$\tilde{W}^\pm, \tilde{W}^0$	W^\pm, W^0	(1 , 3 , 0)
Bino & B	\tilde{B}^0	B^0	(1 , 1 , 0)

After the Higgs gets a non-zero vacuum expectation value (vev), the bino, wino and Higgsino mix to the mass eigenstates neutralino and chargino similarly as in the electroweak gauge sector of the SM.

The superpotential for the MSSM is

$$W_{MSSM} = \bar{u}\mathbf{y}_u QH_u - \bar{d}\mathbf{y}_d QH_d - \bar{e}\mathbf{y}_e LH_d + \mu H_u H_d. \quad (2.31)$$

Here H_u , H_d , Q , L , \bar{u} and \bar{e} are the chiral fields corresponding to the chiral supermultiplets. They are expressed in the weak isospin representation (e.g. $Q_3 = (t, b)$, $\bar{u}_3 = \bar{t}$). The last term is the supersymmetric version of the Higgs mass term and \mathbf{y}_u , \mathbf{y}_d , \mathbf{y}_e are Yukawa coupling matrices in family space, which define the masses of the three families and the *Cabbibo-Kobayashi-Maskawa* (CKM) mixing matrix. It is worth to mention that a general *superpotential* could also contain additional terms, but they would give rise to lepton and baryon number violation which is highly suppressed with respect to the experimental knowledge.

We will consider a simple approximation of this *superpotential*. All Yukawa couplings are set to zero except for the members of the heavy third family.

$$W_{MSSM} \approx y_t(\bar{t}tH_u^0 - \bar{t}bHH_u^+) - y_b(\bar{b}tH_d^- - \bar{b}bH_d^0) - y_\tau(\bar{\tau}\nu_\tau H_d^- - \bar{\tau}\tau H_d^0) \quad (2.32)$$

$$+ \mu(H_u^+ H_d^- - H_u^0 H_d^0) \quad (2.33)$$

The Yukawa interactions are completely symmetric in a general SUSY theory. There-with we get, in addition to the common Higgs-lepton-lepton and Higgs-quark-quark couplings, the squark-higgsino-quark and slepton-higgsino-lepton couplings. However, the interactions due to the superpotential are usually not the most important ones, since the Yukawa couplings are very small. Instead, processes for the superpartners in the MSSM are dominated by the supersymmetric gauge interactions.

To avoid lepton and baryon number violation in the *superpotential* the MSSM is consid-

ered as a theory symmetric under *R-parity* defined as

$$P_R = (-1)^{3(B-L)+2s} \quad (2.34)$$

and which is a multiplicatively conserved quantum number. All the SM particles are labeled with *R-parity* +1 and all their superpartners with -1, so that a vertex must always include an even number of supersymmetric particles which entails that the LSP is stable and provides a good candidate for DM. Nevertheless one can doubt that *R-parity* is an exact symmetry, because in the SM every discrete symmetry is inexact (C, P, T) and we know about processes which can lead to baryon or lepton number violation.

Breaking scenarios

We know that SUSY is not an exact symmetry, at least nowadays. There are two different possibilities how to break a symmetry by either explicit terms in the Lagrangian or via spontaneous symmetry breaking like in the electroweak sector. In fact there is no consensus how to break SUSY “best”. To do phenomenology the introduction of a SUSY breaking term which parametrizes the low-energy scale of the unknown breaking mechanism is needed.

To break a symmetry spontaneously we need a field with a non-vanishing vev at the energy scale where SUSY is broken. This is well-known for the electroweak symmetry breaking. Since the theory must be still Lorentz invariant, only scalar fields may acquire vevs. With regard to SUSY transformations the only field in the chiral multiplet which could obtain such a vev is the auxiliary field F . Looking at our scalar potential $V(\phi) = F_i F^{*i}$ only for a vanishing ϕ we will get a minimum. Hence the scalar potential or the *superpotential* has to be changed. This has been worked out by O’Raifeartaigh. But it has been shown that the *F-term breaking* cannot be accomplished in the MSSM and one has to look beyond. In addition, this is also experimentally excluded due to the occurrence of too low slepton masses.

SUSY-breaking could also be achieved in the gauge supermultiplet. For the same reasons as for *F-term breaking* only the auxiliary field D^α can acquire a non-vanishing vev and we call this type of breaking mechanism the *D-term breaking*. Fayet and Iliopoulos have shown that such a breaking works by adding a new term to the scalar potential in the Lagrangian. Anyway, this type of breaking is not possible only with the particle content of the MSSM. [4]

Most people think the breaking mechanism occurs in a *hidden sector* that is weakly coupled to the chiral supermultiplets in the MSSM. This coupling could be e.g. gravitation

or weak coupling. In this point of view it is possible to break SUSY with F - or D -type mechanisms. Then the *hidden sector* contains unknown particles which show no or less interactions with the visible sector. The breaking in the visible sector happens due to the interaction of the two sectors.

Anyway, even if the breaking mechanism is unknown there should be breaking terms present nowadays wherewith we can do phenomenology. These terms should be soft, of positive mass dimension, so that we do not introduce new divergences. Soft SUSY-breaking terms assure the cancellations of quadratic divergent radiative corrections to scalar (mass)² terms up to all orders in perturbation theory. The mass scale at which SUSY is broken should not be much larger than 1 TeV to avoid the *fine-tuning* problem. The form of a general SUSY-breaking term is restricted. It must be gauge invariant, should be renormalizable and should give all the superpartners different masses. For the MSSM it could be

$$\mathcal{L}_{soft} = -\left(\frac{1}{2}M_a\lambda^a\lambda^a + \frac{1}{6}a^{ijk}\phi_i\phi_j\phi_k + \frac{1}{2}b^{ij}\phi_i\phi_j\right) + c.c - (m^2)_j^i\phi^{j*}\phi_i. \quad (2.35)$$

M_a is a gaugino mass term for each gauge group, m^2 is a scalar mass term and a^{ijk} and b^{ij} are scalar couplings. All these terms definitely break SUSY since they involve only masses for the superpartners. It is worth to mention that we cannot add such mass terms for the SM particles because it would break the electroweak symmetry explicitly. The masses of the SM particles must be generated with spontaneous electroweak symmetry breaking e.g. via the higgs mechanism. For the MSSM the phenomenological breaking term will be

$$\begin{aligned} \mathcal{L}_{soft}^{MSSM} = & -\frac{1}{2}(M_3\tilde{g}\tilde{g} + M_2\tilde{W}\tilde{W} + M_1\tilde{B}\tilde{B} + c.c.) \\ & - (\tilde{u}\mathbf{a}_u\tilde{Q}H_u - \tilde{d}\mathbf{a}_d\tilde{Q}H_d - \tilde{e}\mathbf{a}_e\tilde{L}H_d + c.c.) \\ & - \tilde{Q}^\dagger\mathbf{m}_Q^2\tilde{Q} - \tilde{L}^\dagger\mathbf{m}_L^2\tilde{L} - \tilde{u}\mathbf{m}_u^2\tilde{u}^\dagger - \tilde{d}\mathbf{m}_d^2\tilde{d}^\dagger - \tilde{e}\mathbf{m}_e^2\tilde{e}^\dagger \\ & - m_{H_u}^2H_u^*H_u - m_{H_d}^2H_d^*H_d - (bH_uH_d + c.c), \end{aligned} \quad (2.36)$$

with M_i being the gluino, wino and bino mass terms. The indices for the representations of the gauge groups have been suppressed. The second line represents (scalar)³ couplings and the bold printed expressions are all 3×3 matrices in family space. In the third line are the sfermion mass terms for squarks and sleptons. The last line represents the SUSY-breaking part to the Higgs potential.

With all these new matrices and couplings, the MSSM will gain some kind of arbitrariness,

because we introduce a lot of new parameters for masses, phases and mixing angles. By redefinition of the fields we can “rotate” some parameters away and we end up with 105 parameters in addition to the 19 of the SM. With some special considerations for the breaking we can reduce the enormous amount of arbitrariness in the Lagrangian and we can get a theory with predictive power. There are some experimental discoveries which constrain the parameters, e.g. the amount of CP violation or flavor violation. If e.g. \mathbf{m}_L^2 had non-suppressed off-diagonal elements, unacceptable large lepton flavor changing would be generated. In fact we have several theories for SUSY-breaking assuming some underlying simplicity and symmetry of the Lagrangian. We will briefly mention the most popular model for predictions, the *minimal supergravity* (mSUGRA).

There are mainly two assumptions for mSUGRA breaking. First the *soft supersymmetry breaking universality*, the hypothesis, that all mass matrices are proportional to the unit matrices, second that the triple scalar couplings are proportional to the Yukawa ones and that there is no introduction of new complex phases.

$$\mathbf{m}_Q^2 = m_Q^2 \mathbf{1}, \quad \mathbf{m}_u^2 = m_u^2 \mathbf{1}, \quad \mathbf{m}_d^2 = m_d^2 \mathbf{1}, \quad \mathbf{m}_e^2 = m_e^2 \mathbf{1}, \quad \mathbf{m}_L^2 = m_L^2 \mathbf{1}, \quad (2.37)$$

$$\mathbf{a}_u = A_{u0} \mathbf{y}_u, \quad \mathbf{a}_d = A_{d0} \mathbf{y}_d, \quad \mathbf{a}_e = A_{e0} \mathbf{y}_e, \quad (2.38)$$

$$\arg(M_1) = \arg(M_2) = \dots = \arg(A_{u0}) = 0. \quad (2.39)$$

These assumptions are only approximations since we have already in the SM nonzero phase e.g. for the CP-violation. Nevertheless, up to a certain accuracy this should be correct.

This is the basis for mSUGRA. The breaking occurs in a hidden sector and is connected to the visible MSSM sector mostly through gravitational-strength interactions. Due to the fact that the gravitational force is colorblind, this could be a reasonable assumption. In addition, the assumption of mass and coupling unification at high energy scales has been made. Therefore we have to evaluate the *renormalization group equation* (RGE) and “calculate back” the masses and couplings to the point of the electroweak scale. With all shown assumptions we are left with four parameters

$$m_{1/2} = M_1 = M_2 = M_3, \quad (2.40)$$

$$m_0^2 = m_Q^2 = m_u^2 = m_d^2 = m_e^2 = m_L^2 = m_{H_1}^2 = m_{H_2}^2, \quad (2.41)$$

$$A_0 = A_{u0} = A_{d0} = A_{e0}, \quad (2.42)$$

$$\tan \beta = \frac{\langle H_u^0 \rangle}{\langle H_d^0 \rangle} \quad (2.43)$$

and a relative sign for μ since the Higgs mass is fixed already by the SUSY theory itself. This implies that all the sfermions have been degenerated in mass independent of their flavor and family.

The squarks and sleptons

In the MSSM each fermion has its own superpartner. As we distinguish left and right chiral fermions in the SM we denote different superpartners with L-type and R-type, to see which fermion it belongs to. So we have to introduce 21 new scalar fields. For the squarks we have $\tilde{u}_L, \tilde{u}_R, \tilde{d}_L, \tilde{d}_R$ whereas for the sleptons we have $\tilde{\nu}_{eL}, \tilde{e}_L, \tilde{e}_R$, since the neutrino is also in the MSSM considered as massless. All the sfermions are represented in the same way with the same quantum numbers in the gauge group, e.g. $\tilde{e}_R = \tilde{e}_L$ is a $SU(2)_L$ singlet state.

In general all sfermions with the same quantum numbers can mix with each other and we get a 6×6 (or for sneutrinos 3×3) mixing matrix. The elements depend on the fermion masses and of course on the breaking terms and Higgs mass. Since the experimental observations restrict the flavor mixing dramatically we neglect it as it is done in mSUGRA. The L- and R-type mixing is completely given by the off-diagonal element which is proportional to the fermion masses, so that the L-R mixing will be only important for the heavy third generations ($\tilde{\tau}, \tilde{t}$ and \tilde{b}). The general 2×2 mixing matrix is

$$\mathbf{M}_f^2 = \begin{pmatrix} m_{LL}^2 & m_{LR}^2 \\ m_{LR}^{2*} & m_{RR}^2 \end{pmatrix}. \quad (2.44)$$

The entries are

$$m_{LL}^2 = m_{\tilde{F}}^2 + (T_f^3 - e_f \sin^2 \theta_W) m_Z^2 \cos 2\beta + m_f^2, \quad (2.45)$$

$$m_{RR}^2 = m_{\tilde{F}'}^2 + e_f \sin^2 \theta_W m_Z^2 \cos 2\beta + m_f^2, \quad (2.46)$$

$$m_{LR}^2 = m_f A_f^* - m_f \mu (\tan \beta)^{-2T_f^3}, \quad (2.47)$$

where $m_{\tilde{F}(\tilde{F}'')}$ are soft breaking mass terms, A_f is the trilinear Higgs-sfermion-sfermion coupling, m_f , e_f and T_f^3 are the fermion mass, fractional electric charge and the third component of the weak isospin, θ_W is the Weinberg angle for the electroweak mixing and m_Z is the Z-Boson mass.

We can easily diagonalize this matrix with a unitary matrix $\mathbf{S}^{\tilde{f}}$:

$$\text{diag}(m_1^2, m_2^2) = \mathbf{S}^{\tilde{f}} \mathbf{M}^2 \mathbf{S}^{\tilde{f}\dagger}. \quad (2.48)$$

With the introduction of a mixing angle the matrix $\mathbf{S}^{\tilde{f}}$ can be written as

$$\mathbf{S}^{\tilde{f}} = \begin{pmatrix} \cos \theta_{\tilde{f}} & \sin \theta_{\tilde{f}} \\ -\sin \theta_{\tilde{f}} & \cos \theta_{\tilde{f}} \end{pmatrix}. \quad (2.49)$$

With the convention of $m_{\tilde{f}_1} m_{\tilde{f}_2}$ the mass eigenvalues are

$$m_{\tilde{f}_{1,2}} = \frac{1}{2} \left[m_{LL}^2 + m_{LR}^2 \pm \sqrt{(m_{LL}^2 - m_{RR}^2)^2 + 4|m_{LR}^2|^2} \right] \quad (2.50)$$

and therewith follows the mixing angle

$$\tan 2\theta_{\tilde{f}} = \frac{2m_{LR}}{m_{LL}^2 - m_{RR}^2}. \quad (2.51)$$

2.2 QCD at the LHC

It is well known that QCD is a theory with an asymptotically free behavior at high energies and hence a vanishing coupling α_s . This can be seen after solving the RGE² in lowest order. One gets as the result

$$\alpha_s(\mu_r^2) = \frac{2\pi}{(11 - 2n_f/3) \ln\left(\frac{\mu_r^2}{\Lambda^2}\right)}, \quad (2.52)$$

where μ_r is the artificial renormalization scale parameter and Λ is a scale we find in nature for QCD. Since n_f is the number of quark flavors, the denominator is positive and for a scale $\mu_r > \Lambda$ the coupling becomes smaller than one. For this reason we can treat QCD perturbatively at high energy scales. We refer to reactions at this scale region as hard processes. Below the scale Λ we have to deal with hadronization of quarks and gluons that are nonperturbative problems and which we call soft processes. To make useful predictions it is indispensable to know at which energy scale the transition to the perturbative treatment of QCD takes place. It is known that this happens very rapidly at the order of 1 to 3 GeV, nevertheless, it is still a subject of many measurements [6]. As we will see in higher order corrections of the perturbative series, the coupling in combination with logarithmic prefactors is no longer small, even for large momentum transfers due to soft and collinear parts of the computations. This somehow spoils the convergence of the perturbative series and soft processes become important and enter crucially the hard processes. But due to the *factorization theorem*³, which shows that the separation of the soft and the hard processes can be achieved, we are still able to treat hadron collisions perturbatively at large momentum transfer. To gain the *factorization*, we need to introduce *Parton Distribution Functions* (PDFs), which represent the low energy regime and are therefore not computable with first principles. In this section we will basically deal with the study of PDFs together with the important *Dokshitzer–Gribov–Lipatov–Altarelli–Parisi* equations (DGLAP). For a demonstration we will encounter a crucial process at the LHC, the Drell-Yan process. The next-to-leading order (NLO) computations for slepton pair production at the LHC yield similar problems. Lastly, we will introduce some useful kinematic variables which are convenient for collider physics.

²A pedagogical introduction can be found in Refs. [2] and [5].

³For a detailed study see Ref. [7].

2.2.1 The Drell-Yan process

In 1970 Drell and Yan first developed a model for the production of a lepton pair with two initial state hadrons at high energies [8]. The associated Feynman diagram for this process is shown in Fig. 2.2. Here a quark and an antiquark of the hadrons annihilate into a virtual photon which “decays” into a lepton pair. In addition, we get an undefined hadronic state X in which we are not interested.

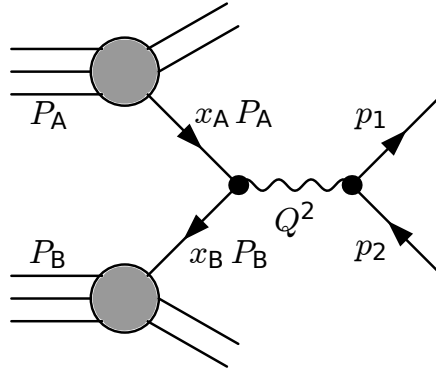


Figure 2.2: Feynman diagram for the Drell-Yan process: $pp \rightarrow l\bar{l} + X$, where X can be any hadronic state.

Due to the *factorization theorem* we can write the cross section for the Drell-Yan process as a convolution of the PDFs, which represent the soft contributions, and the hard partonic subprocess,

$$\sigma_{AB}^H = \sum_{a,b} \int_0^1 \int_0^1 dx_A dx_B f_{a/A}(x_A) f_{b/B}(x_B) \sigma_{ab}(x_A P_A, x_B P_B), \quad (2.53)$$

where $f_{a/A}$ and $f_{b/B}$ are the PDFs of the two initial state hadrons and the sum runs over all partons a, b in the hadrons, including the antipartons. Of course, for the first order computation (LO) only the PDFs of the quarks and their antiquarks lead to contributions. Here the PDFs describe the probability of finding a parton of type a (b) with a longitudinal momentum fraction x_A (x_B) of the hadron A (B), where a (b) denotes the different partons we will consider, i.e. u, d, c, s, g . For higher order processes, e.g. the real quark emission process $gq \rightarrow q\bar{q}q \rightarrow q + l\bar{l}$, it is necessary to use the PDFs for gluons g as well. We will study the PDFs in more detail in the next chapter.

The LO partonic process of the lepton pair production, with a photon as the mediator,

is relatively easy to compute and we get for the unpolarized and spin and color averaged cross section

$$\sigma_{ab} = \frac{1}{3} \frac{4\pi\alpha_{em}^2}{Q^2}, \quad (2.54)$$

where we have made the assumption of massless quarks and leptons. This is reasonable due to the large initial and final state energy of the particles compared to their mass. The squared momentum of the photon is referred to as Q^2 .⁴

Anyway, this result is not precise enough to fit with the experimental data. We need higher order corrections with respect to the strong coupling. Therefore we have to include the virtual diagrams of the quark self energy and the vertex correction.



Figure 2.3: Virtual corrections for the $\mathcal{O}(\alpha_s\alpha)$ contribution to the NLO Drell-Yan cross section, if it is interfered with the LO Feynman diagram. In addition, there would be a third diagram with the antiquark self energy.

As always we handle the appearing ultraviolet (UV) divergences with the method of *renormalization*. That means by a redefinition of our involving masses, fields and couplings we will get rid of them. For specific points in phase space we have to deal with additional divergences, the so called infrared divergences (IR) [10]. But how do we get rid of them? First of all it is important to know that we cannot distinguish between the virtual processes with two final state leptons and the real emission processes with an additional gluon in the final state, which is soft. We cannot detect a gluon with almost no energy. Therefore we have to add real corrections too, since they are of the same order in the perturbative series.

⁴The computation can be found in almost every textbook about particle physics, for example in Refs. [5] and [9].



Figure 2.4: Real correction contributions for the $\mathcal{O}(\alpha_s\alpha)$ contribution to the NLO Drell-Yan cross section. In addition, there is a u-channel for the quark emission and similar antiquark emission diagrams.

Due to the *Bloch-Nordsieck theorem* [11], which is actually for *Quantum Electrodynamics* (QED), the soft divergences will cancel each other. But in QCD we will encounter additional problems. Due to the massless quarks and gluons, which can emit a collinear massless particle, we will encounter also collinear (or mass) singularities. But the *Kinoshita-Lee-Nauenberg theorem* [12] states that also the collinear divergences cancel exactly if we sum over all initial and final degenerate states. The resulting observable is then called an *infrared safe* quantity. However it is not possible to sum over all degenerate states. The soft divergences can be handled at higher scales, because they are power suppressed if the scale is high enough. And due to the *factorization theorem* we can absorb our remaining soft and collinear divergences into the unphysical *bare* PDFs, which will then become scale dependent.

2.2.2 Parton distribution functions

First of all we want to maintain the “naive” parton model which we have used in Eq. (2.53) for LO predictions. We know that hadrons are deeply bound states of quarks. Due to the exchange of soft gluons, the coupling and hence the attractive force between the quarks is large. If the quarks emitted hard gluons, the “recoil” would break the hadron apart. With regard to *Heisenbergs Uncertainty Principle* the time scale for the interaction between the quarks and gluons inside the hadron is large with respect to the scattering of a hadron with e.g. an high energy electron, the *deep inelastic scattering* (DIS). Long before the virtual photon will interact with a parton, the partonic states are already prepared. So the photon “sees” in a good approximation a “frozen sea” of partons inside the hadron. With DIS we can measure the PDFs of a specific hadron [9]. Nevertheless we have to abandon this “naive” parton model, because from experiments of DIS we know that the PDFs depend on the energy scale of the exchanged photon. In

addition, we have still to handle the remaining divergences. Since we cannot calculate the hadronic or even the partonic cross section from first principles, the theory has only a predictive power by relating one cross section to the other.

NLO Drell-Yan process and corrections to PDFs

Now we want to show how a correction to the PDF will enter during a rather simple NLO computation for the Drell-Yan process. For simplification let us only assume real gluon emission and not in addition, the in principle more important, quark emission. Considering again massless quarks we get

$$(p_a - k)^2 = 2p_a \cdot k = p^0 k^0 (1 - \cos \theta) \quad (2.55)$$

in the denominator of our *Feynman amplitude* for such processes (Fig. 2.4 (left)). This is the reason for the already mentioned IR divergences at certain points in phase space, i.e. if the gluons are emitted soft ($k^0 \rightarrow 0$) or collinear ($\theta \rightarrow 0$).

To get a finite result we have to add the already UV renormalized virtual cross section contribution to the real emission part to get rid of some IR divergences. With the method of *dimensional regularization* (DR) [2, 5, 10] and *phase space slicing* the partonic cross sections read [9]

$$\begin{aligned} \frac{d\sigma^r}{dQ^2} &= \sigma_B \frac{\alpha_s}{\pi} C_F D(\epsilon) \left[\frac{2}{\epsilon^2} \delta(1-z) - \frac{2}{\epsilon} \left(\frac{(1+z)^2}{(1-z)^2} \right)_+ + \left(\frac{\ln(1-z)}{1-z} \right)_+ - 2 \frac{1+z^2}{1-z} \ln z \right] \\ &+ O(\epsilon), \end{aligned} \quad (2.56)$$

$$\frac{d\sigma^v}{dQ^2} = \sigma_B \frac{\alpha_s}{\pi} C_F D(\epsilon) \left[-\frac{2}{\epsilon^2} - \frac{3}{\epsilon} - 10 + \frac{2\pi^2}{3} \right] \delta(1-z) + O(\epsilon), \quad (2.57)$$

where z is the momentum fraction of the quark after emitting a gluon, C_F is a color factor and F_+ is a distribution similar to the δ -distribution which gives a finite result after an integration. The expression $D(\epsilon)$ is the usually appearing expansion term by solving the integrals with DR.

$$D(\epsilon) \approx 1 + \epsilon(\ln 4\pi - \gamma_E + \ln \frac{\mu_f^2}{Q^2}) \quad (2.58)$$

If we add Eqs. (2.56) and (2.57) the double poles $1/\epsilon^2$ cancel but we are still left with divergences. How do we get rid of them? Of course we cannot look at the hard process alone due to the confinement. We need to look at the whole hadronic process. Like in

the “naive” parton model it can be shown that the hard (finite) and the long distance (singular) part factorize to

$$d\sigma_{ab} = \int dz_1 dz_2 \phi_{ac}(z_1) d\bar{\sigma}_{cd}(z_1 z_2 s) \phi_{bd}(z_2), \quad (2.59)$$

where ϕ_{ac} (ϕ_{bd}) is similar to the PDF and is called *transition function* or *parton-in-parton distribution function*. It describes the probability of finding a quark inside a quark after a gluon emission. Afterward the quark has the momentum fraction z . The *bare* cross section is $d\sigma$ and the renormalized (finite) cross section is $d\bar{\sigma}$. The *parton-in-parton distribution functions* absorb the last divergences. We can now define a renormalized PDF:

$$\bar{f}(\eta) := \int_0^1 \int_0^1 dx dz f(x) \phi(z) \delta(\eta - xz) = \int_{\eta}^1 \frac{dz}{z} f\left(\frac{\eta}{z}\right) \phi(z) \quad (2.60)$$

$$:= f(\eta) \otimes \phi(z). \quad (2.61)$$

Therewith we can write the cross section in Eq. (2.53) in another way

$$d\sigma_{AB}^H(S) = \int d\eta_a d\eta_b \bar{f}_{c/A}(\eta_a) d\bar{\sigma}_{cd} \bar{f}_{d/B}(\eta_b) \quad (2.62)$$

which is equivalent. Here, $\eta_a, \eta_b \in [0,1]$ are defined as $\eta_a = x_a z_a$ and $\eta_b = x_b z_b$. With this approach we are now able to compute all order corrections to hadronic processes. But what does the *parton-in-parton distribution function* look like in our example? Or similarly, what is the correction of the partonic subprocess to the PDFs? Therefore let us look at the perturbative expansion series of the quantities $d\sigma$, $d\bar{\sigma}$ and ϕ :

$$d\bar{\sigma}(s) = \sum_{n=0}^{\infty} \left(\frac{\alpha_s}{2\pi}\right)^n d\bar{\sigma}^{(n)}(s), \quad (2.63)$$

$$d\sigma(s) = \sum_{n=0}^{\infty} \left(\frac{\alpha_s}{2\pi}\right)^n d\sigma^{(n)}(s), \quad (2.64)$$

$$\phi_{ik}(z) = \delta_{ik} \delta(1-z) + \sum_{n=1}^{\infty} \left(\frac{\alpha_s}{2\pi}\right)^n \phi_{ik}^{(n)}(z). \quad (2.65)$$

The δ -distribution takes into account that at LO no gluon is emitted by the quarks. Now we can write the expansion of the partonic cross section up to first order of perturbation

theory as

$$\begin{aligned} d\sigma_{ab}^0(s) + \frac{\alpha_s}{2\pi} d\sigma^{(1)}(s) = \\ d\bar{\sigma}_{ab}^0(s) + \frac{\alpha_s}{2\pi} \left[d\bar{\sigma}_{ab}^{(1)} + \int_0^1 dz_1 \phi_{ac}^{(1)}(z_1) d\bar{\sigma}_{cb}^{(0)}(z_1 s) + \int_0^1 dz_2 d\bar{\sigma}_{ac}^{(0)}(z_2 s) \phi_{cb}^{(1)}(z_2) \right]. \end{aligned} \quad (2.66)$$

We can see that the unrenormalized LO cross section is the same as the renormalized one, so our LO result is still valid. Let us collect the first order terms in Eq.(2.66) and solve for the renormalized finite NLO cross section.

$$d\bar{\sigma}_{ab}^{(1)}(s) = d\sigma_{ab}^{(1)} - \int_0^1 dz_1 \phi_{ac}^{(1)}(z_1) d\bar{\sigma}_{cb}^{(0)}(z_1 s) - \int_0^1 dz_2 d\bar{\sigma}_{ac}^{(0)}(z_2 s) \phi_{cb}^{(1)}(z_2) \quad (2.67)$$

To get the expression for the *parton-in-parton distribution function* we need the appearance of the divergences which are left in the sum of the real and virtual emission cross sections:

$$\frac{d\sigma^{(1)}}{dQ^2} = \frac{d\sigma^r}{dQ^2} + \frac{d\sigma^v}{dQ^2} = \sigma_B D(\epsilon) \left(-\frac{2}{\epsilon} P_{qq}(z) + R(z) \right), \quad (2.68)$$

where

$$P_{qq} = C_F \left[\left(\frac{(1+z)^2}{(1-z)} \right)_+ + \frac{3}{2} \delta(1-z) \right] \quad (2.69)$$

is one of the Altarelli-Parisi (AP) splitting functions which describe the breaking up of a quark into a gluon and a quark with the momentum fraction z and

$$R(z) = C_F \left[\delta(1-z) \left(\frac{2\pi^2}{3} - 8 \right) + 4(1+z^2) \left(\frac{\ln(1-z)}{1-z} \right)_+ - 2 \left(\frac{1+z^2}{1-z} \right) \ln z \right]. \quad (2.70)$$

Both functions P_{qq} and $R(z)$ are completely finite. Only the AP splitting function is multiplied by a pole $\sim 1/\epsilon$. Hence it is obvious what the *parton-in-parton distribution function* can look like:

$$\phi^{(1)}(z) = -\frac{1}{\epsilon} D(\epsilon) P_{qq}(z). \quad (2.71)$$

The function in Eq. (2.71) is scale and scheme dependent and so are the PDFs, because we can add some arbitrary constant terms which we can absorb. Therefore we need to take the same scheme for the experiments as for the theoretical predictions. E.g. we choose a *parton-in-parton distribution function* in a specific scheme and therewith we “measure” the PDFs with DIS. To make valid predictions we need to use the same *parton-in-parton distribution function* with the same scheme. This scale dependence leads to similar equations as the RGE, the DGLAP equations.

It is now easy to show that with those results our renormalized PDFs are dependent on an arbitrary scale μ_f . If we plug the *parton-in-parton distribution function* expansion stated in Eq. (2.65) into the definition of the renormalized PDF (2.61) we get

$$\bar{f}(\eta) = f_0(\eta) + \frac{\alpha_s}{2\pi} \int_{\eta}^1 \frac{dz}{z} f\left(\frac{\eta}{z}\right) \left(-\frac{1}{\epsilon} - \ln 4\pi + \gamma_E - \ln \frac{\mu_f^2}{Q^2}\right) P_{qq}(z) + \dots \quad (2.72)$$

$$:= f_0(\eta) + \frac{\alpha_s}{2\pi} \int_{\eta}^1 \frac{dz}{z} \bar{f}\left(\frac{\eta}{z}\right) \left(\ln \frac{\mu_f^2}{Q^2}\right) P_{qq}(z) + \dots \quad (2.73)$$

Here we have absorbed the divergent part and some constant quantities directly into the *bare*, not measurable distribution f . The scheme we have used is the common $\overline{\text{MS}}$ -scheme. If we take the derivative with respect to the arbitrary scale μ would get a part of the DGLAP equations.

Again we encounter a somehow arbitrary artificial parameter μ which has a rather similar origin as the renormalization scale μ_r . During the rest of the thesis we will set this scale to $\mu_f = \mu_r = \mu$ and we will only use renormalized quantities without a bar, unless we will mention otherwise. It is important that the PDFs are completely universal and independent of the hard process. They just get contributions from the general *parton-in-parton distribution function*.

DGLAP equations

If we had added the real quark emission process we would also get an evolution equation for the gluon PDF. All in all we get a $(2n_f + 1)$ dimensional matrix equation in the

space of the quarks, gluons and antiquarks.

$$\frac{\partial}{\partial \ln \mu^2} \begin{pmatrix} q_i(x, \mu) \\ g(x, \mu) \end{pmatrix} = \frac{\alpha_s(\mu)}{2\pi} \int_x^1 \frac{dz}{z} \sum_{q_j, \bar{q}_j} \begin{pmatrix} P_{q_i, q_j}(\frac{x}{z}, \alpha_s(\mu)) & P_{q_i, g}(\frac{x}{z}, \alpha_s(\mu)) \\ P_{g, q_j}(\frac{x}{z}, \alpha_s(\mu)) & P_{g, g}(\frac{x}{z}, \alpha_s(\mu)) \end{pmatrix} \begin{pmatrix} q_j(x, \mu) \\ g(x, \mu) \end{pmatrix}. \quad (2.74)$$

The α_s dependence of the AP splitting functions is due to the fact that they are again calculable as a series expansion in α_s , similar as for the *parton-in-parton distribution function*, where trivially the lowest order is independent.

It is relatively easy to derive the DGLAP equation. This is done in a similar fashion as for the RGE. One demands that the physical hadronic Drell-Yan cross section does not depend on an arbitrary scale. Although the partonic cross section and the PDFs will be scale dependent, these dependencies compensate each other. But up to a certain fixed order of perturbation theory the Drell-Yan cross section is indeed scale dependent.

The LO AP splitting functions $P_{ab}^{(0)}(x)$ have an interpretation as the probabilities of finding a type a parton in a parton of type b with the longitudinal momentum fraction x of the mother parton. In LO we have seen that it is exactly the same as the *parton-in-parton distribution function* except the absorbed pole. The transverse momentum it gains is much less than μ^2 [7]. For resummation and for the whole perturbative QCD the DGLAP is essential. Therewith we can evolve the PDF to a different scale for our processes after it has been measured at a certain scale. It assures the predictive power of the theory. The necessary lowest order independent AP splitting functions are [13]:

$$P_{q_i q_j}^{(0)}(z) = \delta_{ij} \frac{8}{3} \left[\left(\frac{1+z^2}{(1-z)} \right)_+ + \frac{3}{2} \delta(1-z) \right], \quad (2.75)$$

$$P_{qg}^{(0)}(z) = \frac{1}{2} (z^2 + (1-z)^2), \quad (2.76)$$

$$P_{gq}^{(0)}(z) = \frac{8}{3} \left[\frac{1+(1-z^2)}{z} \right], \quad (2.77)$$

$$P_{gg}^{(0)}(z) = 12 \left[\left(\frac{z}{(1-z)} \right)_+ + \frac{1-z}{z} + z(1-z) \right] + \delta(1-z) \left(\frac{44}{9} - \frac{2}{3} N_f \right). \quad (2.78)$$

Here N_f is the number of different flavors. Beyond LO, the functions are completely non-trivial and have a complicated flavor structure.

Now we know all the tools to compute higher order corrections to hadronic processes and how to get rid of all the divergences. For a full NLO Drell-Yan computation we also have to take the real quark emissions into account. Then the *parton-in-parton*

distribution function, respectively the PDF evolution, will change to absorb also those divergences. To get the results for the real correction to the DY process the method of *Phase Space Slicing* is widely used for analytical results and has also been used to gain our results. For a numerical approach it is more practical to use another approach to get finite results. This is the so called *dipole subtraction* method. We will explain the method briefly in the chapter about slepton pair production.

In Fig. 2.5 we can see a measurement of a PDF at NLO with the *parton-in-parton distribution functions* defined in the $\overline{\text{MS}}$ -scheme. We will use the same PDFs in the numerical analysis part to make predictions for slepton pair production at the LHC.

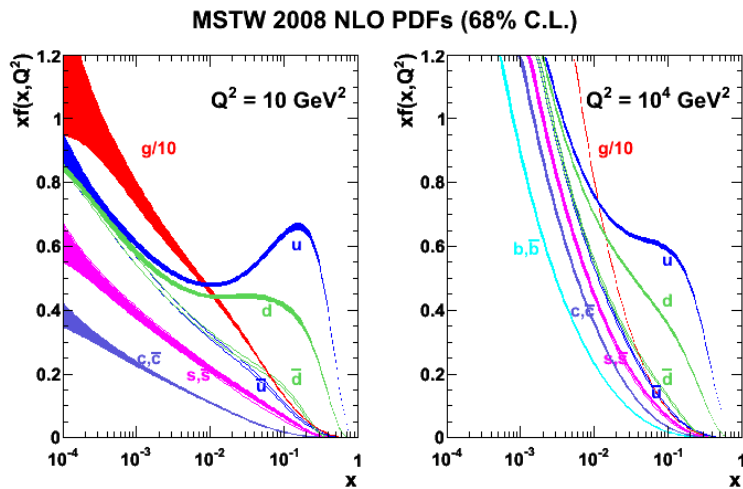


Figure 2.5: Parton Distribution Function (PDF) for a proton at two different energy scales obtained by the MSTW collaboration in 2008 at NLO accuracy with a confidence level $\text{CL} = 68\%$. From Ref. [14].

It can be seen that the distributions are indeed scale dependent. For larger momentum transfers we can resolve more constituents of the hadron and the particle number distribution for small x is larger.

Now we can proceed and write the hadronic and partonic cross sections in some more adjusted variables for collider experiments.

2.2.3 Collider kinematics and important distributions

For collider physics it is common to introduce a useful set of variables which transforms properly under longitudinal boosts. Therefore we choose the \vec{e}_z direction to be the pp collision axis. For the usual coordinates (E, p_x, p_y, p_z) only p_x and p_y are invariant under

a Lorentz boost along the z-axis due to the fact that they are normal to the boost axis. In addition, we do not know the longitudinal momentum of the initial state partons and a measurement of the final velocity along the beam axis would be useless.

Therefore it is common to use projections of the variables into the transverse plane and additional quantities which are invariant under a boost along the z-axis or transform easily.

The transverse momentum

The *transverse momentum* \vec{p}_T is a two component vector in the plane perpendicular to the collision axis. Its absolute value and the transformation formulas are given by

$$p_x = p_T \cos \phi, \quad p_y = p_T \sin \phi, \quad p_T^2 = p_x^2 + p_y^2. \quad (2.79)$$

Trivially it is invariant under a boost along \vec{e}_z and it has another promising feature: Since we assume the partons carry only a longitudinal fraction of the hadron momentum, the \vec{p}_T sum of the final state partons must be zero.

$$\sum_i^N \vec{p}_{T,i} = \vec{0} \quad (2.80)$$

In the rest of the thesis this variable and its properties will be crucial. E.g we can reconstruct the p_T of some undetectable particle like a neutrino, or in the supersymmetric case neutralino and sneutrino.

The rapidity

A quantity which is not invariant under Lorentz boosts but transforms properly is the *rapidity*. It depends on the scattering angle θ , which is the angle between the scattered particle and the beam axis, and the velocity $\vec{\beta} = \vec{p}/E$ and is defined as

$$y := \frac{1}{2} \ln \frac{E + p_z}{E - p_z} = \frac{1}{2} \ln \frac{1 + \beta \cos \theta}{1 - \beta \cos \theta}, \quad (2.81)$$

or equivalently

$$\beta \cos \theta = \tanh y. \quad (2.82)$$

The advantage of this kinematic variable is that it changes under a Lorentz boost along the z-axis only by an additive constant.

For approximately massless particles it is also useful to define the *pseudo-rapidity* η . If $m \ll p_T$, then $\beta \rightarrow 1$ and the *pseudo-rapidity* reads

$$\eta := \frac{1}{2} \frac{1 + \cos \theta}{1 - \cos \theta} = -\ln \tan \left(\frac{\theta}{2} \right), \quad (2.83)$$

With this approximation we get an advantage. Previously we needed two detector types to determine the rapidity of a particle. One for the energy E and another one for the momentum. In the case of *pseudo rapidity* we just need one detector [15].

With the relation $q^2 = (p_a + p_b)^2 = (x_a P_A + x_b P_B)^2 = x_a x_b S$, where \sqrt{S} is the hadronic center of mass (COM) energy, we can write transformations

$$x_a = \sqrt{\frac{q^2}{S}} e^y \quad \text{and} \quad x_b = \sqrt{\frac{q^2}{S}} e^{-y} \quad (2.84)$$

which yield for the Jacobian to change the variables

$$\frac{\partial(q^2, y)}{\partial(x_a, x_b)} = S = \frac{q^2}{x_a x_b}. \quad (2.85)$$

Therewith we can rewrite the LO hadronic cross section for the Drell Yan process (Eq. (2.53)). This reflects more the kinematic observables than the integration over the partonic momentum fractions.

The transverse energy

In addition, one can define the *transverse energy* E_T as the energy in the rest frame of the particle where its momentum in the z-direction equals zero.

$$E_T^2 := p_x^2 + p_y^2 + m^2 = p_T^2 + m^2 = E^2 - p_z^2 \quad (2.86)$$

It is again an often used quantity for collider experiments. Using Eq. (2.81) we can rewrite the *transverse energy* as

$$E = E_T \cosh y. \quad (2.87)$$

For approximately massless particles it is the same as p_T .

The invariant mass

Another widely used quantity, which is by definition invariant under Lorentz transformations, is the *invariant mass* of two final state particles. It is defined as

$$M^2 = (p_1 + p_2)^2. \quad (2.88)$$

In the COM frame and at LO this will yield

$$M^2 = q^2 = s = x_a x_b 2E^2 =: x_a x_b S, \quad (2.89)$$

where $x_{a,b}$ is the momentum fraction of the hadron with momentum $P_{A,B}$.

For a $2 \rightarrow 3$ process the invariant mass of the initial and final states are not the same. Their fraction is denoted as $z = M^2/s$ and will become important in the next chapter.

For a more detailed discussion and further definitions of other useful kinematic variables with respect to LHC physics a good reference would be Ref. [\[15\]](#) or [\[16\]](#).

3 Resummation

In Ch. 2.2 we have given the real gluon emission and virtual correction part to the Drell-Yan cross section. Except the missing real quark emission this is the full inclusive NLO result. As we can see in Eq. (2.70) the NLO cross section has a part which is proportional to

$$\alpha_s(\mu^2) \left[\frac{\ln(1-z)}{1-z} \right]_+, \quad (3.1)$$

remaining after the cancellation of the IR divergences of the virtual and real corrections. We will get the following terms at each order of the perturbative series:

$$\alpha_s(\mu^2)^n \left[\frac{\ln^m(1-z)}{1-z} \right]_+, \quad m \leq 2n - 1, \quad (3.2)$$

where n is the order of the computation $\mathcal{O}(\alpha_s^n)$. The contributions become very large in the limit $z \rightarrow 1$ and spoil the convergence. The limit corresponds to the phase space regions where soft and collinear partons have been emitted. The factors in Eq. (3.2) become larger and larger at each term of the perturbative series spoiling the validity of a fixed order computation. To assure the predictive power we have to sum these contributions up to all orders in certain phase space regions. This is done in the context of resummation.

In this chapter we explain the philosophy of resummation and its applications. It is a very technical procedure, makes use of different theorems and is deeply based on *factorization* [7]. It can be shown that the regions of the large logarithms completely factorize to the LO cross section times an exponential factor, the so called *Sudakov form factor*. Firstly, we will show the *factorization* in a simple example of an infinite emission of soft photons. Afterward, we will discuss and explain the formulas which are necessary to apply resummation to slepton pair production.

Since the whole theoretical background of resummation is rather complicated, the reader is referred to special literature for a more detailed point of view. We recommend Refs.

[17] and [18] for a more pedagogical introduction and Ref. [19] for a more detailed study including *factorization*. The whole chapter is based on Ref. [1].

3.1 The basic ideas behind resummation

Before starting with the special types of resummation let us think about the general ideas behind it and its philosophy. We have already seen that *factorization* is an essential theorem to do perturbative QCD. Let us think about a general physical quantity $R(M^2, m^2)$. This quantity is IR sensitive and the scale m^2 measures the distance to the critical point. Here M^2 could be e.g the transferred momentum of the reaction. In the limit where $m^2 \ll M^2$ it can be shown that we can write the quantity R in a factorized form

$$R(M^2, m^2) = H(M^2/\mu^2)S(m^2/\mu^2). \quad (3.3)$$

This procedure can be highly non trivial and has to be proven before using the application of resummation. To achieve *factorization* we had to introduce potentially large ratios of the scales which depend on the arbitrary value of μ . It is important to mention that the *factorization* often does not hold in the original momentum space, but in a “conjugate space”. This is well known for the common convolution which factorizes in the Mellin space.

Since we know that a physical quantity must be independent of an arbitrary and artificial scale parameter, we can derive evolution equations for H and S :

$$\frac{1}{H} \frac{d \ln H}{d \ln \mu^2} = - \frac{1}{S} \frac{d \ln S}{d \ln \mu^2} := \gamma_S(\mu^2). \quad (3.4)$$

In a similar way, using the same main condition, the RGE can be derived. Like for the running coupling α_s we get a coefficient function here denoted by γ_S , the so called anomalous dimension. Solving Eq. (3.4) for the soft function S yields

$$S(m^2/\mu^2) = S(1) \exp \left[- \int_{m^2}^{\mu^2} \frac{dq^2}{q^2} \gamma_S(q^2) \right] \quad (3.5)$$

and therewith we can rewrite Eq. (3.3) as

$$R(M^2, m^2) = H(1)S(1) \exp \left[- \int_{m^2}^{M^2} \frac{dq^2}{q^2} \gamma_S(q^2) \right], \quad (3.6)$$

where we have set $\mu = M$. The whole dependence on the two scales is now represented by the exponent, the so called *Sudakov form factor*. The coefficient functions S and H are now completely IR safe, finite and computable with perturbation theory. The anomalous dimension γ_S can be expressed in a power series of the strong coupling α_s and can therefore be computed perturbatively.

3.2 Soft photon resummation

In this section we show a simple example of resummation used in an arbitrary emission of soft photons which has been done e.g. by Weinberg [17] and summarized by Peskin [5]. Let us consider a process of n emitted photons by an initial fermion line before taking part in an arbitrary hard process $i\mathcal{M}_0(p_i) = A_0(p_i)u_i$. After n soft photon emissions by the particle i the corresponding matrix element is

$$\begin{aligned} i\mathcal{M} &= \mathcal{A}_0(p_i) \frac{i\not{p}_i + m}{2(p_i \cdot k_1)} (-ie\gamma^{\mu_1}) \epsilon_{\mu_1} \frac{i\not{p}_i + m}{2(p_i \cdot (k_1 - k_2))} (-ie\gamma^{\mu_2}) \epsilon_{\mu_2} \\ &\cdots \frac{i\not{p}_i + m}{2(p_i \cdot (k_1 - k_2 \cdots - k_n))} (-ie\gamma^{\mu_n}) \epsilon_{\mu_n} u_i, \end{aligned} \quad (3.7)$$

where k_r ($r \in \{1, 2, 3, \dots, n\}$) represents the four momentum of the photons. Because of the soft emissions we have already neglected k_r in the numerator and terms of $\mathcal{O}(k_r^2)$ in the denominator. We can easily show, using the Dirac algebra in Eq. (B.1) and the Dirac equation, that the matrix element factorizes to

$$\begin{aligned} i\mathcal{M} &= i\mathcal{M}_0(p_i) e^n \frac{p_i^{\mu_1}}{(p_i \cdot k_1)} \epsilon_{\mu_1} \frac{p_i^{\mu_2}}{(p_i \cdot (k_1 - k_2))} \epsilon_{\mu_2} \\ &\cdots \frac{p_i^{\mu_n}}{(p_i \cdot (k_1 - k_2 \cdots - k_n))} \epsilon_{\mu_n}. \end{aligned} \quad (3.8)$$

Summing over all $n!$ different permutations of n photon emissions yields [5]

$$i\mathcal{M} = i\mathcal{M}_0(p_i) e^n \frac{p_i^{\mu_1}}{(p_i \cdot k_1)} \epsilon_{\mu_1} \frac{p_i^{\mu_2}}{(p_i \cdot k_2)} \epsilon_{\mu_2} \cdots \frac{p_i^{\mu_n}}{(p_i \cdot k_n)} \epsilon_{\mu_n}. \quad (3.9)$$

Since we know that only one of the processes will be realized we have to divide Eq. (3.9) by $n!$ leading to

$$i\mathcal{M} = i\mathcal{M}_0(p_i) \frac{e^n}{n!} \sum_{i=1}^l \prod_{r=1}^n \eta_i \frac{p_i \cdot \epsilon_r}{p_i \cdot k_r}, \quad (3.10)$$

where we have generalized our result for different external fermion lines with a factor $\eta_i = \pm 1$, taking into account if the photon is emitted by a particle or antiparticle.

Before proceeding, let us look at the differential cross section for the emission of one soft photon. Due to the soft approximation the phase space factorizes, too. After summing over all photon polarizations and using the completeness relation the differential cross section is

$$\left(\frac{d\sigma}{d\Omega}\right)_{1\gamma} = \left(\frac{d\sigma_0}{d\Omega}\right) \int_{|\vec{k}| \leq \Delta E} \frac{d^3k}{(2\pi)^3 2E} e^2 \left(\frac{-p_a^2}{p_a \cdot k} + \frac{-p_b^2}{p_b \cdot k} + \frac{2p_a \cdot p_b}{(p_a \cdot k)(p_b \cdot k)} \right) =: \left(\frac{d\sigma_0}{d\Omega}\right) Y, \quad (3.11)$$

where the photon is emitted by either particle a or b . The upper integration limit is ΔE being e.g. the detector resolution. If we consider an amount of n photon emissions we will get n of such factors where we have to divide by all of the permutations, i.e. $n!$. Finally, we get for any number of soft emitted photons

$$\left(\frac{d\sigma}{d\Omega}\right) = \left(\frac{d\sigma_0}{d\Omega}\right) \sum_{n=0}^{\infty} \frac{Y^n}{n!} = \left(\frac{d\sigma_0}{d\Omega}\right) \exp(Y). \quad (3.12)$$

The exponent Y is IR divergent which can easily be seen from the integral in Eq. (3.11). For the compensation we have to include all the virtual corrections up to all orders. In the soft limit it has been shown that we also get a factorized structure [17]. Altogether the differential cross section is

$$\left(\frac{d\sigma}{d\Omega}\right) = \left(\frac{d\sigma_0}{d\Omega}\right) \exp(Y + 2X), \quad (3.13)$$

where $2X$ represents the n loop corrections in the soft limit. The exponent represents the finite probability for the emission of a single soft photon. The whole cross section does not depend on an infrared cut-off scale μ due to the cancellation of the virtual and real scale dependent contributions. The *Sudakov form factor* in the exponential includes all the potentially large logarithms remaining after the IR cancellation. The leading contribution is governed by the famous large double logarithms.

It is worth to mention that this resummation formalism does not hold in the massless approximation of QED due to additional collinear divergences. The generalization for QCD is much more complicated and has been done in Ref. [18]. To get the exponentiation one has to show that the gluon correlation cancels out order by order in perturbation theory. The generalization for QCD has been done in Ref. [18]. In QCD this is also referred to as the *eikonal approximation* and the exponential function is called the *eikonal function*.

3.3 Threshold resummation

In the context of threshold resummation we sum potentially large logarithms in the limit $z := M^2/s \rightarrow 1$, where z is the fraction of the invariant mass of the vector boson and the invariant mass of the two initial state partons before emitting a gluon.

The terms

$$\alpha_s^n \left(\frac{\ln^m(1-z)}{(1-z)} \right)_+ \quad (3.14)$$

are resummed in that formalism to get reasonable results near the threshold $z \rightarrow 1$. Here $m \leq 2n - 1$. We have already seen such terms in Ch. 2.2 in Eq. (2.70).

Let us recall the hadronic cross section of the Drell-Yan process which we can write in a double differential form [7]

$$M^2 \frac{d^2\sigma_{AB}}{dM^2 dp_T^2} \left(\tau = \frac{M^2}{S} \right) = \sum_{ab} \int_0^1 \int_0^1 dx_a dx_b x_a f_{a/A}(x_a, \mu^2) x_b f_{b/B}(x_b, \mu^2) \times z \hat{\sigma}_{ab}(z, M^2, M^2/p_T^2, M^2/\mu^2) \delta(\tau - x_a x_b z), \quad (3.15)$$

where \sqrt{S} is the hadronic COM energy, $f_{a/A}$ and $f_{b/B}$ are the PDFs of the two hadrons A and B , p_T the transverse momentum of the two final state uncolored particles and τ and z are momentum ratios. As we have seen in Ch. 2.2 the partonic cross section $\hat{\sigma}_{ab}$ can be computed as a series expansion in α_s . We can rewrite the convolution in Eq. (3.15) using the Mellin transform

$$\tilde{F}(N) := \int_0^1 dx x^{N-1} F(x) \quad (3.16)$$

as an ordinary product in Mellin space

$$M^2 \frac{d^2 \sigma_{AB}}{dM^2 dp_T^2}(N-1) = \sum_{ab} f_{a/A}(N, \mu^2) f_{b/B}(N, \mu^2) \times \hat{\sigma}_{ab}(N, M^2, M^2/p_T^2, M^2/\mu^2), \quad (3.17)$$

where we have transformed x_a , x_b and z into their Mellin moments. The Mellin transformed functions are indicated only by the change of the argument to their Mellin moments N . We already know that the partonic cross section σ_{ab} can be divergent. Therefore, we will factorize the cross section into the *parton-in-parton distribution functions* and a renormalized finite cross section:

$$M^2 \frac{d^2 \sigma_{ab}}{dM^2 dp_T^2}(N-1) = \sum_{cd} \phi_{c/a}(N, \mu^2) \phi_{d/b}(N, \mu^2) \times \hat{\sigma}_{cd}(N, M^2, M^2/p_T^2, M^2/\mu^2). \quad (3.18)$$

Demanding a factorization and renormalization scale independent hadronic cross section we can derive the DGLAP evolution equation

$$\frac{\partial \phi_{c/a}(N, \mu^2)}{\partial \ln \mu^2} = \sum_b P_{cb}(N, \alpha_s(\mu^2)) \phi_{b/a}(N, \mu^2) \quad (3.19)$$

for the *parton-in-parton distribution functions*. We recall that we can compute the AP splitting functions as a perturbative series. In LO they are given by

$$P_{qq}^{(1)}(N) = C_F \left[\frac{3}{2} + \frac{1}{N(N+1)} - 2 \sum_{k=1}^N \right], \quad (3.20)$$

$$P_{qg}^{(1)}(N) = \frac{1}{2} \left[\frac{2+N+N^2}{N(N+1)(N+2)} \right], \quad (3.21)$$

$$P_{gq}^{(1)}(N) = C_f \left[\frac{2+N+N^2}{N(N^2-1)} \right], \quad (3.22)$$

$$P_{gg}^{(1)}(N) = \beta_0 + 2C_A \left[\frac{1}{N(N-1)} + \frac{1}{(N+1)(N+2)} - \sum_{k=1}^N \right] \quad (3.23)$$

in Mellin space. With the introduction of the so called QCD *evolution operator* $E_{ab}(N, \alpha_s(\mu^2, \mu_0^2))$ defined by

$$\frac{\partial E_{ab}(N, \alpha_s(\mu^2, \mu_0^2))}{\partial \ln \mu^2} = \sum_b P_{cb}(N, \alpha_s(\mu^2)) E_{ab}(N, \alpha_s(\mu^2, \mu_0^2)), \quad (3.24)$$

we can write the solution of the AP Eq. (3.19) as

$$\phi_{c/a}(N, \mu^2) = \sum_b E_{cb}(N, \mu^2, \mu_0^2) \phi_{b/a}(N, \mu_0^2). \quad (3.25)$$

The *evolution operator* can be quite complicated depending on the order of the AP splitting functions. In LO the operator can be written in a closed exponential form. Our renormalized partonic cross section contains potentially large logarithms transforming in Mellin space to

$$\left(\frac{\ln^m(1-z)}{(1-z)} \right)_+ \rightarrow \ln^{m+1} N + \dots \quad (3.26)$$

Near the threshold ($N \rightarrow \infty$) only the LO term will be important and the off-diagonal AP splitting functions are suppressed

$$P_{qq}^{(1)}(N) = C_F \left[\frac{3}{2} - 2 \ln \bar{N} \right] + \mathcal{O} \left(\frac{1}{\bar{N}} \right), \quad (3.27)$$

$$P_{qg}^{(1)}(N) \sim \frac{1}{2N}, \quad (3.28)$$

$$P_{gq}^{(1)}(N) \sim \frac{C_F}{N}, \quad (3.29)$$

$$P_{gg}^{(1)}(N) = \beta_0 - 2C_A \ln \bar{N} + \mathcal{O} \left(\frac{1}{\bar{N}} \right) \quad (3.30)$$

and lead to a simplified evolution equation. Here we have defined $\bar{N} = N \exp(\gamma_E)$, with γ_E being the Euler's constant. The double differential cross section in Eq. (3.18) can be safely integrated over the transverse momentum which yields

$$M^2 \frac{d\sigma_{ab}}{dM^2}(N-1) = \phi_{a/a}(N, \mu^2) \phi_{b/b}(N, \mu^2) \times \hat{\sigma}_{ab}(N, M^2, M^2/\mu^2) + \mathcal{O} \left(\frac{1}{\bar{N}} \right), \quad (3.31)$$

where we have neglected the parton mixing contributions, so that for the Drell-Yan process only the quark and antiquark initial states are important. Our partonic cross

section is completely finite but leads to large logarithms near the threshold. Therefore, we refactorize our expression in a hard IR safe part and a soft part, which contains the potentially large logarithms. It has been shown by Sterman et al. that we can achieve a factorized form [7]

$$M^2 \frac{d\sigma_{ab}}{dM^2}(N-1) = \psi_{a/a}(N, M^2) \psi_{b/b}(N, M^2) \times H_{ab}(M^2, M^2/\mu^2) S_{ab}(N, M^2/\mu^2) + \mathcal{O}\left(\frac{1}{N}\right). \quad (3.32)$$

The hard function H can be safely computed in a perturbative expansion

$$H_{ab}(M^2, M^2/\mu^2) = \sum_{n=0}^{\infty} (\alpha_s(\mu^2))^n H_{ab}^{(n)}(M^2, M^2/\mu^2). \quad (3.33)$$

The new *parton-in-parton distribution functions* are now defined with respect to a certain fraction of energy instead of a longitudinal momentum fraction. They do not depend on the arbitrary scale μ and obey the evolution equations

$$\frac{\partial \psi_{a/a}(N, M^2)}{\partial \ln M^2} = \gamma_a(\alpha_s(M^2)) \psi_{a/a}(N, M^2). \quad (3.34)$$

Here $\gamma_a(\alpha_s)$ is the already mentioned anomalous dimension, which can be computed perturbatively,

$$\gamma_a(\alpha_s) = \frac{1}{Z_a} \frac{\partial Z_a}{\partial \ln \mu^2} = \sum_n \alpha_s^n \gamma^{(n)} \quad (3.35)$$

and corresponds to the N-independent virtual AP splitting functions in the axial gauge. The function S refers to the emission of soft gluons with a large angle with respect to the parent parton. We can solve for $\hat{\sigma}_{ab}$ using Eqs. (3.31) and (3.32):

$$\hat{\sigma}_{ab}(N, M^2, M^2/\mu^2) = H_{ab}(M^2, M^2/\mu^2) \frac{\psi_{a/a}(N, M^2) \psi_{b/b}(N, M^2)}{\phi_{a/a}(N, \mu^2) \phi_{b/b}(N, \mu^2)} S_{ab}(N, M^2/\mu^2) + \mathcal{O}\left(\frac{1}{N}\right) \dots \quad (3.36)$$

We have achieved a *factorization* where all the divergences are absorbed in the *parton-in-parton distribution functions* and the potentially large logarithms are embedded in the soft function S .

The procedure of exponentiating S is rather complicated. First we have to solve the

evolution equations for $\phi_{a/a}$ and $\psi_{a/a}$, which can be done in the region of the threshold. In addition, we have to make use of the gauge invariance and the RGE. Afterward, we can exponentiate the *eikonal function* and we get

$$\hat{\sigma}_{ab}(N, M^2, M^2/\mu^2) = H_{ab}(M^2, M^2/\mu^2) \exp(G_{ab}(N, M^2, M^2/\mu^2)) + \mathcal{O}\left(\frac{1}{N}\right). \quad (3.37)$$

The G function contains finite parts and the large logarithms. It is defined as

$$G_{ab}(N, M^2, M^2/\mu^2) = \ln \Delta_a(N, M^2, M^2/\mu^2) + \ln \Delta_b(N, M^2, M^2/\mu^2) + \ln \Delta_{ab}^{(s)}(N, M^2), \quad (3.38)$$

where

$$\ln \Delta_a(N, M^2, M^2/\mu^2) = \int_0^1 dz \frac{n^{N-1} - 1}{1-z} \int_{\mu^2}^{(1-z)^2 M^2} \frac{dq^2}{q^2} A_a(\alpha_s(q^2)), \quad (3.39)$$

$$\ln \Delta_{ab}^{(s)}(N, M^2) = \int_0^1 dz \frac{n^{N-1} - 1}{1-z} D_{ab}(\alpha_s((1-z)^2 M^2)). \quad (3.40)$$

Function A contains the collinear and soft gluon emission processes of the initial state particles and can be computed perturbatively leading to quadratic logarithms in the highest power. The function in Eq. (3.37) is similar to the function Y in Eq. (3.12) of soft photon resummation. D_{ab} contains the large-angle soft-gluon contributions leading to a single logarithm and being computable with perturbative QCD.

After the integration of the logarithmic functions and a redefinition of the hard function H , we can write the final solution for the threshold resummation as

$$\hat{\sigma}_{ab}(N, M^2, M^2/\mu^2) = \mathcal{H}_{ab}(M^2, M^2/\mu^2) \exp(\mathcal{G}_{ab}(N, M^2, M^2/\mu^2)) + \mathcal{O}\left(\frac{1}{N}\right). \quad (3.41)$$

Now the hard function contains all the finite pieces and, because of the redefinition, we have absorbed the non logarithmic terms.

$$\mathcal{H}_{ab}^{(0)}(M^2, M^2/\mu^2) = H_{ab}^{(0)}(M^2, M^2/\mu^2) \quad (3.42)$$

$$\mathcal{H}_{ab}^{(1)}(M^2, M^2/\mu^2) = H_{ab}^{(1)}(M^2, M^2/\mu^2) + \frac{\pi^2}{6} (A_a^{(1)} + A_b^{(1)}) H_{ab}^{(0)}(M^2) \quad (3.43)$$

The function in the exponent contains only the potentially large logarithmic terms and takes the form

$$\mathcal{G}_{ab} = Lg_{ab}^{(1)}(\lambda) + g_{ab}^{(2)}(\lambda, M^2/\mu^2) + \alpha_s g_{ab}^{(3)}(\lambda, M^2/\mu^2) + \dots, \quad (3.44)$$

where $\lambda = \alpha_s \beta_0 L$ and $L = \ln \bar{N}$. The first order term collects the leading logarithms (LL) and depends only on $A_a^{(1)}$, the second term is the next-to-leading logarithm (NLL) contribution and contains the three functions $A_a^{(1)}$, $A_a^{(2)}$ and $D_{ab}^{(1)}$. Higher order logarithmic terms are governed by $g^{(i)}$.

To use this formula up to NLL accuracy we have to specify our functions A and D :

$$\begin{aligned} 2\lambda\beta_0 g_{ab}^{(1)}(\lambda) &= (A_a^{(1)} + A_b^{(1)})[2\lambda + (1 - 2\lambda) \ln(1 - 2\lambda)], \\ 2\lambda\beta_0 g_{ab}^{(2)}(\lambda, M^2/\mu^2) &= (A_a^{(1)} + A_b^{(1)}) \ln(1 - 2\lambda) \ln \frac{M^2}{\mu^2} \\ &\quad + (A_a^{(1)} + A_b^{(1)}) \frac{\beta_1}{\beta_0^2} [2\lambda + \ln(1 - 2\lambda) + \frac{1}{2} \ln^2(1 - 2\lambda)] \\ &\quad - (A_a^{(2)} + A_b^{(2)}) \frac{1}{\beta_0} [2\lambda + \ln(1 - 2\lambda)] \\ &\quad + (B_a^{(1)} + B_b^{(1)} + D_{ab}^{(1)}) \ln(1 - 2\lambda). \end{aligned} \quad (3.45)$$

The coefficients are

$$\begin{aligned} A_a^{(1)} &= 2C_a, \\ A_a^{(2)} &= 2C_a \left[\left(\frac{67}{18} - \frac{\pi^2}{6} \right) C_A - \frac{5}{9} n_f \right], \\ D_{ab}^{(1)} &= 0, \end{aligned} \quad (3.47)$$

where C_a is $C_q = C_F$ and $C_g = C_A$ representing the common color factors.

Comparing our partonic cross section with the hard function \mathcal{H}_{ab} we get the relations

$$\mathcal{H}_{ab}^{(0)}(M^2, M^2/\mu^2) = \hat{\sigma}_{ab}^{(0)}(M^2, M^2/\mu^2), \quad (3.48)$$

$$\begin{aligned} \mathcal{H}_{ab}^{(1)}(M^2, M^2/\mu^2) &= \hat{\sigma}_{ab}^{(0)}(M^2, M^2/\mu^2) \\ &\quad \times \left[\mathcal{A}_0 + (\delta P_{aa}^{(1)} + \delta P_{bb}^{(1)}) \ln \frac{M^2}{\mu^2} + \frac{\pi^2}{6} (A_a^{(1)} + A_b^{(1)}) \right]. \end{aligned} \quad (3.49)$$

The coefficient \mathcal{A}_0 represents the IR finite part of the renormalized virtual cross section

$$\mathcal{M}^{(1)}\mathcal{M}^{(0)*} + c.c. = \alpha_s \left(\frac{4\pi\mu^2}{M^2} \right)^\epsilon \frac{\Gamma(1-\epsilon)}{\Gamma(1-2\epsilon)} \left(\frac{\mathcal{A}_{-2}}{\epsilon^2} + \frac{\mathcal{A}_{-1}}{\epsilon} + \mathcal{A}_0 \right) |\mathcal{M}^{(0)}|^2 + \mathcal{O}(\epsilon). \quad (3.50)$$

The one-loop amplitude of the $2 \rightarrow 2$ process is denoted as $\mathcal{M}^{(1)}$ and $\mathcal{M}^{(0)}$ is the Born matrix element. To get the renormalized cross section the $\overline{\text{MS}}$ -scheme has been used. The term $\delta P_{aa}^{(1)}$ is the coefficient of the $\delta(1-x)$ part in the AP splitting function $P_{aa}^{(1)}$. These formulas can easily be implemented in a program code but before we have to match the resummed cross section, which is only valid in the soft limit, with our fixed order computations only being valid far from the threshold. This is accounted by

$$\hat{\sigma}_{ab} = \hat{\sigma}_{ab}^{(res)} + \hat{\sigma}_{ab}^{(f.o)} - \hat{\sigma}_{ab}^{(exp)}, \quad (3.51)$$

where $\hat{\sigma}_{ab}^{(exp)}$ represents the overlap of the two contributions. We can obtain the overlap by expanding the resummed cross section up to the same order as the perturbative result:

$$\begin{aligned} \hat{\sigma}^{(exp)}(N, M^2, M^2/\mu^2) &= \tilde{H}_{ab}^{(0)}(M^2, M^2/\mu^2) + \alpha_s \tilde{H}_{ab}^{(1)} - \alpha_s \left(2L - \ln \frac{M^2}{\mu^2} \right) \\ &\quad \sum_c \left[\tilde{H}_{ac}^{(0)}(M^2, M^2/\mu^2) P_{cb}^{(1)}(N) + \tilde{H}_{cb}^{(0)}(M^2, M^2/\mu^2) P_{ca}^{(1)}(N) \right] \\ &\quad - \alpha_s \tilde{H}_{ab}^{(0)}(M^2, M^2/\mu^2) \left[L^2(A_a^{(1)} + A_b^{(1)}) + L(B_a^{(1)} + B_b^{(1)}) \right]. \end{aligned} \quad (3.52)$$

To get the result in the ordinary space we have to do the inverse Mellin transform potentially leading to some complications. For further reading we recommend Refs. [1] and [20].

3.4 Transverse momentum resummation

If we compute the differential transverse momentum distribution, we will encounter terms being proportional to

$$\alpha_s^n \left(\frac{1}{p_T^2} \ln^m \left(\frac{M^2}{p_T^2} \right) \right)_+ \quad (3.53)$$

and leading to large logarithmic contributions in the limit $p_T^2 \rightarrow 0$. To organize and resum these terms we follow the approach of Collins, Soper and Sterman in Ref. [7]. For a refactorization it is common to work with the Fourier transform of the partonic cross section:

$$M^2 \frac{d\sigma_{ab}}{dM^2 dp_T^2}(N) = \int \frac{d^2\vec{b}}{4\pi} \exp(i\vec{b} \cdot \vec{p}_T) \mathcal{W}_{ab}(N+1, M^2, M^2\bar{b}^2, M^2/\mu^2) \quad (3.54)$$

$$= \int_0^\infty db \frac{b}{2} J_0(bp_T) \mathcal{W}_{ab}(N+1, M^2, M^2\bar{b}^2, M^2/\mu^2), \quad (3.55)$$

where b is the impact parameter, $\bar{b} = be^{\gamma_E}/2$ and J_0 is the Bessel function arising after the integration over the angular distribution. In impact-parameter space we get singularities for $M\bar{b} \rightarrow \infty$:

$$\left(\frac{1}{p_T^2} \ln^m \left(\frac{M^2}{p_T^2} \right) \right)_+ \longrightarrow \ln^{m+1}(M^2\bar{b}^2) + \dots \quad (3.56)$$

In the CSS formalism the cross section can be refactorized and the divergences absorbed in the *parton-in-parton distribution functions* $\mathcal{P}_{c/a}(x, k_T, M^2/k_T^2)$ at fixed transverse momentum k_T . The Fourier transformed cross section can be written as

$$\begin{aligned} \mathcal{W}_{ab}(N, M^2, M^2\bar{b}^2, M^2/\mu^2) &= \sum_{cd} H_{cd}(M^2, M^2/\mu^2) \\ &\times \mathcal{P}_{c/a}(N, b^2, M^2\bar{b}^2) \mathcal{P}_{d/b}(N, b^2, M^2\bar{b}^2) S_{cd}(N, M^2\bar{b}^2) \\ &+ \mathcal{O}\left(\frac{1}{M^2\bar{b}^2}\right). \end{aligned} \quad (3.57)$$

The S_{cd} is again the *eikonal function* containing the soft gluon emission parts at fixed transverse momentum. The hard function, absorbing the finite terms of the short distance physics, contains no longer singular terms since it is independent of b . It can be expressed as usual in a power series of α_s :

$$H_{cd}(M^2, M^2/\mu^2) = \sum_{n=0}^{\infty} \alpha_s^n H_{cd}^{(n)}(M^2, M^2/\mu^2). \quad (3.58)$$

After solving the evolution equations for \mathcal{P} and making use of the exponentiation of the eikonal S_{cd} we can write

$$\begin{aligned} \mathcal{W}_{ab}(N, M^2, M^2 \bar{b}^2, M^2/\mu^2) &= \sum_{cd} H_{cd}(M^2, M^2/\mu^2) \\ &\times \mathcal{P}_{c/a}(N, b^2, 1) \mathcal{P}_{d/b}(N, b^2, 1) \exp[G_{cd}(M^2, M^2 \bar{b}^2, M^2/\mu^2)]. \end{aligned} \quad (3.59)$$

Here G_{cd} is the *Sudakov form factor*

$$G_{cd}(M^2, M^2 \bar{b}^2, M^2/\mu^2) = -\frac{1}{2} \int_{1/\bar{b}^2}^{M^2} \frac{dq^2}{q^2} \left[A_c(\alpha_s(q^2)) \ln \frac{M^2}{q^2} + B_c(\alpha_s(q^2)) \right] + (c \leftrightarrow d) \quad (3.60)$$

We can express the $\mathcal{P}_{b/a}$ functions related to the usual k_T integrated *parton-in-parton distribution functions*

$$\mathcal{P}_{b/a}(N, b^2, 1) = \sum_c C_{bc}(N, \alpha_s(1/\bar{b}^2)) \phi_{c/a}(N, 1/\bar{b}^2). \quad (3.61)$$

We can now use the *evolution operator* in Eq. (3.24) to evolve the *parton-in-parton distribution functions* $\phi_{c/a}$ from the factorization scale to the physical and natural scale of the process $1/\bar{b}$. After applying the inverse Fourier transform we get the partonic cross section

$$\begin{aligned} \hat{\sigma}(N, M^2, M^2/p_{\text{T}}^2, N^2/\mu^2) &= \\ &\int_0^\infty db \frac{b}{2} J_0(bp_{\text{T}}) \sum_{cdef} H_{cd}(M^2, M^2/\mu^2) \exp[G_{cd}(M^2, M^2 \bar{b}^2, M^2/\mu^2)] \\ &\times C_{ce}(N, \alpha_s(1/\bar{b}^2)) C_{df}(N, \alpha_s(1/\bar{b}^2)) E_{ea}(N, 1/\bar{b}^2, \mu^2) E_{fb}(N, 1/\bar{b}^2, \mu^2). \end{aligned} \quad (3.62)$$

The functions A , B in the *Sudakov form factor* and the coefficient function C_{ab} can be computed as a power series

$$\begin{aligned} A_a(\alpha_s) &= \sum_{n=1}^{\infty} \alpha_s^n A_a^{(n)}, \quad B_a(\alpha_s) = \sum_{n=1}^{\infty} \alpha_s^n B_a^{(n)}, \\ C_{ab}(N, \alpha_s) &= \delta_{ab} + \sum_{n=1}^{\infty} \alpha_s^n C_{ab}^{(n)}(N). \end{aligned} \quad (3.63)$$

The different accuracies for resummation are completely related to a certain order expansion of the four functions H_{ab} , A_a , B_a and C_{ab} , where for the LL contributions we need only $H_{ab}^{(0)}$ and $A_a^{(1)}$. For the NLL terms we need $H_{ab}^{(0)}$, $A_a^{(1)}$ and $C_{ab}^{(1)}$ and so forth. We can write the *Sudakov form factor* after solving the integrals in Eq. (3.60) as

$$G_{ab}(M^2, M^2 \bar{b}^2, M^2/\mu^2) = L g_{ab}^{(1)}(\lambda) + g_{ab}^{(2)}(\lambda, M^2/\mu^2) + \dots, \quad (3.64)$$

where $\lambda = \alpha_s \beta_0 L$ and $L = \ln M^2 \bar{b}^2$. The first and the second term describe the LL and NLL accuracy, respectively. They can be expressed as follows

$$\begin{aligned} 2\lambda \beta_0 g_{ab}^{(1)}(\lambda) &= (A_a^{(1)} + A_b^{(1)})[\lambda + \ln(1 - \lambda)], \quad (3.65) \\ 2\lambda \beta_0 g_{ab}^{(2)}(\lambda, M^2/\mu^2) &= (A_a^{(1)} + A_b^{(1)}) \left[\frac{\lambda}{1 - \lambda} + \ln(1 - \lambda) \right] \ln \frac{M^2}{\mu^2} \\ &\quad + (A_a^{(1)} + A_b^{(1)}) \frac{\beta_1}{\beta_0^2} \left[\frac{\lambda + \ln(1 - \lambda)}{1 - \lambda} + \frac{1}{2} \ln^2(1 - \lambda) \right] \\ &\quad - (A_a^{(2)} + A_b^{(2)}) \frac{1}{\beta_0} \left[\frac{\lambda}{1 - \lambda} + \ln(1 - \lambda) \right] \\ &\quad + (B_a^{(1)} + B_b^{(1)}) \ln(1 - \lambda). \quad (3.66) \end{aligned}$$

The A and B functions coincide with the expressions in the threshold resummation Sec. 3.3 in Eq. (3.47). There is a freedom in the definition of the functions $H_{ab}^{(1)}$, $C_{ab}^{(1)}$, and $B_{ab}^{(2)}$. We follow the CSS formalism where the functions H_{ab} is expressed as

$$H_{ab}(M^2, M^2/\mu^2) = \hat{\sigma}_{ab}^{(0)}(M^2, M^2/\mu^2) \quad (3.67)$$

and the specific choices of the coefficient functions are [7]

$$C_{ab}^{(1)}(N) = \delta_{ab} \left[C_a \frac{\pi^2}{6} + \frac{1}{2} \mathcal{A}_0 \right] - P_{ab}^{(1),\epsilon}(N), \quad (3.68)$$

$$B_a^{(2)} = -2\delta P_{aa}^{(2)} + \beta_0 \left[\frac{2\pi^2}{3} C_a + \mathcal{A}_0 \right]. \quad (3.69)$$

where, similar to the threshold formalism $P_{ab}^{(1),\epsilon}$ is the $\mathcal{O}(\epsilon)$ term in the AP splitting kernel expansion and $\delta P_{aa}^{(2)}$ is the two-loop AP splitting function coefficient in front of $\delta(1 - x)$.

For the final resummation formula we have to do the inverse transform to switch back to the physical space and the matching, which works in an analogous way as for threshold

resummation:

$$\hat{\sigma}_{ab} = \hat{\sigma}_{ab}^{(res)} + \hat{\sigma}_{ab}^{(f.o)} + \hat{\sigma}_{ab}^{(exp)}, \quad (3.70)$$

where the expansion is

$$\begin{aligned} \hat{\sigma}_{ab}^{(exp)}(N, M^2, M^2/p_T^2, M^2/\mu^2) &= H_{ab}^{(0)}(M^2, M^2/\mu^2) + \alpha_s H_{ab}^{(1)}(M^2, M^2/\mu^2) \\ &\quad - \alpha_s \left(\mathcal{J} - \ln \frac{M^2}{\mu^2} \right) \sum_c \left[H_{ac}^{(0)}(M^2, M^2/\mu^2) P_{cb}^{(1)}(N) + P_{ca}^{(1)}(N) H_{cb}^{(0)}(M^2, M^2/\mu^2) \right] \\ &\quad + \alpha_s \sum_c \left[H_{ac}^{(0)}(M^2, M^2/\mu^2) C_{cb}^{(1)}(N) + C_{ca}^{(1)}(N) H_{cb}^{(0)}(M^2, M^2/\mu^2) \right] \\ &\quad - \alpha_s H_{ab}^{(1)}(M^2, M^2/\mu^2) \left[\frac{\mathcal{J}^2}{4} (A_a^{(1)} + A_b^{(1)}) + \frac{\mathcal{J}^2}{2} (B_a^{(1)} + B_b^{(1)}) \right], \end{aligned} \quad (3.71)$$

with

$$\mathcal{J} = \int_0^\infty db \frac{b}{2} J_0(bp_T) \ln(M^2 \bar{b}^2) \quad (3.72)$$

containing the p_T dependence.

4 Slepton pair production

After studying the basics of SUSY, QCD and resummation we can focus on the slepton pair production at the LHC. We divide the chapter in three parts. The first one deals with the computations of the fixed order differential cross sections. In the second one we discuss the chosen benchmark points (BPs) in the SUSY parameter space and show the numerical results for total cross sections, invariant mass and transverse momentum distributions up to NLL accuracy. The third part deals with implications for DM. A previous study for slepton pair production at hadron colliders has been done in Ref. [20].

4.1 Analytical results

In this section we present all the necessary fixed order computations to make predictions for the cross section of slepton pairs at the LHC.

The process $pp \rightarrow \tilde{l}^*$ can only occur with the annihilation of an incoming quark and antiquark. For this reason there will be only s-channel diagrams, with different mediators and their interference terms, contributing to the cross section at LO. Due to very small Yukawa couplings compared with the gauge couplings we neglect the Higgs mediated processes and consider only the electroweak gauge bosons γ , Z , and W^\pm in the propagator. We have to compute the partonic subprocesses

$$q\bar{q} \rightarrow \gamma, Z \rightarrow \tilde{l}^*, \quad (4.1)$$

$$q\bar{q}' \rightarrow W^-, W^+ \rightarrow \tilde{l}\tilde{\nu}^*, \tilde{l}^*\tilde{\nu} \quad (4.2)$$

for a neutral or a charged final state generally depicted as the Feynman diagram in Fig. 4.1.

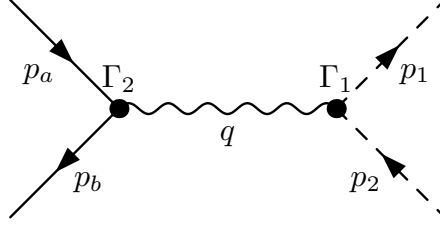


Figure 4.1: Generic Feynman diagram for slepton pair production at LO with a vector boson $V \in \{\gamma, Z, W^\pm\}$ as the mediator. The variables $p_{a,b}$, q and $p_{1,2}$ describe the four momentum of the incoming quark and antiquark, the virtual boson and the final state sleptons, respectively.

The computation and result for the general LO squared matrix element of the generic process can be found in App. B in Eq. (B.18), where we have averaged (summed) over the incoming (outgoing) spin, polarization and color states.

$$|\overline{\mathcal{M}}_B|^2 = \frac{1}{12} \frac{1}{(q^2 - m_{V_1}^2)} \frac{1}{(q^2 - m_{V_2}^2)} (C_1 R_2 C_3^* R_4^* + C_1 L_2 C_3^* L_4^*) [tu - m_1^2 m_2^2] \quad (4.3)$$

To compute a certain process we have to exchange the generic coupling constants L and R with

$$[L_{qq'\gamma}, R_{qq'\gamma}] = -e_f \delta_{qq'} , \quad (4.4)$$

$$[L_{qq'Z}, R_{qq'Z}] = (2T_f^3 - 2e_f x_W) \delta_{qq'} , \quad (4.5)$$

$$[L_{\nu\nu'Z}, R_{\nu\nu'Z}] = \left[\frac{-e}{2s_W c_W}, 0 \right] \delta_{\nu\nu'} , \quad (4.6)$$

$$[L_{qq'W}, R_{qq'W}] = \left[\frac{-ef}{\sqrt{2}s_W} V_{qq'}, 0 \right] , \quad (4.7)$$

$$[L_{\bar{l}l'\gamma}, R_{\bar{l}l'\gamma}] =: C = -e \delta_{\bar{l}l'} , \quad (4.8)$$

$$[L_{\bar{l}l'Z}, R_{\bar{l}l'Z}] =: C = \frac{-e}{c_W s_W} \delta_{\bar{l}l'} \\ \times [2x_W U_{1,2}^* U_{1,2} - U_{1,1}^* U_{1,1} (1 - x_W), 2x_W U_{2,2}^* U_{2,2} - U_{2,1}^* U_{2,1} (1 - x_W)] , \quad (4.9)$$

$$[L_{\bar{l}l'W^-}, R_{\bar{l}l'W^-}] =: C = \frac{-e}{\sqrt{2}s_W} \delta_{\bar{l}l'} U_{i,1} , \quad (4.10)$$

$$[L_{\bar{l}l'W^+}, R_{\bar{l}l'W^+}] =: C = \frac{-e}{\sqrt{2}s_W} \delta_{\bar{l}l'} U_{i,1}^* , \quad (4.11)$$

where we have used the abbreviations $s_W := \sin \theta_W$, $c_W := \cos \theta_W$ and $x_W^2 := s_W$ for the electroweak mixing. The CKM and LR-type mixing matrices are represented by $V_{qq'}$

and U_{ij} , e_f represents the fractional part of the electrical coupling constant e and T_f^3 the third isospin component of the certain flavour. Afterward, we sum the squared matrix elements over all the different initial state partons and possible interference diagrams. Therewith, with the flux of the initial and the phase space of the final state particles we can write the differential partonic cross section for the individual processes as

$$d\sigma_B = \frac{1}{2s} |\overline{M}_B|^2 d\text{PS}^{(2)}, \quad (4.12)$$

where

$$d\text{PS}^{(2)} = \frac{1}{(2\pi)^{n-2}} \frac{d^{D-1}p_1}{2E_1} \frac{d^{D-1}p_2}{2E_2} \delta^n(p_a + p_b - p_1 - p_2) \quad (4.13)$$

is the D -dimensional phase space factor which yields

$$d\text{PS}^{(2)} = \frac{1}{8\pi s} \left(\frac{4\pi}{Q^2}\right)^\epsilon \frac{\Gamma(1-\epsilon)}{2-\epsilon} \delta\left(1 - \frac{Q^2}{s}\right) dQ^2 \quad (4.14)$$

after integrating over D -dimensional spherical coordinates [9]. Since the LO cross section does not suffer any divergences, we can express the phase space factor in $D = 4$ dimensions without any concern which yields for the differential cross section

$$\frac{d\sigma_B}{dt} = \frac{1}{16s^2} |\overline{M}_B|^2. \quad (4.15)$$

For the hadronic LO cross section we can now embed Eq. (4.15) in the convolution with the PDFs in Eq. (2.53), substitute the kinematic variables with the desired ones and integrate them partially for differential distributions or completely for the total cross section.

The NLO corrections of $\mathcal{O}(\alpha_s)$ are caused by virtual loop diagrams interfered with the LO diagrams and by real quark and gluon emission. For the virtual corrections we can use the same formula as in Eq. (4.15) by only exchanging the LO order matrix elements with the virtual contributions depicted in Fig. 4.2. The four diagrams arise because of the QCD self energies and vertex correction and their supersymmetric counterparts. All the computations up to the UV finite¹ virtual squared matrix elements have been presented in App. B.2. The remaining IR divergences will be handled, together with the real corrections, with the common approach called *dipole subtraction* later in this section.

¹The physical quantities have been renormalized by using the $\overline{\text{MS}}$ -scheme, where we absorb the divergent part and some finite contributions proportional to $\Delta = \frac{1}{\epsilon} - \ln 4\pi + \gamma_E$.

To get numerical results we have to exchange the new arising couplings with the expressions stated in Eqs. (4.16) and (4.17) for QCD and SUSY-QCD:

$$[L_{qq'g}, R_{qq'g}] = -g_3 T^a \delta_{qq'} , \quad (4.16)$$

$$[L_{\tilde{q}_i q_I \tilde{g}}, R_{\tilde{q}_i q_I \tilde{g}}] = -g_3 \sqrt{2} T^a \left[-Z^{Ii*}, Z^{(I+3)i*} \right] . \quad (4.17)$$

Here I and i are flavour indices, a represents a color index and Z mixing matrices. All the Feynman rules for the MSSM can be found in Ref. [21].

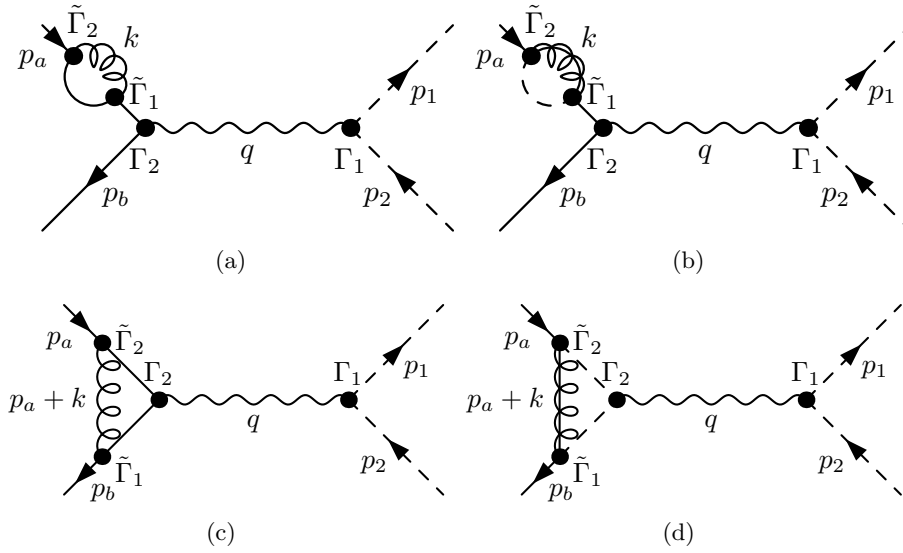


Figure 4.2: Feynman diagrams for the virtual self energy of quarks in SM-QCD (a) and SUSY-QCD (b) and for the vertex corrections due to gluon (c) or gluino (d) exchange. To get the virtual NLO contributions the diagrams have to be multiplied with the Born diagram depicted in Fig. 4.1.

Examples for the real corrections are shown in Fig. 4.3. The corresponding squared matrix elements can be found in App. B.3.

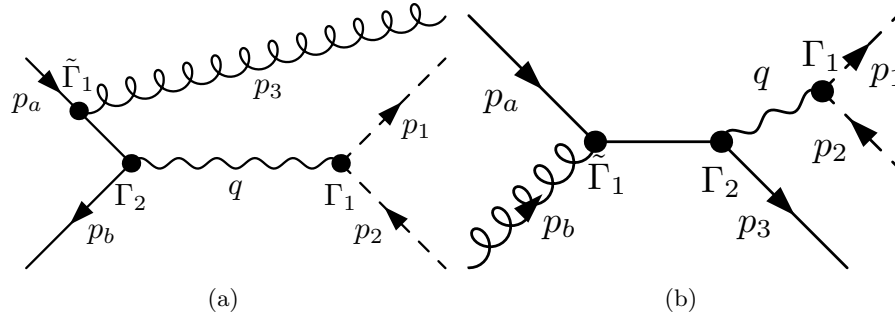


Figure 4.3: Feynman diagrams contributing to the real corrections corresponding to real gluon emission (a) and real quark emission (b). In addition, one has to consider real antiquark emission and the arising u- and t-channels which can be generated by *crossing*.

The main difference, with respect to the former computation parts, is the larger phase space factor due to the additional final state parton:

$$d\sigma_r = \frac{1}{2s} |\overline{\mathcal{M}}_r|^2 d\text{PS}^{(3)}. \quad (4.18)$$

According to the Drell-Yan process, discussed in Ch. 2.2, we have to deal with arising IR divergences. It can be shown that the differential cross section in Eq. (4.18) factorizes in a soft, collinear and hard real emission part.

$$d\sigma_r = d\sigma_r^{(\text{soft})} + d\sigma_r^{(\text{coll})} + d\sigma_r^{(\text{hard})} \quad (4.19)$$

Since we have to sum over all degenerated initial and final states, we take into account the soft and collinear parts to compute the full inclusive NLO slepton pair production cross section. If we add the hard emission part we get the NLO slepton pair production result including a hard jet allowing the slepton pair to get a nonzero transverse momentum. Similar to the virtual contribution of the QCD vertex correction, the former parts are IR divergent.

The dipole subtraction method

We can get rid of the remaining IR divergences, either with the approach of *Phase Space Slicing* or the *dipole subtraction method*, which is more convenient for a numerical approach. Additionally, because of the convolution of the partonic cross section and the PDFs, a numerical approach for the computation of the hadronic cross section is even indispensable and the analytical integrations in the partonic subprocesses can be very

painful.

In this subsection we briefly present the basic ideas of the *dipole subtraction method* based on Catani and Seymour [22].

We can write the full NLO finite cross section for the production of a slepton pair and an additional jet as

$$\begin{aligned} \sigma_{ab}^{NLO}(p_a, p_b, \mu^2) = & \int_{m+1} (d\sigma_{ab}^R(p_a, p_b) - d\sigma_{ab}^A(p_a, p_b)) \\ & + \left[\int_{m+1} d\sigma_{ab}^A(p_a, p_b) + \int_m d\sigma_{ab}^V(p_a, p_b) + \int_m d\sigma_{ab}^C(p_a, p_b, \mu) \right], \end{aligned} \quad (4.20)$$

where we have introduced a local counterterm $d\sigma_{ab}^A$ which assures the IR finiteness. The term $d\sigma_{ab}^C$ acts like a collinear counterterm. The latter is factorization scale dependent and has to be chosen with respect to the renormalization scheme used for the PDFs. For slepton pair production $m = 2$. The NLO correction terms have to be computed in D -dimensions for the virtual part and in 4-dimensions for the real emission part. It can be shown that the counterterm $d\sigma^A$ can be written as a color and spin projection of the Born cross section

$$d\sigma^A = \sum_{\text{dipoles}} d\sigma^B \otimes (dV_{\text{dipole}} + dV'_{\text{dipole}}) \quad (4.21)$$

and similar for the collinear contribution. The dipole factors are universal and the collinear part exhibits the already shown AP splitting functions. To take all diagrams into account we have to sum over all $(m + 1)$ configurations leading to the given m -parton state.

Since it is cumbersome to state all the necessary formulas we refer to Ref. [22], where we can look up the needed dipole terms.

4.2 Numerical results

To get numerical results we have extended a program which was originally written for gaugino pair production in $p\bar{p}$ - and pp -collisions with NLL accuracy by Jonathan Debove [1]. We have considered different BPs with respect to the current limits for SUSY particles. Before we will present the final results, we briefly describe the experimental constraints leading to our chosen benchmark scenarios.

4.2.1 Experimental constraints

For charged sleptons the cleanest searches originate from LEP. The mass limits are mostly quoted for the R-type charged sleptons since they are lighter. The $\tilde{\mu}$ pair production takes place only in the s-channel via γ/Z -exchange. The limits, which are calculated with the assumption of mass unification, depend on the difference between the slepton and the lightest neutralino mass, since its dominant decay is $\tilde{\mu}_R \rightarrow \mu \tilde{\chi}_1^0$. Therefore a mass below 94 GeV is excluded. For the selectron there is in addition a t-channel neutralino exchange. With a neutralino mass below 85 GeV the R-type selectron must be heavier than 100 GeV. Independent of the neutralino mass both types of the selectron have a lower mass limit of 73 GeV. Depending on the neutralino mass, the limit ranges for the lighter $\tilde{\tau}_1$ between 87 and 93 GeV.

The limits for the neutral sleptons, the sneutrinos, arise mostly from the invisible Z-width. Therewith we get a lower bound of 45 GeV. Together with the mass unification it is approximately 94 GeV. All the mentioned results are presented in Ref. [16] with the corresponding references to the experimental works.

With the end of the 7 and 8 TeV runs of the LHC we can also derive lower mass limits for the MSSM particles, especially for colored supersymmetric particles. The newest results have been published by the ATLAS collaboration². They have shown, for scenarios where a R-type slepton directly decays into a charged lepton and a neutralino, that masses between 90 and 185 GeV are excluded for a neutralino with $m_{\tilde{\chi}_1^0} \approx 20$ GeV. Furthermore, they state that the colored sparticles, the gluinos and squarks, are excluded for masses smaller than 1 TeV. It is worth to mention that most of the constraints arise from the assumptions of constrained models like mSUGRA. For less constrained models the limits are weaker.

The eventual discovery of the Higgs particle and its stated mass of roughly 125 GeV set further limits for the mSUGRA parameter space and the resulting sparticle mass spectrum. This is different to the SM where the Higgs mass is considered as a free parameter. It has been shown by Bayesian analysis and using *likelihood* analysis methods that e.g. $m_{\tilde{q}} > 1.5$ TeV and $m_{\tilde{\tau}} > 590$ GeV is excluded for the low mass region [23]. This is not really a problem, but unlikely, because of the large discrepancy of the slepton and lepton masses which evokes again the *fine-tuning* problem.

²The public results can be found on the homepage <https://twiki.cern.ch/twiki/bin/view/AtlasPublic/SupersymmetryPublicResults>.

4.2.2 Benchmark scenarios

Under consideration of the previously presented current constraints we have chosen specific BPs. Motivated by the measurements of the anomalous momentum of the muon $(2 - g)_\mu$ only BPs with a positive off-diagonal Higgs mixing parameter $\mu > 0$ and $\tan\beta = 10$, $A_0 = 0$ GeV or $\tan\beta = 40$, $A_0 = -500$ GeV have been used. We have chosen three BPs lying on the two model lines 10.1, 10.3 and 40.1 [24] depicted in Fig. 4.4. These are widely used for analysis by the SUSY working groups of ATLAS and CMS experimentalists and have been discussed with the LHC Physics Center at CERN (LPCC).

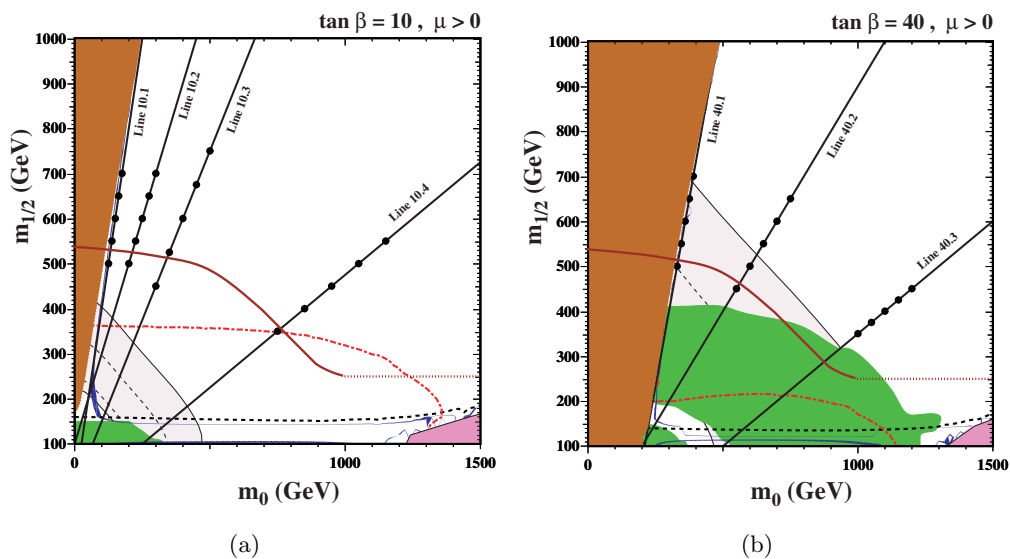


Figure 4.4: The cMSSM planes for $(m_0, m_{1/2})$ for $\tan\beta = 10$, $\mu > 0$ and $A_0 = 0$ in (a) and $\tan\beta = 40$, $\mu > 0$ and $A_0 = -500$. The brown shaded region represents benchmark points where the lightest stable particle (LSP) is charged, in the pink region there is no consistent electroweak vacuum, the green regions are excluded because of large flavor violation in $b \rightarrow s\gamma$ and the gray shaded regions are favored for the reason of the magnetic moment of the muon $(g-2)_\mu$. There are exclusion lines for charginos (near-horizontal black dashed lines), for Higgs boson (near-horizontal red dot-dashed lines) (both LEP) and LHC excluded areas below the purple lines. Our chosen benchmark points are some of the black points on the black solid lines which are spaced regularly along these lines. For the cold dark matter density we get correct results at the dark blue strips in the cMSSM. From Ref. [24].

According to the LPCC numbering scheme, we have chosen the BPs in Tab. 4.1.

The BP 1 exhibits the lightest supersymmetric particle mass spectrum due to the low unification masses m_0 and $m_{1/2}$. The squark and gluino masses are slightly lighter than 1 TeV and are therefore close to the exclusion limits. The lightest slepton is $\tilde{\tau}_1$ with $m \approx 176$ GeV and the LSP is the $\tilde{\chi}_1^0$ with a mass of roughly 162 GeV. The point lies on the model line 10.1 with $\tan \beta = 10$, $A_0 = 0$ and $m_0 = 0.25 \times m_{1/2}$.

Table 4.1: Selection of benchmark points on the cMSSM model. We show the mSUGRA parameters and the resulting averaged slepton, gluino and averaged squark masses rounded to 5 GeV accuracy.

Point	$(m_{1/2}, m_0)$ (GeV)	A_0 (GeV)	$\tan \beta$	$\langle m_{\tilde{l}} \rangle$ (GeV)	$\langle m_{\tilde{g}} \rangle$	$\langle m_{\tilde{q}} \rangle$ (GeV)
1	(400, 100)	0	10	250	840	935
18	(600, 400)	0	10	525	1275	1370
31	(600, 400)	-500	40	500	1275	1365

The second BP 18, lying on the model line 10.3 defined by $m_0 = 1.5 \times m_{1/2}$, differs only in the larger unification masses compared to BP 1. In this scenario the lightest slepton is again the $\tilde{\tau}_1$ and with its mass of $m \approx 451$ GeV, close to the averaged mass $\langle m_{\tilde{l}} \rangle$ of the sleptons. The gluinos and squarks now weigh more than 1.2 TeV.

For a good comparison the last BP 31 agrees in the unification masses with BP 18, but differs in the trilinear coupling A_0 and $\tan \beta$ shown in Tab. 4.1. The averaged masses are approximately the same, but the large A_0 and $\tan \beta$ induce an important mixing among the third generation sleptons and squarks. Still being the lightest slepton, the mass of the $\tilde{\tau}_1$ now differs in more than 200 GeV with respect to the averaged slepton mass. As in all the chosen BPs the neutralino $\tilde{\chi}_1^0$ is the LSP. The BP 31 lies on the model line 40.1 defined by $0.5 \times m_{1/2} + 100$ GeV shown in Fig. 4.4.

During the rest of this chapter we analyze the total cross sections for the model lines and use the three presented BPs for the demonstration of resummation effects in the invariant mass and transverse momentum distributions. The same BPs have been chosen in Ref. [25] to study the production of gaugino pairs at the LHC.

4.2.3 Total cross sections

For all the presented results we have used the MSTW 2008 LO and NLO set for the PDFs [14], except for the numerical cross checks with PROSPINO v. 2.1 [26] where we have used the PDF sets CTEQ 6.1 from the CTEQ collaboration [27], taking into account the five light flavors and the gluon. We have not used a Gaussian distribution to simulate small initial transverse momentum of the partons. The top quark mass has

been set to 173.1 GeV and the masses of the electroweak bosons to $m_Z = 91.1876$ GeV and $m_W = 80.403$ GeV [16]. The CKM matrix has been set to the identity in flavor space and we have considered only an LR-type mixing of the heavy third sfermion generations. The supersymmetric spectra have been created with the software `SUSPECT` v. 2.41 [28] which evolves the universal parameters of e.g. mSUGRA at the GUT scale to the low-energy supersymmetric masses and parameters through renormalization group running at two-loop level. Additionally we have used the *zero-width approximation*. In all computations we have used the same fixed value for the renormalization and factorization scale μ . We have set it to the average of the final state particle mass, which we call the central scale, and varied it by a factor of 0.5 and 2 to get a reasonable scale uncertainty.

Before we have made new predictions for cross sections, we checked the program by comparing with `PROSPINO` v. 2.1 up to NLO accuracy. In Tab. 4.2 we present some numerical cross checks for the total cross sections computed with the program `PROSPINO` v. 2.1.

Table 4.2: Numerical comparison with the program `PROSPINO` v. 2.1 for total cross sections up to NLO accuracy. The coupling constants have been computed with the universal value of G_f , the squark mixing has been set to zero and the scale to the averaged mass of the final state sleptons. All the total cross sections are shown in fb and have been computed for BP 1 using the PDF set CTEQ 6.1 [27] of the CTEQ collaboration.

Process	LO	LO _{prosp}	LO _{dev}	NLO	NLO _{prosp}	NLO _{dev}
$pp \rightarrow \tilde{e}_L \tilde{e}_L^*$	1.508	1.500	0.53%	1.755	1.759	0.57%
$pp \rightarrow \tilde{e}_L \tilde{\nu}_L^*$	4.431	4.407	0.45%	5.054	5.058	0.20%
$pp \rightarrow \tilde{\tau}_1 \tilde{\tau}_2^*$	0.1081	0.1073	0.93%	0.1278	0.1280	0.78%
$pp \rightarrow \tilde{\tau}_1 \tilde{\tau}_1^*$	11.52	11.58	0.52%	13.95	14.00	0.71%

The squark mixing has been set to zero. We have made sure that we use the same parameters in the two programs, but there could still be a difference leading to a harmless discrepancy. The coupling constants have been computed with the universal value of G_f with respect to `PROSPINO` v. 2.1. All the results for the total cross sections, computed at the central scale, differ only in an amount of less than one percent, which assures correct predictions for our further computations.

We will present all of our total cross section results with two uncertainties. The first one, already mentioned, is the scale uncertainty due to the varied scale factor and for the second one we will use a definition made by the MSTW collaboration to take into

account the different fits for the NLO PDF sets. The PDF error is obtained by the expressions

$$(\Delta\sigma_{\text{up}})^2 = \sum_{k=1}^n \{\max(\sigma_k^+ - \sigma_0, \sigma_k^- - \sigma_0, 0)\}^2, \quad (4.22)$$

$$(\Delta\sigma_{\text{down}})^2 = \sum_{k=1}^n \{\max(\sigma_0 - \sigma_k^+, \sigma_0 - \sigma_k^-, 0)\}^2, \quad (4.23)$$

where σ_0 is the cross section using the central PDF set and σ_k^\pm are the values resulting from the $\pm\sigma$ variation along the k -eigenvector of the covariance matrix of the PDF set [14].

Total cross sections for BP 1, 18 and 31

In Tabs. 4.3 - 4.6 we present the LO, NLO and NLL results for the total cross sections for the three different BPs and four elected reference processes. All the results are computed with a hadronic COM energy of $\sqrt{S} = 8$ TeV. In the first, second and third column we state the BP and the masses of the produced slepton particles. The first error reflects the scale uncertainty and the second one the PDF error, which is of course not present in the LO predictions.

Table 4.3: The total cross sections for \tilde{e}_L pair production at the LHC with a COM energy of $\sqrt{S} = 8$ TeV in a proton-proton collision. In the columns we present the BPs, the corresponding slepton masses, the LO cross sections with scale uncertainty and the NLO and (NLO+NLL) matched resummation results with additional PDF uncertainty computed with the MSTW 2008 PDF sets [14].

BP	$m_{\tilde{e}_L}$ (GeV)	$m_{\tilde{e}_L}$ (GeV)	σ_{LO} (ab)	σ_{NLO} (ab)	σ_{res} (ab)
1	288.1	288.1	1416.7 ^{+7.1%} _{-6.4%}	1795.9 ^{+2.6%} _{-2.6%} ^{+1.8%} _{-1.1%}	1808.9 ^{+0.2%} _{-0.4%} ^{+3.2%} _{-1.1%}
18	563.4	563.4	43.2 ^{+11.3%} _{-9.7%}	52.8 ^{+3.6%} _{-3.9%} ^{+3.8%} _{-1.1%}	54.1 ^{+0.2%} _{-0.6%} ^{+3.6%} _{-1.7%}
31	564.0	564.0	48.4 ^{+10.0%} _{-8.4%}	52.4 ^{+3.6%} _{-3.8%} ^{+3.8%} _{-1.5%}	53.7 ^{+0.2%} _{-0.6%} ^{+3.9%} _{-1.5%}

Table 4.4: Same as in Tab. 4.3 for selectron-sneutrino pair production.

BP	$m_{\tilde{e}_L}$ (GeV)	$m_{\tilde{\nu}_L}$ (GeV)	σ_{LO} (ab)	σ_{NLO} (ab)	σ_{res} (ab)
1	288.1	277.4	$3953.1^{+7.1\%}_{-6.3\%}$	$4949.1^{+2.6\%+2.0\%}_{-2.6\%-1.2\%}$	$4983.1^{+0.4\%+2.0\%}_{-0.5\%-1.2\%}$
18	563.4	558.1	$119.7^{+11.7\%}_{-10.0\%}$	$142.4^{+3.8\%+2.5\%}_{-4.1\%-1.5\%}$	$147.6^{+0.2\%+2.5\%}_{-1.2\%-1.6\%}$
31	564.0	558.6	$118.8^{+11.8\%}_{-10.1\%}$	$141.2^{+5.4\%+3.6\%}_{-5.8\%-2.2\%}$	$146.4^{+0.2\%+2.5\%}_{-0.7\%-1.5\%}$

Table 4.5: Same as in Tab. 4.3 for $\tilde{\tau}_1\tilde{\tau}_2^*$ pair production.

BP	$m_{\tilde{\tau}_1}$ (GeV)	$m_{\tilde{\tau}_2}$ (GeV)	σ_{LO} (ab)	σ_{NLO} (ab)	σ_{res} (ab)
1	175.7	290.3	$100.5^{+6.0\%}_{-5.4\%}$	$129.0^{+2.4\%+1.6\%}_{-2.3\%-1.1\%}$	$129.5^{+0.3\%+1.7\%}_{-0.5\%-1.1\%}$
18	451.4	562.9	$0.98^{+11.2\%}_{-9.2\%}$	$1.21^{+3.3\%+3.3\%}_{-4.1\%-1.7\%}$	$1.24^{+0.8\%+3.2\%}_{-0.8\%-1.6\%}$
31	296.2	536.9	$17.6^{+9.7\%}_{-8.5\%}$	$22.0^{+3.2\%+2.3\%}_{-3.2\%-1.4\%}$	$22.3^{+0.4\%+2.4\%}_{-0.4\%-1.3\%}$

Table 4.6: Same as in Tab. 4.3 for $\tilde{\tau}_1\tilde{\tau}_1^*$ pair production except that the total cross sections are presented in fb.

BP	$m_{\tilde{\tau}_1}$ (GeV)	$m_{\tilde{\tau}_1}$ (GeV)	σ_{LO} (fb)	σ_{NLO} (fb)	σ_{res} (fb)
1	175.7	175.5	$10.98^{+4.0\%}_{-3.9\%}$	$14.18^{+2.1\%+1.4\%}_{-1.9\%-1.0\%}$	$14.19^{+0.5\%+1.5\%}_{-0.7\%-1.0\%}$
18	451.4	451.4	$0.150^{+10.1\%}_{-8.7\%}$	$0.185^{+3.3\%+2.7\%}_{-3.4\%-1.3\%}$	$0.188^{+0.0\%+2.7\%}_{-0.1\%-2.3\%}$
31	296.2	296.2	$1.065^{+7.3\%}_{-6.5\%}$	$1.346^{+2.6\%+1.8\%}_{-2.7\%-1.1\%}$	$1.357^{+0.2\%+1.8\%}_{-0.4\%-1.1\%}$

We can see, e.g. in Tab. 4.3, that the NLO corrections to the LO cross section mean a roughly 30% contribution with respect to the LO result. The scale uncertainty is smaller, since we add one more order in perturbation theory with respect to α_S depending on the renormalization and factorization scale. It has been reduced by roughly a factor of 2-3. The NLL results matched to the NLO cross section mean a change by an amount of less than 3%. Due to the fact that we sum the series up to all orders in a certain phase space region the scale error has been reduced tremendously. For resummation, the error is dominated by the PDF uncertainty and is of similar size or slightly larger than in the NLO prediction arising from the Mellin transform in the approach of threshold resummation.

For the selectron and the sneutrino pair production, the cross section decreases by going from BP 1 to 18, while it is rather the same as in BP 31 due to the roughly identical averaged sparticle masses. We can see that the cross section decreases by one order of

magnitude while increasing the mass by a factor of 2. If we consider processes where slepton mixing effects are taken into account we will see a large difference between BP 18 and 31. We get an increased cross section in Tabs. 4.5 and 4.6 due to the lighter mass of $\tilde{\tau}_1$ for BP 31.

Since the $\tilde{\tau}_1$ is the lightest slepton we will get the largest cross section. The lowest cross section corresponds to the $\tilde{\tau}_1\tilde{\tau}_2$ pair production. It can be produced only with the decay of the neutral Z boson instead of the additional photon channel for the other neutral final state slepton pairs. The cross section is roughly lowered by a factor of 100 with respect to the $\tilde{\tau}_1$ pair production. The cross section for selectron sneutrino pair production is also quite large due to the positive charge in the final state which is easier to produce in a proton-proton collision.

Total cross sections for model lines 10.1, 10.3 and 40.1

In order to get a larger overview for slepton pair production with respect to the large parameter space we present the cross sections for the $\tilde{\tau}_1$ pair production for some points defined by LPCC numbering scheme lying on the three model lines 10.1, 10.3 and 40.1. For the computations we have used the same parameters as in the previous section. The results for the different model lines are presented in Figs. 4.5 - 4.7.

In Fig. 4.5 see that for the lightest mass, which corresponds to our BP 1, we get the largest cross section. There is an exponential dependence on the mass which shows the linear behavior. The mass $m_{\tilde{\tau}}$ increases from 180 to 330 GeV while decreasing the cross section by almost two orders of magnitude. In addition, the impact of the NLO corrections to the LO cross section is clearly visible. The NLO line is very close to the NLL line and lies in the PDF uncertainty band of the NLL cross section. The main advantage of the resummed cross section is its reduced scale dependence to make more precise predictions with respect to the artificial and arbitrary renormalization and factorization scales. In Figs. 4.6 and 4.7 we see exactly the same behavior.

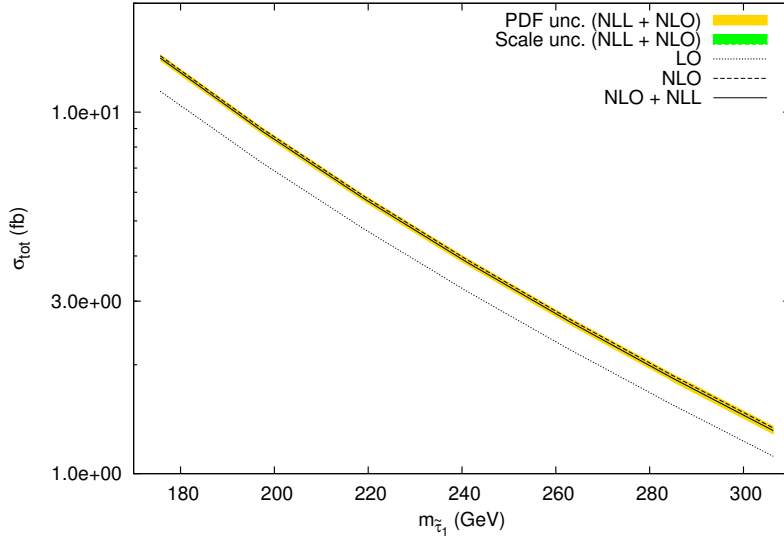


Figure 4.5: The total cross section at LO (dotted), NLO (dashed) and NLO+NLL (full) with its scale (green) and PDF (yellow) uncertainty for the production of a $\tilde{\tau}_1^* \tilde{\tau}_1$ pair at the LHC as a function of their degenerate mass $m_{\tilde{\tau}_1}$ with $\sqrt{S} = 8$ TeV for BPs 1-7 of the LPCC numbering scheme lying on model line 10.1.

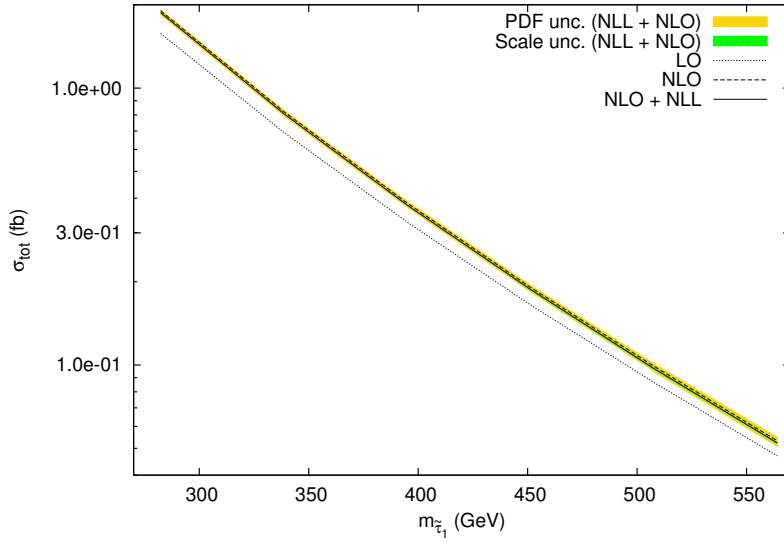


Figure 4.6: Same as in Fig. 4.5 for BPs 15-20.

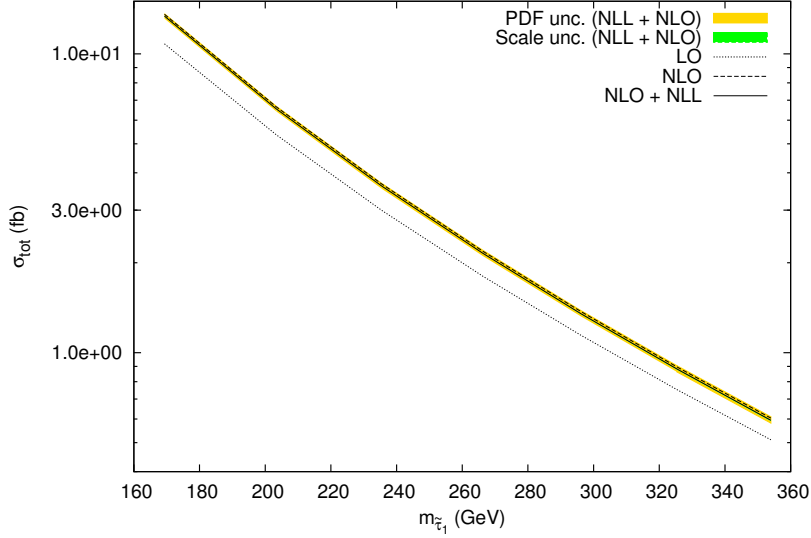


Figure 4.7: Same as in Fig. 4.5 for BPs 27-33.

4.2.4 Invariant mass distributions

In this section we present our results for the invariant mass distributions which are widely used by experimentalists to determine the properties of new particles. We have used the same PDF sets and parameters as in the total cross section part. The invariant mass distributions for a L-type selectron pair is shown in Fig. 4.8 for BP 1 and in 4.9 for BP 31. We have included the distributions for LO, NLO and resummation, where we have computed the latter with the threshold formalism and matched to the NLO. For the first BP in Fig. 4.8 we see that the invariant mass distributions start at the threshold of the partonic COM energy $\sqrt{s} = 2m_{\tilde{e}_L}$ and rise very rapidly up to a peak at roughly 750 GeV. Afterward, they fall very steeply due to the s-channel propagator and less parton luminosity with higher momenta. In the region close to the peak we see large contributions (up to 30 %) arising from the NLO corrections to the Born approximation. The resummed correction with respect to NLO is smaller than 5 %. Much closer to the production threshold, resummation corrections are less contributing and limited up to 1 % due to the less emitted soft gluons in that region. At higher invariant masses the distribution goes asymptotically to zero due to the restricted momentum of the initial state partons. In addition, we show the uncertainties arising from the scale variation and the different PDF fits. We can see that the scale uncertainty becomes smaller in the large-M region, where threshold resummation contributions are more effective. The

distributions in Fig 4.9 for BP 31 show up a similar behavior as the previous one except a shifted production threshold and a lowered maximum due to the larger masses. This effects also slightly larger corrections arising from resummation since we come closer to the hadronic threshold.

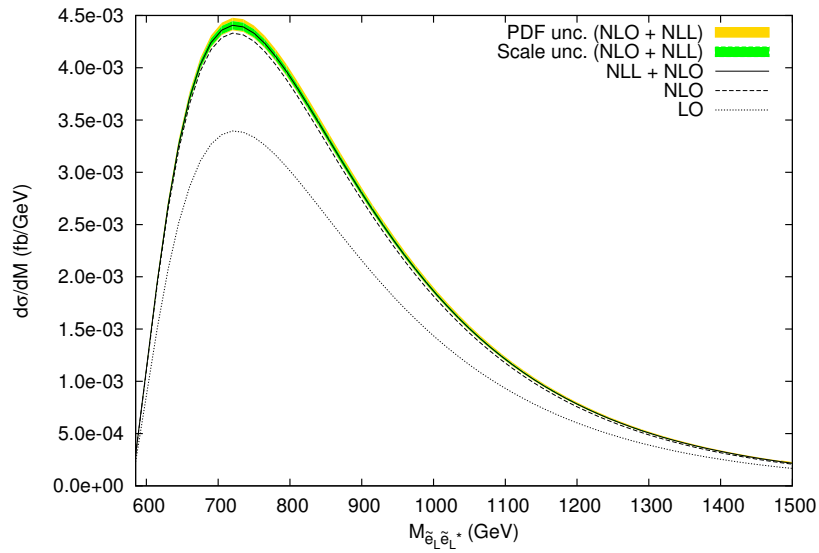


Figure 4.8: The invariant mass distributions at LO (dotted), NLO (dashed) and NLO+NLL (full) with its scale (green) and PDF (yellow) uncertainty for the production of a $\tilde{e}^*\tilde{e}_L$ pair at the LHC with $\sqrt{S} = 8$ TeV and using BP 1.

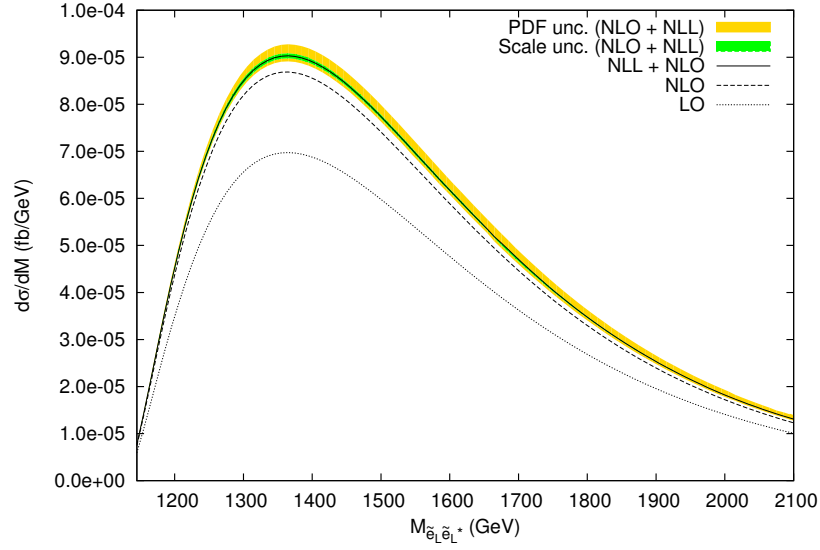


Figure 4.9: Same as in Fig. 4.8 for BP 31.

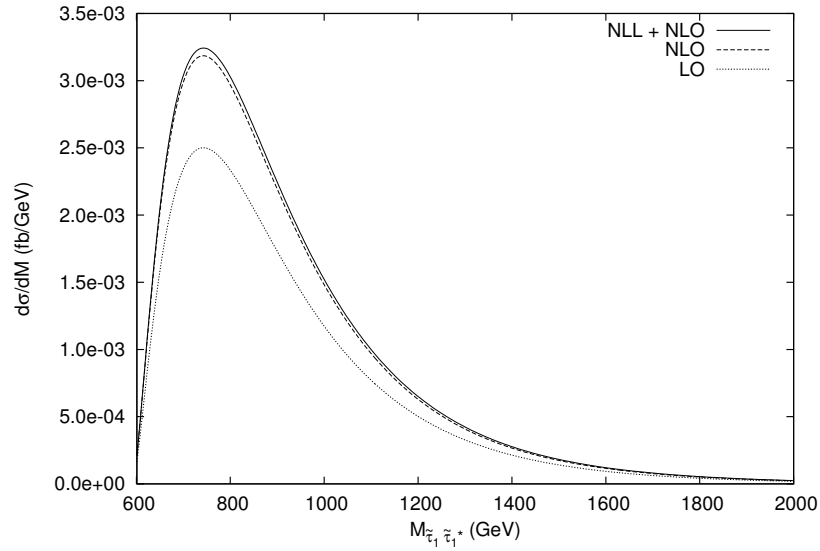


Figure 4.10: The invariant mass distributions at LO (dotted), NLO (dashed) and NLO+NLL (full) for the production of a $\tilde{\tau}_1^* \tau_1^*$ pair at the LHC with $\sqrt{S} = 8$ TeV and using BP 31.

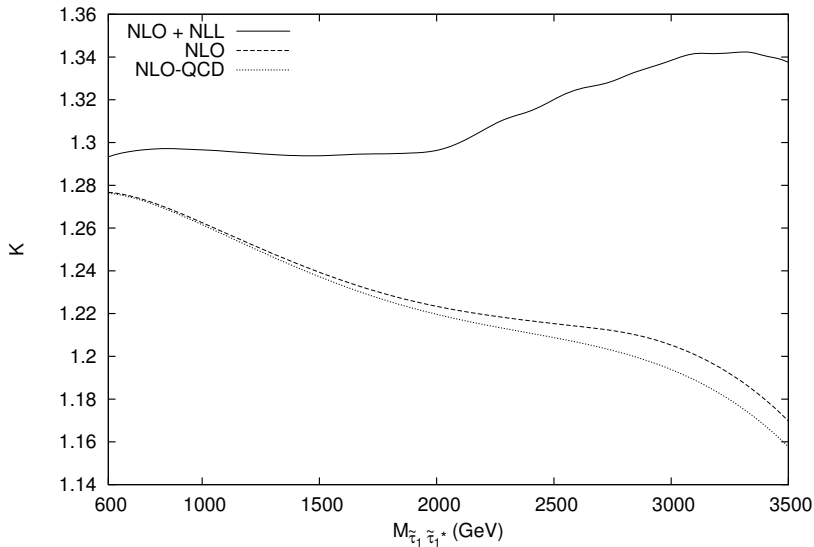


Figure 4.11: The K-factors as defined in Eq. (4.24) for the invariant mass distribution presented in Fig. 4.10. We show the relevance of the NLO-QCD, NLO including SUSY QCD and resummation (NLL + NLO) corrections.

To study the NLO and resummation effects contributing to the invariant mass distributions we show the K-factor distribution in Fig. 4.11 defined as

$$K^i = \frac{d\sigma^i/dM}{d\sigma^{\text{LO}}/dM} \quad (4.24)$$

for $\tilde{\tau}_1$ pair production shown in Fig. 4.10. In Eq. (4.24) i labels the NLO-QCD, NLO and threshold resummation results, where NLO includes also the SUSY-QCD induced effects. We see that the threshold resummation effects are less important in the small-M region since it is far from the hadronic threshold energy. Close to the threshold, for large invariant masses, the impact of resummation on the K-factor is quite large, as expected. In the small-M region the NLO K-factor is dominated by the QCD part, whereby the contributions due to SUSY QCD are more important in the intermediate-M region arising from the gluino vertex correction and in the large-M region starting from the production threshold for squark pairs. Similar results can be found in Ref. [20] for $\sqrt{S} = 14$ TeV.

4.2.5 Transverse momentum distributions

Finally, we present the transverse momentum distributions which show the tremendous impact and the necessity for transverse momentum resummation close to the zero transverse momentum limit. If we write the expression for the NLO transverse momentum distribution we would see that it diverges for $p_T \rightarrow 0$ and leads in addition to large logarithmic contributions shown in the transverse momentum resummation section. Therefore it is indispensable that we organize and sum the logarithmic contributions restoring the convergence properties of the perturbative series and leading to reliable results in the low- p_T region.

In Figs. 4.12 - 4.14 we show the transverse momentum distributions for the production of a $\tilde{\tau}_1^* \tilde{\tau}_1$, $\tilde{\tau}_1^* \tilde{\tau}_2$ and $\tilde{e}_L^* \tilde{\nu}_L$ pairs, respectively. It is worth to mention that for LO the result would lead to a δ -distribution due to trivial momentum conservation conditions. The NLO and resummation predictions fall steeply in the intermediate p_T -region and go to zero for p_T due to the restricted energy of the initial state particles. In the low- p_T region we see the expected results of the divergent NLO and convergent resummation predictions with a finite peak.

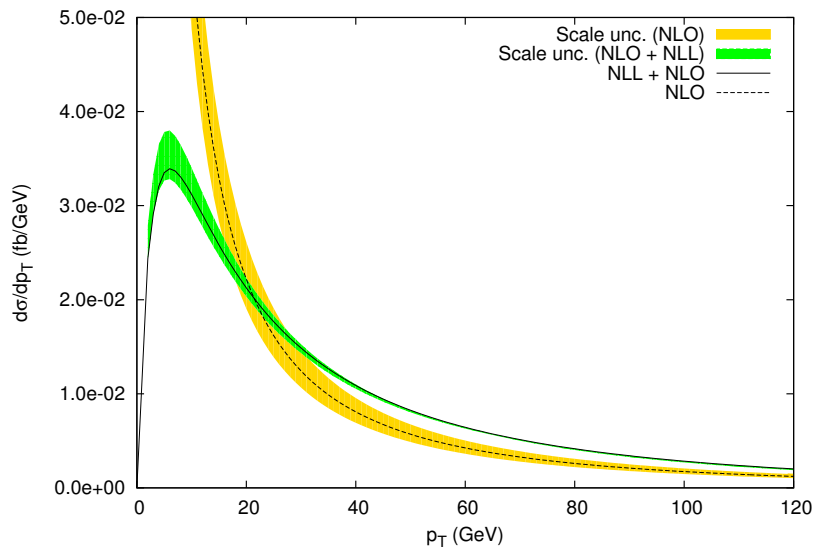


Figure 4.12: The transverse momentum distribution for NLO (dashed) and NLO+NLL (full) with its scale uncertainties (green and yellow) for the production of a $\tilde{\tau}_1^* \tilde{\tau}_1$ pair at the LHC with $\sqrt{S} = 8$ TeV and BP 31.

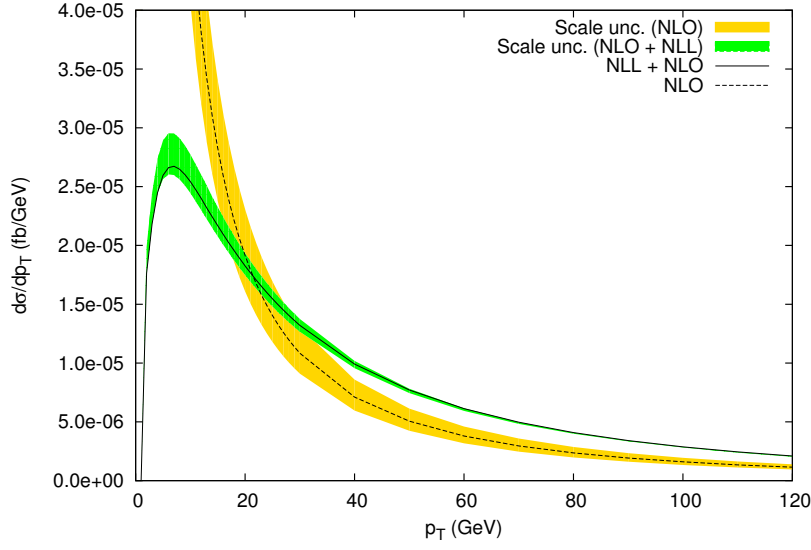


Figure 4.13: Same as in Fig. 4.12 for the production of a $\tilde{\tau}_1^* \tilde{\tau}_2$ pair.

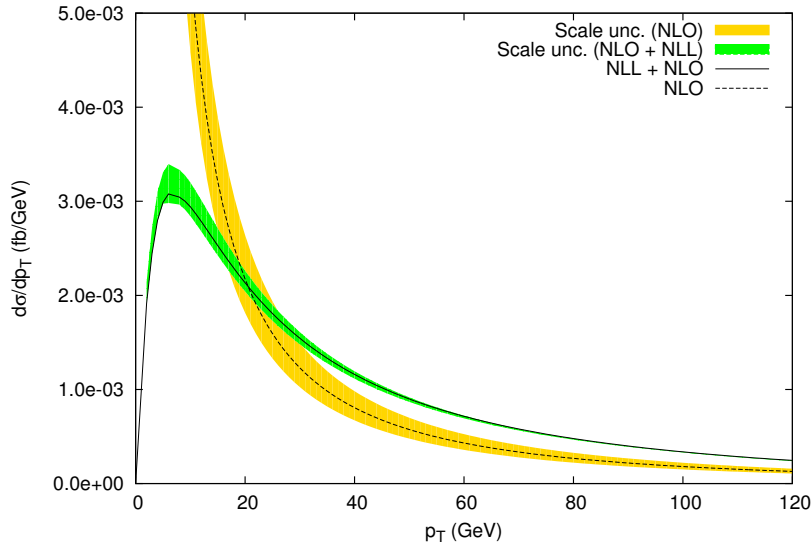


Figure 4.14: Same as in Fig. 4.12 for the production of a $\tilde{e}_L^* \tilde{\nu}_L$ pair.

The reason for the low scale dependence of the resummation predictions are basically the same as in the previous parts. They are especially reduced in the kinematic region $p_T \rightarrow 0$, where we sum all the large logarithms in the transverse momentum resummation formalism. In the large- p_T region resummation becomes less important and the scale

uncertainty gets close to the NLO one. The PDF uncertainties have been neglected. They lead to an approximately fixed uncertainty of 5% for NLO and resummation predictions.

4.3 Implications for dark matter

In modern astrophysics and particle physics DM has become a paradigm. Its existence is widely accepted and some of its properties are well known. We know that the identity of DM is not completely unconstrained. It must be massive, act via gravitational force and therefore give an explanation for the trajectories of the objects in the universe. Of course it must be “dark”, which means that it must be electrically neutral and should have less or no interaction to ordinary matter. Due to the anisotropy of the cosmic microwave background we know that it must be non-baryonic. In addition it must be cold in order to give correct structure formation. Finally every possible DM candidate must be stable or at least long lived to give an explanation for the relic abundance of $\Omega_{DM} = 0.23$. [29]

The only stable “massive” neutral particle in the SM is the neutrino. Since the discovery of neutrino oscillation, it also has a small rest mass, but it is too small to be slowed down by gravitation so that it cannot form cold dark matter. Thus the neutrino can only be a constituent of hot DM. Several models BSM have been proposed, e.g fourth generation neutrinos, axions or new weakly interacting massive particles (WIMPS). The latter can be found in SUSY fulfilling all the mentioned constraints for DM. In the constrained MSSM (cMSSM), or mSUGRA, the only still allowed possibility is the neutralino as the LSP, which gives a promising DM candidate. Nevertheless, with the inclusion of neutrino masses in models also beyond the MSSM its supersymmetric partner, the sneutrino, can be the LSP and gives a reasonable DM candidate with all its properties.

In this section we investigate the sneutrino as a possible DM candidate with models beyond the cMSSM through the inclusion of R-type sneutrinos. First, we will briefly study the possibility for sneutrinos being the LSP. Then we will state the results for recent constraints of its properties through the approach of direct and indirect detection. Afterward, we will focus on an analysis type, called the monojet analysis, which is widely used to constrain parameters for models BSM at hadron colliders, especially for DM candidates.

4.3.1 Sneutrino as a dark matter candidate

The sneutrino as the LSP and therefore being a possible explanation for DM has been investigated in the past in many different works [30]. First of all it is not a priori clear which particle will be the LSP in the cMSSM. It has been shown, using recent experimental constraints, that the sneutrino cannot be the LSP in the cMSSM. The

mass limits are set by searches for SUSY at colliders and for sneutrinos lighter than $m_Z/2$ by the invisible Z-width [31]

$$\Delta\Gamma_Z = \frac{\Gamma_\nu}{2} \left[1 - \left(\frac{2m_{\tilde{\nu}}}{m_Z} \right)^2 \right]^{3/2} \theta(M_Z - 2m_{\tilde{\nu}}) < 2 \text{ MeV}, \quad (4.25)$$

where $\Gamma_\nu = 167 \text{ MeV}$ is the invisible Z-boson width for the decay into one neutrino species. This leads to a lower mass limit for the MSSM sneutrino of 43.7 GeV for one or 44.7 GeV for three sneutrinos degenerate in mass.

The upper mass bounds usually arise from collider experiments through non-observation of their corresponding charged sleptons. Being the LSP, it must fulfill

$$m_{\tilde{\nu}} < m_{\tilde{e}_R} \quad \text{and} \quad m_{\tilde{\nu}} < m_{\tilde{\chi}_0^1}. \quad (4.26)$$

With the knowledge of the current mass constraints for the charged sleptons and the neutralino, the allowed mSUGRA parameter space, that has been computed, yielded to the upper limit of

$$m_{\tilde{\nu}}^{\text{LSP}} < 44.2 \text{ GeV}. \quad (4.27)$$

This result from Ref. [32] is inconsistent with three degenerate sneutrinos and leaves a rather small parameter space for the sneutrino as the LSP. In addition it has been shown that in this small parameter space the amount of the relic density cannot be explained [30].

With the extension of the MSSM, including right handed neutrinos and therewith their R-type superpartners, we enlarge the parameter space which opens new possibilities for the sneutrino being the LSP and a good DM candidate. Many recent searches, with models like NMSSM, SUSY-LR, seesaw and inverse seesaw mechanism and special breaking models with the inclusion of Dirac mass terms, have been made, all leading to reasonable values for sneutrino DM. Let us focus on a class of models with an extended superpotential by right handed superfields \hat{N}^I , containing sterile R-type sneutrinos, one for each family I . It follows

$$W = \epsilon_{ij} \left(\mu \hat{H}_i^1 \hat{H}_i^2 - Y_l^{IJ} \hat{H}_i^1 \hat{L}_j^I \hat{R}^J + Y_\nu^{IJ} \hat{H}_i^2 \hat{L}_j^I \hat{N}^J \right), \quad (4.28)$$

where $Y_{\nu,l}^{IJ}$ are Yukawa coupling matrices in flavor space chosen to be real and diagonal. Y_ν^{II} determines the Dirac type neutrino masses $m_D^I = v_2 Y_\nu^{II}$, where v_2 is the vev of

\hat{H}_i^2 . Of course the SUSY-breaking potential, including additional mass terms for the superpartners, changes as well to

$$V_{\text{soft}} = (M_L^2)^{IJ} \tilde{L}_i^{I*} \tilde{L}_i^J + (M_N^2)^{IJ} \tilde{N}^{I*} \tilde{N}^J - \left[\epsilon_{ij} \left(\Lambda_i^{IJ} H_i^1 \tilde{L}_i^J \tilde{R}^J + \Lambda_\nu^{IJ} H_i^2 \tilde{L}_i^J \tilde{N}^J \right) + \text{h.c.} \right]. \quad (4.29)$$

With Eqs. (4.28) and (4.29) we get the sneutrino mass potential, which can be written in a compact form, using the definition of the vector $\Phi^\dagger = (\tilde{\nu}_L, \tilde{N}^*)$:

$$V_{\text{mass}} = \frac{1}{2} \Phi_{LR}^\dagger M_{LR}^2 \Phi_{LR}. \quad (4.30)$$

By neglecting the small Dirac masses m_D we get for the squared mass matrix

$$M_{LR}^2 = \begin{pmatrix} m_L^2 + \frac{1}{2} m_Z^2 \cos 2\beta & F^2 \\ F^2 & m_N^2 \end{pmatrix}, \quad (4.31)$$

where

$$F^2 = v \Lambda_\nu \sin \beta \quad (4.32)$$

and $v^2 = v_1^2 + v_2^2 = 246 \text{ GeV}$, $\tan \beta = v_1/v_2$ and $\Lambda_\nu =: 1/\sqrt{2} A_{\tilde{\nu}}$ is a trilinear coupling. After diagonalizing and redefining the fields we will get the masses for the two sneutrino mass eigenstates

$$m_{\tilde{\nu}_{1,2}}^2 = \frac{1}{2} \left(m_+^2 \pm \sqrt{m_-^4 + 2A_{\tilde{\nu}}^2 v^2 \sin^2 \beta} \right), \quad (4.33)$$

where $m_\pm^2 := m_L^2 \pm m_N^2 + m_Z^2/2$. By convention it has been chosen that $m_{\tilde{\nu}_1} < m_{\tilde{\nu}_2}$. Since $m_{\tilde{N}}$ is a new free parameter, independent of the trilinear coupling or other mass parameters, we are allowed to vary it freely. Therefore, we can achieve a large mixing and a reduction of the lighter sneutrino mass just by changing the parameter $m_{\tilde{N}}$ and without varying the trilinear coupling. For $m_{\tilde{N}} \ll m_{\tilde{L}}$ we can avoid the collider limits and the only constraints arise from the invisible Z-width. The eigenstates can be written in a similar way as for the third generation charged sleptons with the introduction of a mixing angle.

$$\begin{pmatrix} \tilde{\nu}_1 \\ \tilde{\nu}_2 \end{pmatrix} = \begin{pmatrix} \cos \theta_{\tilde{\nu}} & -\sin \theta_{\tilde{\nu}} \\ \sin \theta_{\tilde{\nu}} & \cos \theta_{\tilde{\nu}} \end{pmatrix} \begin{pmatrix} \tilde{\nu}_R \\ \tilde{\nu}_L \end{pmatrix}, \quad \sin^2 \theta_{\tilde{\nu}} = \frac{\sqrt{2} A_{\tilde{\nu}} v \sin \beta}{m_{\tilde{\nu}_1} - m_{\tilde{\nu}_2}}. \quad (4.34)$$

The R-type sneutrino is sterile, which means that it only interacts with the Higgs field. The L-type field is multiplied by a factor $\sin \theta$ and leads to a variation of the interaction Lagrangian

$$\mathcal{L}_{\tilde{\nu}_1 \tilde{\nu}_1 Z} \rightarrow \sin^2 \theta_{\tilde{\nu}} \mathcal{L}_{\tilde{\nu}_L \tilde{\nu}_L Z} \quad (4.35)$$

followed by a modified contribution to the invisible Z-width

$$\Delta\Gamma_Z = \sin^4 \theta_{\tilde{\nu}} \frac{\Gamma_{\nu}}{2} \left[1 - \left(\frac{2m_{\tilde{\nu}}}{m_Z} \right)^2 \right]^{3/2} \theta(M_Z - 2m_{\tilde{\nu}}) < 2 \text{ MeV}. \quad (4.36)$$

Therewith, sneutrino masses of $\mathcal{O}(1 \text{ GeV})$ are possible, whereby the mixing angle must be small, which means the sneutrino is mostly R-type and possesses only a small fraction of the active component. In Ref. [33] a full analysis of the physical parameter space, i.e. the sneutrino mass $m_{\tilde{\nu}_1}$ and the mixing angle $\theta_{\tilde{\nu}_1}$, has been done with respect to the invisible Z-width constraints, recent Higgs and SUSY mass limits, DM constraints from the relic abundance as well as from direct and indirect detection experiments. It has been found that the sneutrino, as a DM candidate fulfilling all the limits, is viable in the parameter regions

$$1 \text{ GeV} \leq m_{\tilde{\nu}_1} \leq 8 \text{ GeV} \quad \text{and} \quad 0.1 \leq \sin \theta_{\tilde{\nu}} \leq 0.4. \quad (4.37)$$

In addition the cascade decay of the squarks and gluinos, decaying into neutralinos $\tilde{N}_{1,2}$ and then invisibly into a $\tilde{\nu}_1 \nu$ pair has been studied [34]. They have also investigated the dominant decay of a chargino into a charged lepton and the sneutrino with recent LHC results, supporting the possibility of light sneutrino DM below 10 GeV.

An analysis method which has not been made so far in this context is the monojet analysis.

4.3.2 The monojet analysis

There are many different ways to constrain the parameter space for DM candidates in different models. In Fig. 4.15 we have sketched the different possibilities to look for DM. The up going arrow indicates the direct search via WIMP-Nucleon scattering which is done, e.g. by the XENON experiment [35]. In backward direction we have the indirect DM search investigating DM annihilation, e.g. with the PAMELA satellite. Collider searches are done in forward direction, where we try to generate DM particles through the collision of SM particles.

Nevertheless, we get a problem with this kind of detection form since we know that the DM particle is electrically neutral and only weakly interacting. We cannot measure it with our detectors. What we need is an additional electrically interacting particle, like a photon (monophoton) or an emitted parton transforming to a jet via hadronization (monojet). We concentrate on the latter, where we measure a jet with some transverse momentum recoiling against “nothing”, potentially DM.

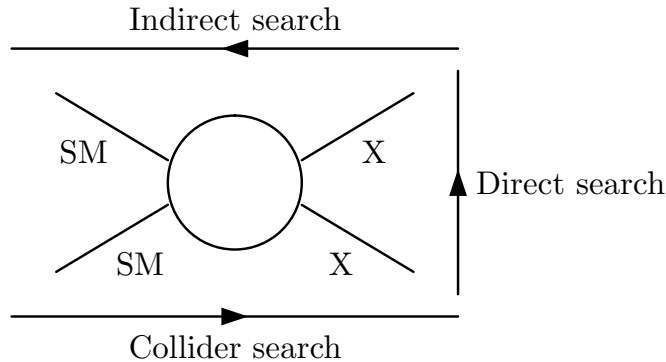


Figure 4.15: Sketch of different detection methods for dark matter. The time direction is indicated by the outer arrows.

The main idea is rather simple. First we have to estimate the SM background leading to monojet events, basically provided by the decay of the Z-boson into two neutrinos or the decay of a W-boson into an undetected charged lepton and neutrino. After computing the SM predictions we compare the results with the experimental data for monojet events. The discrepancy is an open slot for new weakly interacting particles and perhaps a DM candidate. Therewith we can get an upper bound for DM creation cross section at the LHC, leading to limits for our parameterspace. Practically it is not that simple.

For our analysis we will focus on the results for a monojet analysis made by CMS [36] with an integrated luminosity of $L = 5.0 \text{ fb}^{-1}$ and a hadronic COM energy of $\sqrt{S} = 7 \text{ TeV}$. The data has been recorded by using a trigger, which requires an event including a jet with a certain transverse momentum and missing energy. Using Monte Carlo event generators they have produced DM signal samples with different contact interactions and found some good values for the triggers. The missing energy was set to $\cancel{E}_T > 350 \text{ GeV}$ and the jet with the highest transverse momentum requiring $p_T > 110 \text{ GeV}$ and $\eta(j_1) < 2.4$. Events with more than two jets, where $p_T(j_2) > 30 \text{ GeV}$ have been discarded. If the azimuth angle between the highest and the second highest p_T jet is $\Delta\phi(j_1, j_2) < 2.5$, a second jet will be allowed. For reducing background events

originated by Z and W production and top quark decays with isolated muons or electrons with $p_T > 10$ GeV are rejected. In addition, they made an analysis with $\cancel{E}_T > 250, 300$ and 400 GeV. The background samples are also generated by Monte Carlo programs. Here they have used MADGRAPH v. 5 [37] interfaced to PYTHIA [38] for generating parton showers. For a more detailed view we recommend Ref. [36]. The summarized results for the upper limit in the non-SM cross sections are shown in Tab. 4.7.

Table 4.7: Summarized results from Ref. [36] showing the estimated SM background events, the observed data and the observed upper limits for non-SM events corresponding to an integrated luminosity of 5.0 fb^{-1} and a COM energy of 7 TeV. The uncertainties include statistical and systematical terms. In the last row the limit is determined with a confidence level of 95 %. The method which has been used for the errors is the so called CLS-method.

\cancel{E}_T (GeV)	≥ 250	≥ 300	≥ 350	≥ 400
Events in SM	7842 ± 367	2757 ± 167	1225 ± 101	573 ± 65
Events in data	7584	2774	1142	522
Observed upper limits	600	368	158	95
Observed upper σ_{tot} (fb)	120	73.6	31.6	19

For our analysis we have computed the cross section for the production of one hard jet combined with two light sneutrinos. Due to our assumption of massless partons we get $\cancel{E}_T \approx p_T$. We have set the lower limit of the p_T integration to the values of \cancel{E}_T stated in Tab. 4.7. Instead of using the zero-width approximation we have implemented the width of the Z-boson $\Gamma_Z = 2.4952 \text{ GeV}$ [16]. The central scale value has been used. All the other parameters are the same as in the previous sections. In Figs. 4.16 - 4.19 we show different contour plots for the physical parameter space $m_{\tilde{\nu}_1}$ and $\sin \theta_{\tilde{\nu}}$ leading to different total cross sections.

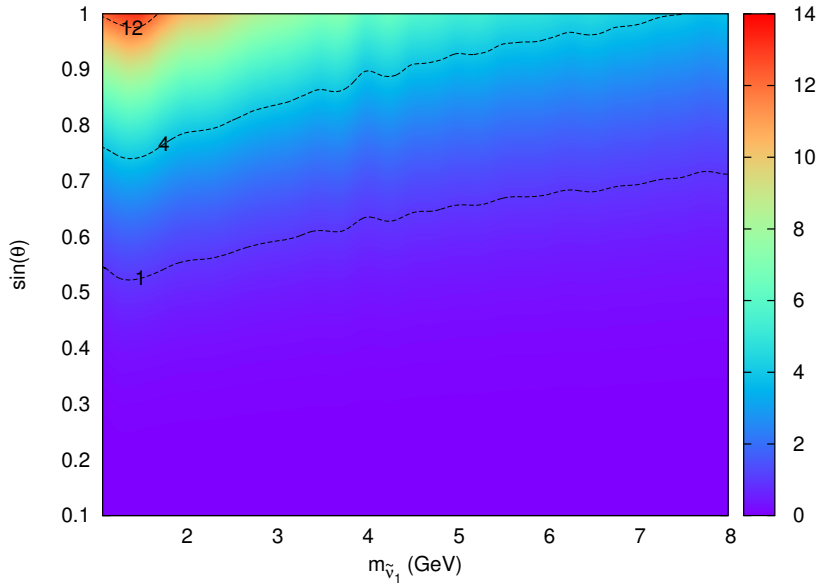


Figure 4.16: Contour plot for the 2-dimensional parameter space $(m_{\tilde{\nu}_1}, \sin \theta)$. The color represents the total cross section value in fb. We have used the central scale value, a COM energy of 7 TeV and the MSTW@NLO 2008 PDF set. For the transverse momentum we require $p_T > 350$ GeV.

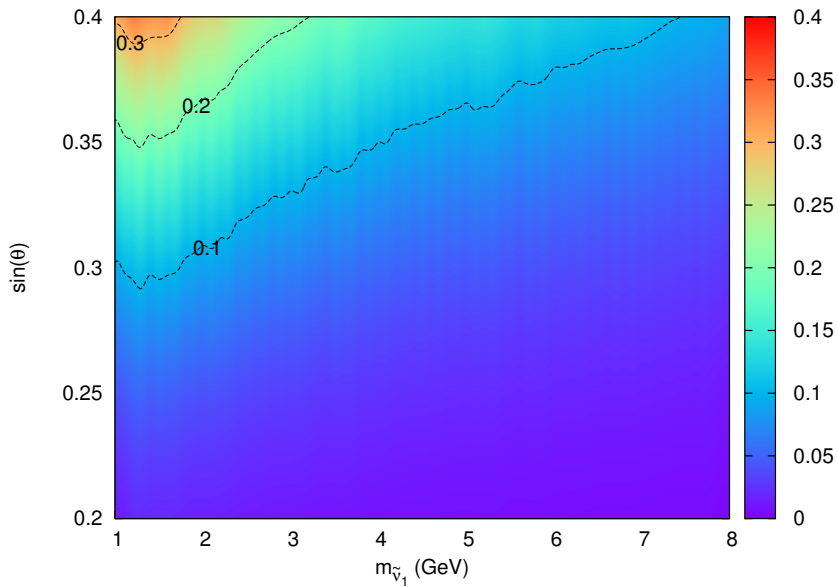


Figure 4.17: Close-up of Fig. 4.16 showing the allowed parameter space for cold sneutrino DM.

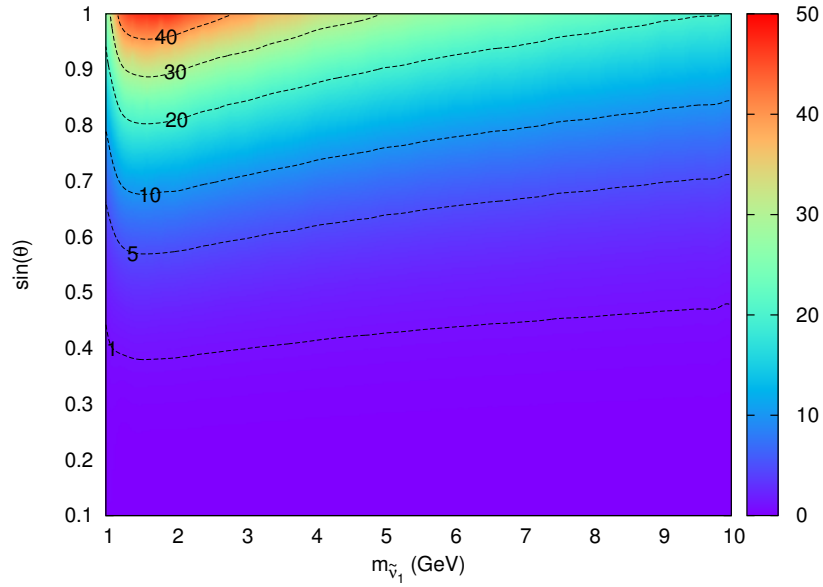


Figure 4.18: Same parameters as in Fig. 4.16, except $p_T > 250$ GeV.

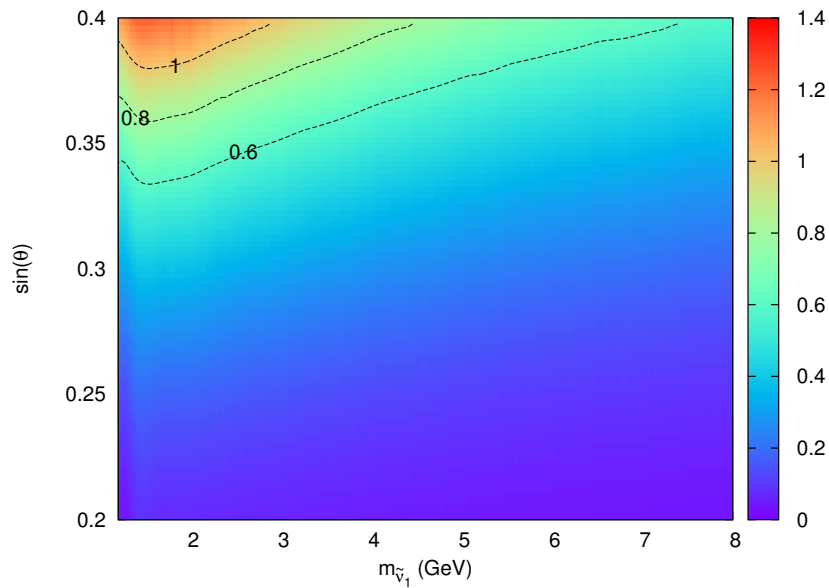


Figure 4.19: Close-up of Fig. 4.18 showing the allowed parameter space for cold sneutrino DM.

In Fig. 4.17 we see the relevant parameter space for cold sneutrino DM. As expected the cross section increases with the mass decreasing. The cross section strongly depends

on the mixing angle since it goes with the fourth power due to the modified interaction Lagrangian. With the largest allowed value for the mixing angle and a mass of roughly 1 GeV we get a cross section in the region of 0.3 fb. Comparing this with the upper bound of 31.6 fb stated in Tab. 4.7, the difference is given by a factor of 100. Even with the already excluded regions in the parameter space, the cross sections shown in Fig. 4.16 are still three times too large. Different p_T -cuts show similar results, as can be seen in Figs. 4.18 and 4.19. If we increase the cut by a factor of 1.4, the cross section will decrease by a factor of 0.3. This seems to be reasonable with respect to the steep increasing and after the maximum exponentially decreasing p_T -distributions.

For the whole parameter space the cross section is smaller than the given upper limit. Nowadays, it is impossible to constrain the parameters. Nevertheless, we are looking forward to new monojet data of the finished 8 TeV and the following 14 TeV runs of the LHC. Until now ATLAS has achieved an integrated luminosity of roughly 20 fb^{-1} ³. For the 14 TeV run we expect an integrated luminosity of $\mathcal{O}(100 \text{ fb}^{-1})$. This will lead to a reduced statistical error and therefore a smaller open “slot” for non-SM events. We are confident that we will be able to set constraints to the sneutrino DM parameter space soon.

³The current results can be found on https://twiki.cern.ch/twiki/bin/view/AtlasPublic/LuminosityPublicResults#2012_pp_Collisions

5 Conclusion and outlook

In this work we have presented slepton pair production at the LHC including resummation techniques apart from the usual fixed order computations. In addition, we have investigated the sneutrino as a possible candidate for DM.

Firstly, we have discussed the important basics of SUSY, secondly we have studied the theoretical background to apply perturbative QCD techniques to slepton pair production in proton-proton collisions. This has been followed by the presentation of the threshold and transverse momentum formalism for summing potentially large logarithms arising in the NLO real corrections.

Before we have made predictions for cross sections, invariant mass and transverse momentum distributions, we have discussed the experimental constraints setting exclusion limits for supersymmetric particles. We have seen that until now charged sleptons with a mass of $\mathcal{O}(100 \text{ GeV})$ are still compatible with the experimental data of the LHC. The crucial factor for the choice of our used BPs has been given by the mass limits on squarks and gluinos which must be roughly of the order $\mathcal{O}(1 \text{ TeV})$. With the eventual discovery of the Higgs there are even stronger constraints, especially for the mass spectrum constrained MSSM.

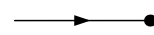
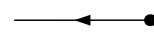
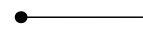


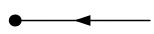
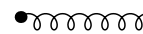
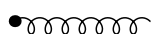
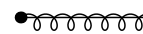
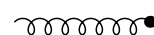
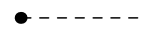
The largest cross section has arisen from the $\tilde{\tau}_1$ -pair production since it is the lightest in the considered benchmark scenarios. Due to the resummation approach the scale uncertainty has been reduced by at least a factor of 4 up to roughly a factor of 8. In the invariant mass distributions it has been shown that resummation becomes more important in the high invariant mass region, as expected. For the transverse momentum distribution the resummation formalism assures the convergence in the low- p_T region. Due to the experimental constraints, given by LHC and the invisible Z-width, it is no longer possible for the sneutrino to be the LSP in mSUGRA models. We have investigated the sneutrino as a DM candidate by adding a sterile R-type sneutrino field. Former searches have shown that a scenario with sneutrino DM is possible in the parameter space $1 \text{ GeV} \leq m_{\tilde{\nu}_1} \leq 8 \text{ GeV}$ and $0.1 \leq \sin \theta_{\tilde{\nu}} \leq 0.4$. Applying monojet results of the LHC for a luminosity of 5 fb and a COM energy of 7 TeV it was not possible to set

further limits on the two-dimensional, of the other parameters of mSUGRA independent, parameter space. We are still a factor of roughly 100 away from constraints with a monojet analysis apart from the limits due to direct detection, the relic abundance and cascade decay. Nevertheless, we look forward to the next results of the recently finished 8 TeV run and we are very confident that we can set new boundaries on the parameters at least after the 14 TeV because of the larger luminosity.

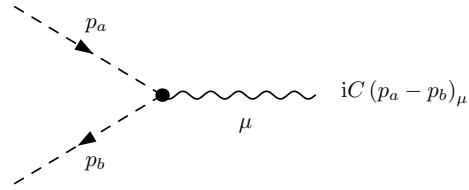
To enlarge the underlying symmetry and to do further phenomenology with additional models the part of gaugino pair production made by Jonathan Debove and the slepton pair production will be combined with the recently finished work of David R. Lamprea presented in Ref. [39] who has investigated resummation predictions for new electroweak gauge bosons. This opens the field of SUSY-LR models which obey a large symmetry and could be very successful, e.g. for further sneutrino DM phenomenology. Finally the program code will be published to get additional advises and to allow particle physicists to use further tools for comparison with experimental data.

A Feynman rules

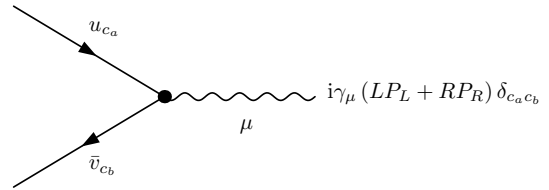
During the computations we will use the following Feynman rules:

	$u(p, s, c)$	incoming quark		
	$\bar{v}(p, s, c)$	incoming antiquark		$i \frac{\not{p}}{p^2} \delta_{c_a c_b}$ massless quark propagator
	$\bar{u}(p, s, c)$	outgoing quark		$-i \frac{g^{\mu\nu}}{q^2 - m_V^2}$ generic vector boson propagator
	$v(p, s, c)$	outgoing antiquark		$-i \frac{g^{\mu\nu}}{k^2} \delta_{ab}$ gluon propagator
	$\epsilon_\mu^a(k, \lambda)$	incoming gluon		$-i \frac{\not{k}}{k^2 - m_{\tilde{g}}^2} \delta_{c_a c_b}$ gluino propagator
	$\epsilon_\mu^{a*}(k, \lambda)$	outgoing gluon		$\frac{i}{k^2 - m_{\tilde{q}}^2} \delta_{c_a c_b}$ squark propagator

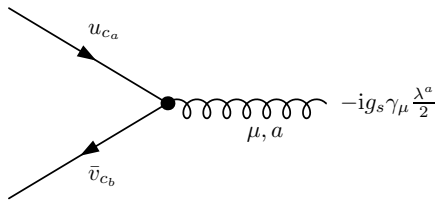
generic sfermion-sfermion-vector coupling:



generic fermion-fermion-vector coupling:



fermion-fermion-gluon coupling:



generic quark-squark-gluino coupling:

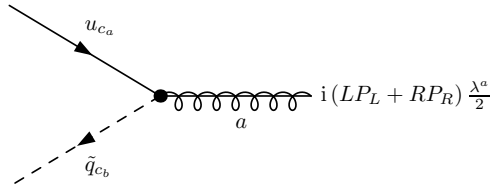


Figure A.1: Feynman rules for LO and NLO slepton pair production.

B Feynman amplitudes

In this chapter we will present the necessary LO and NLO unpolarized Feynman amplitudes for slepton pair production at hadron colliders. During all the computations the initial state particles are considered as massless. To evaluate the arising traces the computer program FORM has been used.

The following relations are useful for simplifications:

$$\{\gamma_\mu, \gamma_\nu\} = 2g_{\mu,\nu}, \quad (\text{B.1})$$

$$g_\mu^\mu = D, \quad (\text{B.2})$$

$$\gamma^\mu \gamma_\mu = D, \quad (\text{B.3})$$

$$\gamma_\mu \not{a} \gamma^\mu = (2 - D) \not{a}, \quad (\text{B.4})$$

$$\gamma_\mu \not{a} \not{b} \gamma^\mu = 4a \cdot b + (D - 4) \not{a} \not{b}, \quad (\text{B.5})$$

$$\gamma_\mu \not{a} \not{b} \not{c} \gamma^\mu = -2 \not{c} \not{b} \not{a} - (D - 4) \not{a} \not{b} \not{c}, \quad (\text{B.6})$$

$$\not{a} \gamma_\mu \not{a} = 2a_\mu \not{a} - \gamma_\mu a^2, \quad (\text{B.7})$$

$$\not{a} \gamma_\mu \not{b} = -\not{b} \gamma_\mu \not{a} + 2a_\mu \not{b} + 2b_\mu \not{a} - 2a \cdot b \gamma_\mu, \quad (\text{B.8})$$

$$\not{p} u = \bar{u} \not{p} = 0, \quad (\text{B.9})$$

$$\not{p} v = \bar{v} \not{p} = 0. \quad (\text{B.10})$$

To get shorter expressions we make redefinitions of the generic couplings

$$\Gamma_\mu^{\text{vqq}} = \gamma_\mu (LP_L + RP_R) =: \gamma_\mu \Gamma, \quad (\text{B.11})$$

$$\Gamma_\mu^{\text{vslsl}} = C(p_1 - p_2)_\mu =: (p_1 - p_2)_\mu \bar{\Gamma} \quad (\text{B.12})$$

and for the hermitean conjugate couplings

$$(\Gamma_\mu^{\text{vqq}})^\dagger = (RP_L + LP_R) \gamma_\mu =: \bar{\Gamma} \gamma_\mu, \quad (\text{B.13})$$

$$(\Gamma_\mu^{\text{vslsl}})^\dagger = C^*(p_1 - p_2)_\mu =: (p_1 - p_2)_\mu \bar{\Gamma}. \quad (\text{B.14})$$

Disregarding the different coupling constants and mediator masses we can compute all the diagrams with a general mediator V and its mass m_V .

B.1 Leading-order process

The only contributing diagram to the Born cross section is depicted in Fig. B.1.

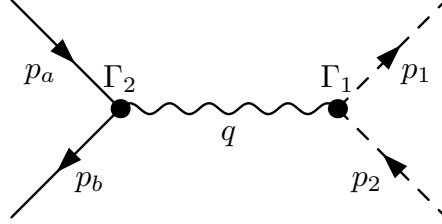


Figure B.1: Generic Feynman diagram for slepton pair production at LO.

With respect to the Feynman rules of App. A the matrix element can be written as

$$i\mathcal{M}_B = \frac{-ig_{\mu\nu}}{q^2 - m_{V_1}^2} iC_1(p_1 - p_2)_\mu [\bar{v}_b i\gamma_\nu (L_2 P_L + R_2 P_R) u_a] \delta_{c_a c_b}. \quad (\text{B.15})$$

For the unpolarized averaged Feynman amplitude we get

$$\begin{aligned} |\overline{\mathcal{M}_B}|^2 &= \overline{\mathcal{M}_B \mathcal{M}_B^*} = \frac{|f_c|^2}{4 \cdot 9} \frac{1}{(q^2 - m_{V_1}^2)} \frac{1}{(q^2 - m_{V_2}^2)} \\ &\Gamma_1 \bar{\Gamma}_3 (p_1 - p_2)^\mu (p_1 - p_2)^\nu \text{Tr} \left[\not{p}_b \gamma_\mu \Gamma_2 \bar{\Gamma}_4 \not{p}_a \gamma_\nu \right], \end{aligned} \quad (\text{B.16})$$

where $|f_c|^2$ represents the color factor

$$|f_c|^2 = \sum_{c_a, c_b} \delta_{c_a c_b} = 3. \quad (\text{B.17})$$

The factors 4 and 9 in the denominator arise due to the spin and color averaging, respectively.

After evaluating the trace and using the common Mandelstam variables our result finally is

$$|\overline{\mathcal{M}_B}|^2 = \frac{1}{12} \frac{1}{(q^2 - m_{V_1}^2)} \frac{1}{(q^2 - m_{V_2}^2)} (C_1 R_2 C_3^* R_4^* + C_1 L_2 C_3^* L_4^*) [tu - m_1^2 m_2^2]. \quad (\text{B.18})$$

B.2 Virtual corrections

In this section we compute corrections of the order $\mathcal{O}(\alpha_s\alpha)$ to the Born cross section. Therefore, we have to take into account contributions of the SM-QCD diagrams for the virtual self energy of the quark and antiquark and the vertex corrections with an internal gluon. In addition, we have to compute the MSSM-QCD corrections which correspond here to the squark self energy and the vertex correction with an internal gluino. The diagrams will be interfered with the Born matrix element \mathcal{M}_B^* .

B.2.1 The quark self energy

We compute the Feynman diagram in Fig. B.2 using the approach of *dimensional regularization* (DR). To preserve a dimensionless coupling we introduce the renormalization scale μ_r . To get a common expression for the tensor integrals, we use the reduction formalism discussed in Ref. [41].

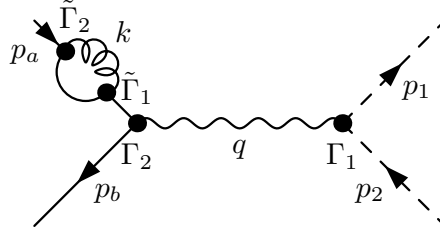


Figure B.2: Feynman diagram for the self energy of an external quark. In addition one has to take into account the self energy of the antiquark b leading to a similar Feynman amplitude.

The matrix element can be written as

$$i\mathcal{M} = \mu_r^{4-D} g_s^2 \frac{g_{\mu\nu}}{q^2 - m_{V_1}^2} \Gamma_1(p_1 - p_2)_\mu \frac{1}{p_a^2} \delta_{c_a c_b} C_f \int \frac{d^D k}{(2\pi)^D} \frac{[\bar{v}_b \gamma_\nu \Gamma_2 \not{p}_a \gamma_\rho (k + \not{p}_a) \gamma^\rho u_a]}{k^2 (p_a + k)^2} \quad (\text{B.19})$$

$$=: \mu^{4-D} g_s^2 \frac{g_{\mu\nu}}{q^2 - m_{V_1}^2} \Gamma_1(p_1 - p_2)_\mu \frac{1}{p_a^2} \delta_{c_a c_b} C_f [\bar{v}_b \gamma_\nu \Gamma_2 \not{p}_a \Sigma(p_a) u_a]. \quad (\text{B.20})$$

$\Sigma(p_a)$ contains the divergent tensor integral and can be expressed in terms of scalar

integrals:

$$\Sigma(p_a) := \mu_r^{4-D} g_s^2 \int \frac{d^D k}{(2\pi)^D} \gamma_\rho \frac{k + \not{p}_a}{k^2 (p_a + k)^2} \gamma^\rho \quad (\text{B.21})$$

$$\stackrel{(B.4)}{=} -i \frac{D-2}{(4\pi)^2} \left(\gamma_\mu B^\mu + \not{p}_a B_0 \right) \quad (\text{B.22})$$

$$= -i \frac{D-2}{(4\pi)^2} \not{p}_a \left(B_1(p_a^2, 0, 0) + B_0(p_a^2, 0, 0) \right) \quad (\text{B.23})$$

$$= -i \frac{D-2}{(4\pi)^2} \not{p}_a \frac{1}{2} B_0(p_a^2, 0, 0). \quad (\text{B.24})$$

Now we can rewrite the squared matrix element in terms of the LO Feynman amplitude

$$\overline{\mathcal{M}\mathcal{M}}_B^* = \frac{1}{(4\pi)^2} |\overline{\mathcal{M}}_B|^2 C_f g_s^2 \frac{D-2}{2} B_0(p_a^2, 0, 0). \quad (\text{B.25})$$

Since $p_a^2 = m_a^2 = 0$ all the arguments of the scalar B function are zero. It has been shown that this integral does not contribute [40].

B.2.2 SUSY self energy for quarks

For the SUSY quark self energy diagrams, one of them is shown in Fig. B.3, the computation is similar to the previous one for the squark self energy.

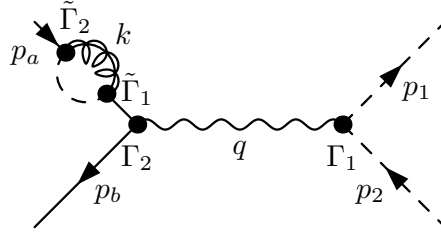


Figure B.3: Feynman diagram for the SUSY quark self energy.

With our Feynman rules we can write the matrix element as

$$i\mathcal{M} = \frac{g_{\mu\nu}}{q^2 - m_{V_1}^2} C_1 (p_1 - p_2)_\mu \frac{1}{p_a^2} \delta_{c_a c_b} C_f \mu_r^{4-D} \int \frac{d^D k}{(2\pi)^D} \frac{\left[\bar{v}_b \gamma_\nu \Gamma_2 \not{p}_a \tilde{\Gamma}_1 (k + m_{\tilde{g}}) \tilde{\Gamma}_2 u_a \right]}{\left(k^2 - m_{\tilde{g}}^2 \right) \left((p_a + k)^2 - m_{\tilde{q}}^2 \right)}. \quad (\text{B.26})$$

We can define

$$\Sigma := \mu_r^{4-D} \int \frac{d^D k}{(2\pi)^D} \frac{\not{k} + m_{\bar{g}}}{(k^2 - m_{\bar{g}}^2) \left((p_a + k)^2 - m_{\bar{q}}^2 \right)} \quad (\text{B.27})$$

$$= \frac{i}{4\pi^2} (\gamma_\mu B^\mu + m_{\bar{g}} B_0) = \frac{i}{4\pi^2} (\not{p}_a B_1 + m_{\bar{g}} B_0) \quad (\text{B.28})$$

containing the divergent scalar integrals. If we compute the squared matrix element, only the term proportional to B_1 will contribute. The term proportional to B_0 will be zero because of an odd amount of γ matrices. After evaluating the resulting traces in D -dimensions we get the squared Feynman amplitude

$$\overline{\mathcal{M}\mathcal{M}_B^*} = \frac{C_f}{(4\pi)^2} |\overline{\mathcal{M}_B}|^2 (\tilde{L}_1 \tilde{R}^*_2 + \tilde{R}_1 \tilde{L}^*_2) B_1(p_a^2, m_{\bar{g}}^2, m_{\bar{q}}^2), \quad (\text{B.29})$$

where we have used the common color factor

$$C_f = (T^a T^a) = \frac{4}{3}. \quad (\text{B.30})$$

To get the Feynman amplitude for the antiquark self energy we have to change $p_a \leftrightarrow p_b$.

B.2.3 The gluon vertex correction

For the SM vertex correction we have to compute the diagram shown in Fig. B.4.

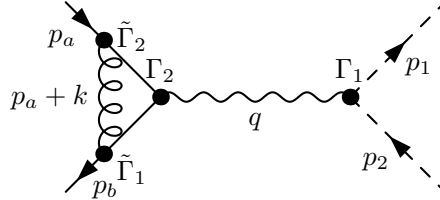


Figure B.4: Feynman diagram for the QCD vertex correction.

Before we write down the whole amplitude, we focus on the hadronic part of the matrix element. We can write the part of the vertex correction as

$$i\Lambda_\mu = ig_s^2 \mu^{\frac{4-D}{2}} \int \frac{d^D k}{(2\pi)^D} \frac{-ig^{\rho\sigma} \left[\gamma_\rho i(\not{p}_a + \not{p}_b + \not{k}) i\gamma_\mu \Gamma_2 i\not{k} \gamma_\sigma \right]}{k^2 (p_a + k)^2 (p_a + p_b + k)^2} \quad (\text{B.31})$$

$$= ig_s^2 \frac{\mu^{\frac{4-D}{2}}}{(2\pi)^D} \int d^D k \frac{\left[\gamma_\rho (\not{p}_a + \not{p}_b + \not{k}) \gamma_\mu \Gamma_2 \not{k} \gamma_\rho \right]}{k^2 (p_a + k)^2 (p_a + p_b + k)^2}. \quad (\text{B.32})$$

It can be expressed in terms of the generic tensor integrals

$$i\Lambda_\mu = ig_s^2 \frac{i}{(4\pi)^2} \gamma_\rho (\gamma_\sigma \gamma_\mu \gamma_{\sigma'} C^{\sigma\sigma'} + \not{p}_a \gamma_\mu \gamma_\sigma C^\sigma + \not{p}_b \gamma_\mu \gamma_\sigma C^\sigma) \gamma^\rho \quad (\text{B.33})$$

Before we rewrite the tensor integrals in terms of the scalar integrals, let us have a look at the squared Feynman amplitude:

$$\overline{\mathcal{M}\mathcal{M}_B^*} = \frac{|f_c|^2}{4 \cdot 9} \text{Tr} [T^a T^a] \frac{1}{(q^2 - m_{\tilde{V}_1}^2)} \frac{1}{(q^2 - m_{\tilde{V}_2}^2)} \quad (\text{B.34})$$

$$\Gamma_1 \bar{\Gamma}_3 (p_1 - p_2)^\mu (p_1 - p_2)^\nu \text{Tr} [\not{p}_b \Lambda_\mu \Gamma_2 \bar{\Gamma}_4 \not{p}_a \gamma_\nu] . \quad (\text{B.35})$$

Since we deal with massless particles, all the terms in Λ proportional to \not{p}_a on the left- or to \not{p}_b on the right-hand side will vanish due to the Dirac equation. Therewith and with the help of Eq. (B.6), we can write the virtual correction in terms of scalar integrals and the LO amplitude

$$\overline{\mathcal{M}\mathcal{M}_B^*} = \frac{1}{2} g_s^2 \frac{1}{(4\pi)^2} |\overline{\mathcal{M}_B}|^2 \quad (\text{B.36})$$

$$[4p_a \cdot p_b (C_{23} + C_{11}) - 2(4 - D)p_a \cdot p_b (C_{23} + C_{12}) + (2 - D)^2 C_{24}] , \quad (\text{B.37})$$

where we have used the tensor reduction formalism presented in Ref. [41]. The arguments of the C functions are only $(p_a + p_b)^2$ due to the massless approximation.

B.2.4 The SUSY vertex correction

The MSSM-QCD vertex correction corresponds to the exchange of a gluino by two squarks depicted in Fig. B.5.

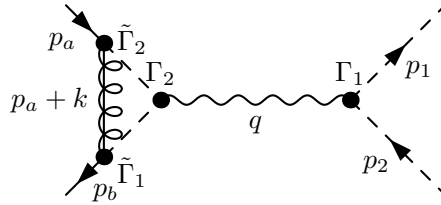


Figure B.5: Feynman diagram for the MSSM-QCD vertex correction.

Again we define the vertex correction as

$$i\Lambda_\mu = i\Gamma_2\mu^{\frac{4-D}{2}} \int \frac{d^D k}{(2\pi)^D} \frac{\tilde{\Gamma}_1(\not{p}_b + \not{k} + m_{\tilde{g}})\tilde{\Gamma}_2(p_b - p_a - 2k)_\mu}{(k^2 - m_{\tilde{q}_1}^2)((p_a + k)^2 - m_{\tilde{g}}^2)((p_a + p_b + k)^2 - m_{\tilde{q}_2}^2)}. \quad (\text{B.38})$$

We can write the squared amplitude in a compact form:

$$\overline{\mathcal{M}\mathcal{M}_B^*} = \frac{|f_c|^2}{4 \cdot 9} \text{Tr}[T^a T^a] \frac{1}{(q^2 - m_{V_1}^2)} \frac{1}{(q^2 - m_{V_2}^2)} \quad (\text{B.39})$$

$$\Gamma_1 \bar{\Gamma}_3 (p_1 - p_2)^\mu (p_1 - p_2)^\nu \text{Tr}[\not{p}_b \Lambda_\mu \bar{\Gamma}_4 \not{p}_a \gamma_\nu] \Gamma_2. \quad (\text{B.40})$$

The only contributing parts are

$$\Lambda_\mu \sim \not{k}(p_b - p_a - 2k)_\mu \quad (\text{B.41})$$

and therefore the vertex correction can be expressed as

$$\Lambda_\mu \sim p_{b\mu} \gamma_\sigma C^\sigma - p_{a\mu} \gamma_\sigma C^\sigma - 2\gamma^\sigma C_{\sigma\mu}. \quad (\text{B.42})$$

Using again the massless quark approximation, we end up with the squared Feynman amplitude:

$$\overline{\mathcal{M}\mathcal{M}_B^*} = 2C_{24} \frac{1}{(4\pi)^2} \frac{1}{2} \frac{1}{12} \frac{1}{(q^2 - m_{V_1}^2)} \frac{1}{(q^2 - m_{V_2}^2)} \quad (\text{B.43})$$

$$\left((\tilde{L}_1 \tilde{R}_2) C_1 R_2 C_3^* R_4^* + (\tilde{R}_1 \tilde{L}_2) C_1 L_2 C_3^* L_4^* \right) [tu - m_1^2 m_2^2]. \quad (\text{B.44})$$

B.3 The real corrections

B.3.1 Real gluon emission

For the real gluon emission we have to consider two diagrams, where either the gluon is emitted by the quark or the antiquark. The former is shown in Fig. B.6.

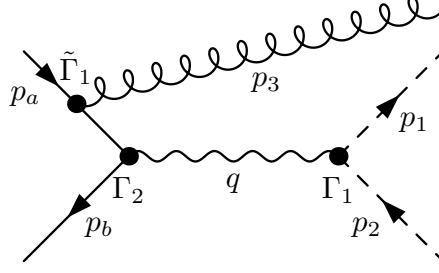


Figure B.6: Feynman diagram for the real gluon emission.

The two matrix elements can be written as

$$i\mathcal{M}_a = \frac{-ig_{\mu\nu}}{q^2 - m_{V_1}^2} C_1 (p_1 - p_2)_\mu \left[\bar{v}_b \gamma_\nu (L_2 P_L + R_2 P_R) i \frac{\not{p}_a - \not{p}_3}{p_a^2 - p_3^2} (-ig_s) \gamma_\rho u_a \right] \epsilon_\rho^a T^a, \quad (\text{B.45})$$

$$i\mathcal{M}_b = \frac{-ig_{\mu,\nu}}{q^2 - m_{V_1}^2} C_1 (p_1 - p_2)_\mu \left[\bar{v}_b (-ig_s) \gamma_\rho i \frac{\not{p}_b - \not{p}_3}{p_b^2 - p_3^2} \gamma_\nu (L_2 P_L + R_2 P_R) u_a \right] \epsilon_\rho^a T^a. \quad (\text{B.46})$$

To write the squared amplitude in a compact form we introduce the hadronic tensor $H_{\mu\nu}$ and the sleptonic one $L^{\mu\nu}$. This yields

$$\rightarrow |\overline{\mathcal{M}}|^2 \equiv L^{\mu\nu} H_{\mu\nu} = L^{\mu\nu} \left(H_{\mu\nu}^{aa} + H_{\mu\nu}^{bb} + H_{\mu\nu}^{ab} + H_{\mu\nu}^{ba} \right), \quad (\text{B.47})$$

where the different exponents correspond to the different realizations of the process. The interference term is denoted by $H_{\mu\nu}^{ab}$ and $H_{\mu\nu}^{ba}$. We include the electroweak propagators into the definition of $L^{\mu\nu}$ and all strong correction parts in $H_{\mu\nu}$. For the summation over the gluon polarizations we use the common relation

$$\sum_\lambda \epsilon_\rho \epsilon_{\rho'}^* \sim -g_{\rho\rho'}, \quad (\text{B.48})$$

yielding

$$L^{\mu\nu} = \frac{1}{q^2 - m_{V_1}^2} \frac{1}{q^2 - m_{V_2}^2} C_1 (p_1 - p_2)^\mu C_3^* (p_1 - p_2)^\nu, \quad (\text{B.49})$$

$$H_{\mu\nu}^{aa} = -\frac{|f_c|^2}{36} \frac{g_s^2}{(2p_a \cdot p_3)^2} \text{Tr} \left[\not{p}_b \gamma_\mu \Gamma_2 (\not{p}_a - \not{p}_3) \gamma_\rho \not{p}_a \gamma^\rho (\not{p}_a - \not{p}_3) \bar{\Gamma}_2 \gamma_\nu \right], \quad (\text{B.50})$$

$$H_{\mu\nu}^{bb} = -\frac{|f_c|^2}{36} \frac{g_s^2}{(2p_b \cdot p_3)^2} \text{Tr} \left[\not{p}_a \bar{\Gamma}_4 \gamma_\nu (\not{p}_b - \not{p}_3) \gamma_\rho \not{p}_b \gamma^\rho (\not{p}_b - \not{p}_3) \gamma_\mu \Gamma_2 \right], \quad (\text{B.51})$$

$$H_{\mu\nu}^{ab} = -\frac{|f_c|^2}{36} \frac{g_s^2}{4p_a \cdot p_3 p_b \cdot p_3} \text{Tr} \left[\not{p}_b \gamma_\mu \Gamma_2 (\not{p}_a - \not{p}_3) \gamma_\rho \not{p}_a \bar{\Gamma}_4 \gamma_\nu (\not{p}_b - \not{p}_3) \gamma^\rho \right], \quad (\text{B.52})$$

$$H_{\mu\nu}^{ba} = -\frac{|f_c|^2}{36} \frac{g_s^2}{4p_a \cdot p_3 p_b \cdot p_3} \text{Tr} \left[\not{p}_b \gamma_\rho (\not{p}_b - \not{p}_3) \gamma_\mu \Gamma_2 \not{p}_a \gamma^\rho (\not{p}_b - \not{p}_3) \bar{\Gamma}_4 \gamma_\nu \right]. \quad (\text{B.53})$$

The large traces have been computed with FORM. The color factor is $|f_c|^2 = 3 \text{Tr} \lambda^a \lambda^a$.

B.3.2 Real quark emission

For the real quark emission we can have a s-channel, an u-channel and the interference terms. The diagrams are shown in Fig. B.7.

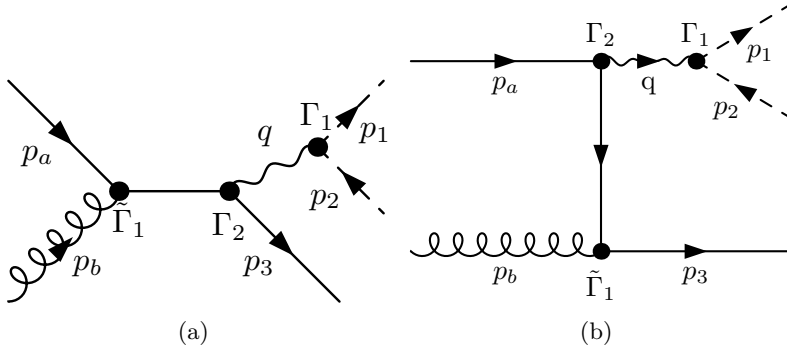


Figure B.7: Feynman diagrams for real quark emission.

Since the sleptonic tensor will be the same as in the real gluon emission we will just

state the hadronic tensor, where we have to consider a different color factor.

$$H_{\mu\nu}^{ss} = -\frac{|f_c|^2}{96} \frac{g_s^2}{(2p_a \cdot p_b)^2} \text{Tr} \left[\gamma_\rho \not{p}_a \gamma^\rho (\not{p}_a + \not{p}_b) \gamma_\mu \Gamma_4 \not{p}_3 \gamma_\nu \Gamma_2 (\not{p}_a + \not{p}_b) \right], \quad (\text{B.54})$$

$$H_{\mu\nu}^{uu} = \frac{|f_c|^2}{96} \frac{g_s^2}{(2p_b \cdot p_3)^2} \text{Tr} \left[\not{p}_a \gamma_\mu \Gamma_4 (\not{p}_3 - \not{p}_b) \gamma_\rho \not{p}_3 \gamma^\rho (\not{p}_3 - \not{p}_b) \gamma_\nu \Gamma_2 \right], \quad (\text{B.55})$$

$$H_{\mu\nu}^{su} = \frac{|f_c|^2}{96} \frac{g_s^2}{4p_b \cdot p_3 p_a \cdot p_b} \text{Tr} \left[\gamma_\rho \not{p}_a \gamma_\mu \Gamma_4 (\not{p}_3 - \not{p}_a) \gamma^\rho \not{p}_3 \gamma_\nu \Gamma_2 (\not{p}_a + \not{p}_b) \right], \quad (\text{B.56})$$

$$H_{\mu\nu}^{us} = -\frac{|f_c|^2}{96} \frac{g_s^2}{4p_a \cdot p_b p_b \cdot p_3} \text{Tr} \left[\gamma_\rho (\not{p}_3 - \not{p}_a) \gamma_\mu \Gamma_2 \not{p}_a \gamma^\rho (\not{p}_b + \not{p}_a) \gamma_\nu \Gamma_4 \not{p}_3 \right]. \quad (\text{B.57})$$

B.3.3 Real antiquark emission

Similar as for the real quark emission we will have a s-channel and a t-channel diagram.

The computation is more or less the same as for the real quark emission.

C Gaugino pair production

The extended program code was originally made for gaugino pair production [1]. We have used it to update the resummation predictions for gaugino cross sections, invariant mass and transverse momentum distributions for the same BPs and same setup as for the slepton pair production done in this thesis. The whole work including all further references can be found in Ref. [25].

Due to the same quantum numbers the Higgsino and the electroweak gauginos will mix after the electroweak symmetry breaking. The neutral $\tilde{H}_{1,2}^0$ mixes with \tilde{B} and \tilde{W}^0 to form four neutral mass eigenstates χ_i^0 with $i \in \{1,2,3,4\}$ called neutralinos. The χ_1^0 is in most mSUGRA scenarios the LSP. In addition the charged fields $\tilde{H}_{1,2}^\pm$ can mix with the winos \tilde{W}^\pm giving two mass eigenstates χ_k^\pm called charginos. The mixing depends on the values of $\tan\beta$, μ and the trilinear coupling in the mSUGRA parameter space.

Since gauginos are fermionic the production of pairs is closely related to the Drell-Yan process. However at LO we have additional t- and u-channels due to squark exchange which are depicted in Fig. C.1. This leads to many different diagrams for NLO corrections including self-energies, vertex corrections and “boxes”. The computations can be found in Ref. [1].

We have updated the results for gaugino-pair production for the 8 TeV run of the LHC

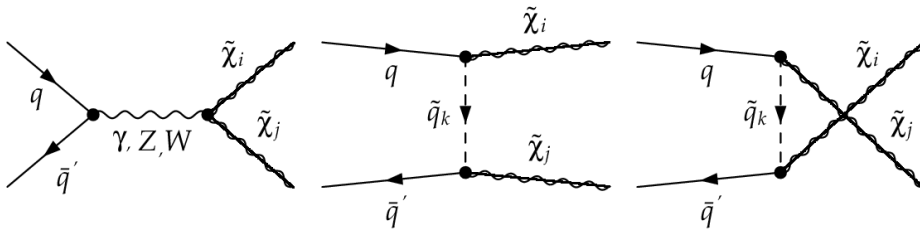
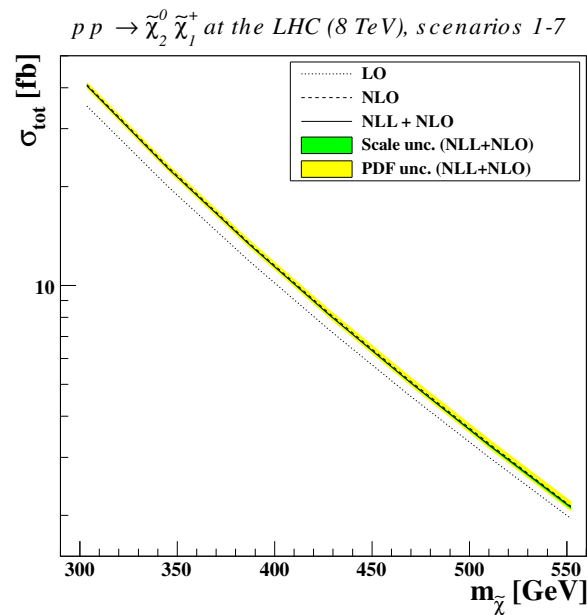


Figure C.1: Leading-order Feynman diagrams for gaugino pair production at hadron colliders. Here the virtual particle corresponds to an electroweak gauge boson (left) or squark (center and right). From Ref. [42].

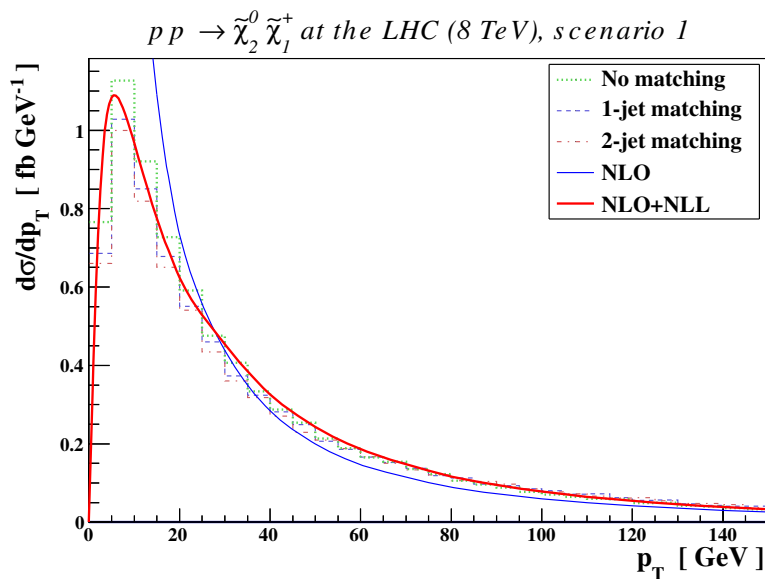
and newer PDF sets, the same as for slepton pair production, i.e. MSTW 2008 NLO. In

Fig. C.2 (a) we show the results for the total cross section for model line 10.1 of a $\tilde{\chi}_2^0\tilde{\chi}_1^+$, the so called golden channel. The cross section decreases exponentially by increasing the almost degenerated mass of the gauginos. Comparing Fig. C.2 (a) and 4.5 we can see that even for larger masses of the gauginos the cross section is roughly three times larger than for the sleptons. In Tab. C.1 results for all possible final states are shown while using BP 1 of the LPCC numbering scheme. We can see that the cross section for the golden channel is enhanced. This is a common feature to many SUSY models, where the $\tilde{\chi}_1^0$ is mostly bino like. For further results including different BPs see [25]. In addition we show again the scale and PDF uncertainties with the expected behavior for NLO matched to NLL. We expect that the gauginos will be found as one of the first SUSY particles since the cross section is quite large with respect to the other supersymmetric particles.

Finally we present a transverse momentum distribution of the golden channel in Fig. C.2 (b). We see the typical behavior for the NLO and resummation results. In addition we have included results generated with MADGRAPH v.5 [37] interfaced to PYTHIA [38] for generating one and two additional jets. This Monte Carlo tool is widely used by experimental collaborations. We can see that the results for resummation fit the curve for 1-jet-matching quite well. This is obvious since the resummation code [1] includes the emission of one hard jet.



(a) The total cross section at LO (dotted), NLO (dashed) and NLO+NLL (full) with its scale (green) and PDF (yellow) uncertainty for the production of a $\tilde{\chi}_2^0 \tilde{\chi}_1^+$ pair as a function of their almost degenerate mass $m_{\tilde{\chi}}$ at the LHC with $\sqrt{S} = 8$ TeV and benchmark points 1-7 on model line 10.1.



(b) Transverse momentum distribution for the production of a $\tilde{\chi}_2^0 \tilde{\chi}_1^+$ pair at the COM energy of 8 TeV in a proton-proton collision for BP 1. NLO, NLO+NLL and results from Monte Carlo event generators matched to 1 and 2 jets are shown.

Figure C.2: Total cross sections for model line 10.1 (a) and the transverse momentum distributions for NLO, resummation and Monte Carlo event generators. From Ref. [25].

Table C.1: Total cross sections related to the production of various gaugino pairs of masses m_1 and m_2 , presented together with the associated scale and PDF uncertainties for the LHC running at a center-of-mass energy of $\sqrt{s} = 8$ TeV in the context of the benchmark point 1 of the LPCC numbering scheme. The cross sections are given at the leading order and next-to-leading order of perturbative QCD and matched to threshold resummation. The PDF uncertainties are not shown for the LO results. Any cross section smaller than 0.1 fb is omitted.

Process	m_1 (GeV)	m_2 (GeV)	LO (fb)	NLO (fb)	NLO+NLL (fb)
$pp \rightarrow \chi_1^0 \chi_1^0$	161.7	161.7	$0.81^{+5.8\%}_{-5.3\%}$	$1.06^{+3.5\%+2.8\%}_{-3.0\%-2.0\%}$	$1.03^{+0.5\%+2.9\%}_{-0.6\%-2.0\%}$
$pp \rightarrow \chi_1^0 \chi_1^-$	161.7	303.5	$0.16^{+6.0\%}_{-5.5\%}$	$0.20^{+2.5\%+2.9\%}_{-2.4\%-2.4\%}$	$0.20^{+0.0\%+2.9\%}_{-0.3\%-2.5\%}$
$pp \rightarrow \chi_2^0 \chi_2^0$	303.8	303.8	$0.85^{+9.2\%}_{-7.9\%}$	$1.07^{+3.5\%+3.1\%}_{-3.5\%-2.2\%}$	$1.05^{+0.0\%+3.5\%}_{-0.4\%-1.9\%}$
$pp \rightarrow \chi_2^0 \chi_3^0$	303.8	526.5	$0.21^{+9.4\%}_{-8.1\%}$	$0.25^{+2.6\%+3.2\%}_{-2.9\%-2.3\%}$	$0.25^{+0.1\%+3.2\%}_{-0.5\%-2.3\%}$
$pp \rightarrow \chi_2^0 \chi_1^-$	303.8	303.5	$14.46^{+6.7\%}_{-6.1\%}$	$17.25^{+1.6\%+3.0\%}_{-1.7\%-2.6\%}$	$17.05^{+0.2\%+3.1\%}_{-0.7\%-2.6\%}$
$pp \rightarrow \chi_3^0 \chi_4^0$	526.5	542.4	$0.83^{+11.0\%}_{-9.3\%}$	$0.97^{+2.8\%+3.9\%}_{-3.3\%-2.4\%}$	$0.96^{+0.4\%+3.8\%}_{-0.9\%-2.5\%}$
$pp \rightarrow \chi_3^0 \chi_1^-$	526.5	303.5	$0.12^{+9.4\%}_{-8.1\%}$	$0.15^{+2.6\%+3.8\%}_{-2.9\%-2.9\%}$	$0.15^{+0.1\%+3.8\%}_{-0.6\%-3.0\%}$
$pp \rightarrow \chi_3^0 \chi_2^-$	526.5	542.2	$0.42^{+11.2\%}_{-9.5\%}$	$0.50^{+2.8\%+4.9\%}_{-3.3\%-3.6\%}$	$0.49^{+0.4\%+4.9\%}_{-0.9\%-3.5\%}$
$pp \rightarrow \chi_4^0 \chi_2^-$	542.4	542.2	$0.39^{+11.3\%}_{-9.6\%}$	$0.47^{+2.7\%+4.9\%}_{-3.2\%-3.6\%}$	$0.46^{+0.5\%+4.9\%}_{-1.1\%-3.7\%}$
$pp \rightarrow \chi_1^+ \chi_1^0$	303.5	161.7	$0.38^{+6.0\%}_{-5.4\%}$	$0.46^{+2.5\%+2.8\%}_{-2.4\%-2.1\%}$	$0.46^{+0.2\%+2.9\%}_{-0.5\%-2.1\%}$
$pp \rightarrow \chi_1^+ \chi_2^0$	303.5	303.8	$35.16^{+6.3\%}_{-5.8\%}$	$40.90^{+1.6\%+2.9\%}_{-1.7\%-2.2\%}$	$40.51^{+0.0\%+2.9\%}_{-0.3\%-2.2\%}$
$pp \rightarrow \chi_1^+ \chi_3^0$	303.5	526.5	$0.34^{+9.2\%}_{-7.9\%}$	$0.40^{+2.6\%+3.7\%}_{-2.9\%-2.4\%}$	$0.40^{+0.0\%+3.6\%}_{-0.3\%-2.5\%}$
$pp \rightarrow \chi_1^+ \chi_1^-$	303.5	303.5	$25.64^{+6.6\%}_{-5.9\%}$	$30.37^{+1.7\%+2.7\%}_{-1.9\%-2.0\%}$	$30.04^{+0.0\%+2.7\%}_{-0.5\%-2.1\%}$
$pp \rightarrow \chi_2^+ \chi_3^0$	542.2	526.5	$1.27^{+11.1\%}_{-9.4\%}$	$1.46^{+2.9\%+4.4\%}_{-3.3\%-2.7\%}$	$1.45^{+0.3\%+4.3\%}_{-0.7\%-2.9\%}$
$pp \rightarrow \chi_2^+ \chi_4^0$	542.2	542.4	$1.21^{+11.2\%}_{-9.5\%}$	$1.37^{+2.7\%+4.4\%}_{-3.2\%-2.8\%}$	$1.36^{+0.4\%+4.6\%}_{-0.8\%-2.6\%}$
$pp \rightarrow \chi_2^+ \chi_2^-$	542.2	542.2	$0.86^{+10.9\%}_{-9.3\%}$	$1.00^{+2.6\%+4.0\%}_{-3.1\%-2.4\%}$	$0.99^{+0.4\%+4.1\%}_{-0.9\%-2.4\%}$

Acknowledgements

I would like to thank the following people and express my gratitude to them:

- David R. Lamprea for the great collaboration, many good discussions and teaching me some of his computer science know how.
- Prof. Dr. Michael Klasen, for giving me the opportunity to work on that interesting topic, the freedom to develop some parts on my own and of course the things he taught me.
- The rest of the group Klasen for creating a nice working atmosphere and teaching me many things.
- Dr. Benjamin Fuks for helping me whenever I needed help.
- My girlfriend, Rebecca Hagen, for her mental support and brightened words needed during this work.
- My brother Marco Rothering and my parents for giving me the best family background and helping me with many things.
- My former teacher Dr. Wolfgang Speller who evoked my passion for physics during school.
- My friends, especially Joshua Sibbing and Marcel Pollmann, for many things.

Bibliography

- [1] Jonathan Debove. *QCD resummation for gaugino-pair hadroproduction*. PhD thesis, U. Grenoble, 2010.
- [2] Lewis H. Ryder. *Quantum Field Theory*. Cambridge University Press, 2 edition, June 1996.
- [3] Stephen P. Martin. *A Supersymmetry primer*. 1997.
- [4] Ian J.R. Aitchison. *Supersymmetry and the MSSM: An Elementary introduction*. 2005.
- [5] Michael E. Peskin and Dan V. Schroeder. *An Introduction To Quantum Field Theory (Frontiers in Physics)*. Westview Press, 1995.
- [6] Walter Greiner. *Quantum Chromodynamics*. Springer-Verlag Berlin Heidelberg, Berlin, Heidelberg, third revised and enlarged edition edition, 2007.
- [7] John C. Collins, Davison E. Soper, and George F. Sterman. Factorization of Hard Processes in QCD. *Adv. Ser. Direct.High Energy Phys.*, 5:1–91, 1988.
- [8] S.D. Drell and Tung-Mow Yan. Massive Lepton Pair Production in Hadron-Hadron Collisions at High-Energies. *Phys.Rev.Lett.*, 25:316–320, 1970.
- [9] B. Pötter. *Calculation Techniques in Perturbative QCD: The Drell-Yan Process*. 1997.
- [10] Taizo Muta. *Foundations of quantum chromodynamics*. World Scientific, Singapore, 1987.
- [11] F. Bloch and A. Nordsieck. Notes on the radiation field of the electron. *Phys. Rev.*, 52:54–59, 1937.
- [12] T. Kinoshita and A. Ukawa. *Mass Singularities of Feynman Amplitudes*. 1975.

-
- [13] R. Keith Ellis, W. James Stirling, and B. R. Webber. *QCD and Collider Physics*, volume 8. Cambridge University Press, 1996.
- [14] A.D. Martin, W.J. Stirling, R.S. Thorne, and G. Watt. Parton distributions for the LHC. *Eur. Phys. J.*, C63:189–285, 2009.
- [15] Andrew R. Baden. Jets and kinematics in hadronic collisions. *International Journal of Modern Physics A*, 13(11):1817–1845, 1998.
- [16] J. Beringer et al. Review of Particle Physics (RPP). *Phys. Rev.*, D86:010001, 2012.
- [17] Steven Weinberg. Infrared photons and gravitons. *Phys. Rev.*, 140:B516–B524, 1965.
- [18] S. Catani and L. Trentadue. Resummation of the QCD Perturbative Series for Hard Processes. *Nucl. Phys.*, B327:323, 1989.
- [19] George F. Sterman. Partons, factorization and resummation, TASI 95. 1995.
- [20] Benjamin Fuks. *QCD-resummation and non-minimal-flavour violation for supersymmetric particle productions at hadron colliders*. PhD thesis, U. Grenoble, 2007.
- [21] Janusz Rosiek. Complete set of Feynman rules for the MSSM: Erratum. 1995.
- [22] Stefano Catani and Michael H. Seymour. A general algorithm for calculating jet cross sections in nlo qcd. 1996. <http://arxiv.org/abs/hep-ph/9605323>.
- [23] Sujeet Akula, Pran Nath, and Gregory Peim. Implications of the Higgs Boson Discovery for mSUGRA. *Phys. Lett.*, B717:188–192, 2012.
- [24] S.S. AbdusSalam, B.C. Allanach, H.K. Dreiner, J. Ellis, U. Ellwanger, et al. Benchmark Models, Planes, Lines and Points for Future SUSY Searches at the LHC. *Eur. Phys. J.*, C71:1835, 2011.
- [25] Benjamin Fuks, Michael Klasen, David R. Lamprea, and Marcel Rothering. Gaugino production in proton-proton collisions at a center-of-mass energy of 8 TeV. *JHEP*, 1210:081, 2012.
- [26] W. Beenakker, R. Hopker, M. Spira, and P.M. Zerwas. Squark and gluino production at hadron colliders. *Nucl. Phys.*, B492:51–103, 1997.

-
- [27] Daniel Stump, Joey Huston, Jon Pumplin, Wu-Ki Tung, H.L. Lai, et al. Inclusive jet production, parton distributions, and the search for new physics. *JHEP*, 0310:046, 2003.
- [28] Abdelhak Djouadi, Jean-Loic Kneur, and Gilbert Moultaka. SuSpect: A Fortran code for the supersymmetric and Higgs particle spectrum in the MSSM. *Comput. Phys. Commun.*, 176:426–455, 2007.
- [29] Pat Scott. Searches for Particle Dark Matter: An Introduction. 2011.
- [30] Chiara Arina and Nicolao Fornengo. Sneutrino cold dark matter, a new analysis: relic abundance and detection rates. *JHEP*, 2007(11):029, 2007.
- [31] W-M Yao et al. Review of particle physics. *Journal of Physics G: Nuclear and Particle Physics*, 33(1):1, 2006.
- [32] Thomas Hebbeker. Can the sneutrino be the lightest supersymmetric particle? *Phys.Lett.*, B470:259–262, 1999.
- [33] G. Belanger, M. Kakizaki, E.K. Park, S. Kraml, and A. Pukhov. Light mixed sneutrinos as thermal dark matter. *JCAP*, 1011:017, 2010.
- [34] Genevieve Belanger, Sabine Kraml, and Andre Lessa. Light Sneutrino Dark Matter at the LHC. *JHEP*, 1107:083, 2011.
- [35] Elena Aprile. The XENON Dark Matter Experiment. 2005.
- [36] Serguei Chatrchyan et al. Search for Dark Matter and Large Extra Dimensions in pp Collisions Yielding a Photon and Missing Transverse Energy. *Phys. Rev. Lett.*, 108:261803, 2012.
- [37] Johan Alwall, Michel Herquet, Fabio Maltoni, Olivier Mattelaer, and Tim Stelzer. MadGraph 5 : Going Beyond. *JHEP*, 1106:128, 2011.
- [38] Torbjorn Sjostrand, Stephen Mrenna, and Peter Z. Skands. PYTHIA 6.4 Physics and Manual. *JHEP*, 0605:026, 2006.
- [39] David R. Lamprea. Resummation predictions for new electroweak gauge boson production at the LHC, 2012.
- [40] Stefan Pokorski. *Gauge Field Theories; 2nd ed.* Cambridge monographs on mathematical physics. Cambridge Univ. Press, Cambridge, 2000.

-
- [41] G. Passarino and M.J.G. Veltman. One Loop Corrections for $e^+ e^-$ Annihilation Into $\mu^+ \mu^-$ in the Weinberg Model. *Nucl. Phys.*, B160:151, 1979.
- [42] Jonathan Debove, Benjamin Fuks, and Michael Klasen. Model-independent analysis of gaugino-pair production in polarized and unpolarized hadron collisions. *Phys.Rev.*, D78:074020, 2008.
- [43] Benjamin Fuks. Transverse-momentum, threshold and joint resummations for slepton pair production at hadron colliders. 2007.
- [44] Giuseppe Bozzi, Benjamin Fuks, and Michael Klasen. Joint resummation for slepton pair production at hadron colliders. *Nucl. Phys.*, B794:46–60, 2008.
- [45] Jonathan Debove, Benjamin Fuks, and Michael Klasen. Transverse-momentum resummation for gaugino-pair production at hadron colliders. *Phys. Lett.*, B688:208–211, 2010.
- [46] Jonathan Debove, Benjamin Fuks, and Michael Klasen. Threshold resummation for gaugino pair production at hadron colliders. *Nucl. Phys.*, B842:51–85, 2011.
- [47] Jonathan Debove, Benjamin Fuks, and Michael Klasen. Joint Resummation for Gaugino Pair Production at Hadron Colliders. *Nucl. Phys.*, B849:64–79, 2011.

Ich versichere hiermit, dass ich meine Masterarbeit „ *Resummation predictions for slepton particle production at the LHC and implications for dark matter*“ selbstständig und ohne fremde Hilfe angefertigt habe, und dass ich alle von anderen Autoren wörtlich übernommenen Stellen, wie auch die sich an die Gedankengänge anderer Autoren eng anlehrenden Ausführungen meiner Arbeit besonders gekennzeichnet und die Quellen zitiert habe.

Münster, den 12. November 2012
